QUANTIFYING THE ROLES OF CHEMICAL AND MICROBIAL WEATHERING IN ACID-SULFATE HYDROTHERMAL SYSTEMS

By

Charity M. Phillips Lander

Submitted to the graduate degree program in Geology and the Graduate Faculty of the University of Kansas in partial fulfillment of the requirements for the degree of Doctor of Philosophy.

_____

Chairperson: David A. Fowle

_____

Co-Chairperson: Jennifer A. Roberts

_____

Andreas Moeller

_____

Andrea Brookfield

_____

P. Scott Hefty

Date Defended: August 14, 2014

The Dissertation Committee for Charity M. Phillips Lander
certifies that this is the approved version of the following dissertation:

QUANTIFYING THE ROLES OF CHEMICAL AND MICROBIAL WEATHERING IN ACID-SULFATE HYDROTHERMAL SYSTEMS

_____

Chairperson: David A. Fowle

_____

Chairperson: Jennifer A. Roberts

Date approved: August 14, 2014

Abstract

Although the roles of microbial and chemical processes are relatively well-studied in neutral-chloride hydrothermal systems, very few studies have addressed these processes in acid-sulfate hydrothermal systems. This study aims to survey the roles of chemical and microbial weathering in acid-sulfate hydrothermal systems in order to provide greater understanding of the geochemical processes operating in low pH (2-4) and relatively high temperature (43-90^{o}C) enviroments. These data provide insight into both modern and ancient life in extreme environments, as well as which processes are abiotically controlled.

Field microcosm experiments indicate initial dissolution in Las Pailas hydrothermal system, located on the southwest flank of Rincón de la Vieja, Costa Rica, is likely driven by microorganisms. These microorganisms increase the short-term volumetric weathering rate of anorthoclase containing Fe-oxide and apatite mineral inclusions by an order of magnitude relative to abiotic controls. However, weathering of other silicates by microorganisms appeared to be relatively similar to abiotic controls. These results indicate that microbially induced silicate dissolution facilitates phosphate solubulization in acid-sulfate hydrothermal systems. These results are similar to previous research conducted in low temperature (T), circum-neutral pH systems, despite the higher reaction rates due to increased T and acid attack in this extreme environment.

The net result of increased weathering is the mobilization of trace metals into solution. Hydrothermal fluid fluxes contain abundant trace metals, however, these metals preferentially partition into the sediments at Las Pailas. In other hydrothermal systems and acid mine drainage environments, trace metals preferentially bind to iron oxides. Microorganisms in these systems typically facilitate the formation of Fe-oxides to which trace metals bind. In circum-neutral hydrothermal systems, associated with low-sulfidation epithermal ore deposits, microorganisms form shallow epithermal ore deposits. Sequential extraction of Las Pailas sediments indicates microorganisms also concentrated trace metals, particularly copper, gold and silver in the Las Pailas sediments, despite the acidic pH. However, microorganisms in this acid-sulfate system appear to sequester trace metals by binding them to microbial cell surfaces, exopolymeric substances, and iron oxides produced and entrained within biofilm. These

data suggest microorganisms may create shallow/surficial indicators of epithermal Au-Ag ore formation at depth. Moreover, the association of microbial biomarkers and influences on the isotopic record suggest microorganisms may play a role in ore formation that occurs below the limit for life (~121^{o}C) and that microorganisms may have been involved in ore formation throughout geologic time.

Not all processes in acid-sulfate hydrothermal systems, however, are microbially controlled. Weathering not only concerns itself with the dissolution of primary mineral phases, but also the formation of secondary mineral phases, particularly nontronite and kaolinite formation. Pailas de Agua I, one of the hot springs in the Las Pailas hydrothermal field, contains abundant clay minerals. To assess the influence of microorganisms on secondary mineral formation in Las Pailas, a model hydrothermal solution, based on the solution geochemisty of Pailas de Agua I, was created. Experiments using this solution were performed at high (80^{o}C) and low (25^{o}C) temperatures, with and without the addition of fluoride and microbial surrogates to determine the influence of temperature, Al-complexation by fluoride and microbial processes on clay formation. Results indicate that high temperature experiments form nontronite and kaolinite regardless of experimental conditions. However, in low temperature solutions, fluoride plays a key role in Al-complexation and aids in authigenic nontronite precipitation. Microbial surrogates play little role in clay formation in acidic pH systems, in contrast to, clay mineral formation in many circum-neutral pH systems, which is microbially influenced. Acid-sulfate hydrothermal systems have been proposed as an analog for Mars because of mineralogical similarities between the two systems. These data indicate that while clay minerals on Mars may be good indicators of water in Mars' history, they do not specifically indicate an environment of formation, nor should they be used as an indicator of past life on Mars. Moreover, these data suggest that the kickstarting of the "clay mineral factory" on early Earth may not be the result of microbial processes.

These results indicate that many microbial processes, including microbially induced mineral dissolution and trace metal immobilization, may be ubiquitous in nature regardless of whether exceptional preservation of microbial structures occurs. However, the mechanisms that underpin these processes may

differ between environments. Most importantly, despite the common association between microorganisms and clay minerals in modern environments, authigenic clay formation may occur in the absence of microbial surrogates, if/when Al-complexing ligands are present in solution. Both abiotic and biological processes influence weathering in acid-sulfate hydrothermal systems and these processes may likely be differentiable in the rock record through examination of associations between biomarker associations with sediments, even in the absence of exceptional preservation.

Dedication

For Geoffrey.
You taught me how to be a better person.
I am forever in your debt.

Acknowledgments

I am eternally grateful that I have been surrounded by wonderful people throughout my life who have helped me achieve everything I have today. I have been blessed to have the right people show up at key points in my life and provide for my temporal, intellectual, emotional, and spiritual needs. I would be remiss if I did not acknowledge members of the Church of Jesus Christ of Latter-day Saints, who fed me when I was hungry, clothed me, and provided safe shelter for me. I very often wonder if I would be where I am today had I not been provided these key necessities.

I would not have completed my PhD were it not for my husband, Geoffrey Lander, who knows me better than I know myself. He is my super hero and guardian angel. Without his generous, empathetic, and courageous heart, I very literally would not be here today. Geoffrey sacrificed all creature comforts in order to provide me a safe and comfortable home while I was studying. No one outside of our family will truly understand the depth of commitment and sacrifice required to successfully navigate the uncertainties of military life and maintain a strong marriage while separated by half a continent or more. I hope to be half the human he is. I would also like to thank Kerri-Leigh Grady, Hilary Trout, Karen Santiano Francis, Sylvia Hauser, Kathleen Harris Causey, Tammy Jacobsen, Kim Place-Gateau, Natalia Flechsig, and Tess Crazybull for their support and friendship. Although our paths through military life have been different, they have been among the few people who understand the sacrifices and strain we have experienced over the past decade of war. They have helped me get back up when I have fallen and are among the best cheerleaders a girl could ever have.

One of the biggest challenges I had to overcome during my PhD was the paralyzing anxiety which I developed as a result of some of the challenges I have previously faced. I could barely string two words together in public when I got to KU. Jennifer Roberts spent countless hours discussing science with me in advance of my comprehensive exam in order to show me I knew the material. Jen then turned around and

helped me practice answering questions at the white board to get me comfortable with the format. She is greatly responsible for my success in this and other areas. I am incredibly grateful that she has been patient, kind, and given me the room and time I needed to develop my research and thinking skills. I have learned more from her than I could possibly quantify. Whatever my next chapter brings, I hope Jen and I will be friends until we are both old and grey.

Liz Gravatt got me interested in equitation and whether she realizes it or not, much of my self-confidence has been derived from learning to ride. I was terrified of horses at the first lesson and Coco, The Wonder Pony, was a gentle soul who accepted me as I am. Liz's strength and leadership combined with Coco's patient, calm demeanor helped me to see that I did not need to be angry to be strong. In fact, she, Coco, Merika, and Rocky each taught me that in order to be strong, one must face only the problem directly in front of you, leaving all other baggage at the door. In so doing, I gained the confidence that I could manage a thousand pound animal and/or a difficult faculty member without anger. The peace that Liz and the ponies have given me is one of the greatest gifts I have ever been given.

Intellectually, I have been blessed to have the opportunity to develop a broad background in the geosciences as a result of wonderful pedagogical instruction at every level. I would not be a geologist today without the love and support of Glen F. Embree, my undergraduate advisor. He knew of my passion for all things volcanic, but he encouraged me to develop a broad background in geology. His words encouraged me to develop both intellectual breadth and depth and to chase interesting questions that crossed my path, whether or not they were within my chosen specialty. My success as a geoscientist can be largely credited to this early mentorship. I am grateful to Yildirim Dilek, my master's thesis advisor who demanded perfection from me in all I did and who believed in me even if he was terrible at expressing it.

At KU, I am particularly grateful for the help and support I have received from the faculty and staff, as well as my committee. I have been very blessed with a supportive committee. Andreas Moeller is gifted and pedagogy and has always been ready with good tea and conversation. Andrea Brookfield stepped up

at the last minute to help me get finished. Craig Marshall always exacted the highest standards from me and Scotty Hefty has always asked good questions and helped me strive to do my best. I am extremely indebted to Luis Gonzalez, our Chair, who has supported me through the travails of the PhD and both of my advisors, Jennifer Roberts and David Fowle for their support. I am grateful for Steve Case's support both while I was an NSF GK-12 Fellow and after and for teaching me to better communicate my science to a broad diversity of geoscience audiences. I am also grateful for both Ted Peltier and Gwen MacPherson who taught me geochemistry until I got it.

I am also grateful for the lab supporting cast of my PhD movie, including Karla Leslie and Arne Sturm who taught me lab technique (or how not to screw up in the lab), Paul Kenward and Pete Schillig who taught me how to have a sense of humor and maintain my insanity in graduate school, Maggie Schmerge, Blair Schneider, Aimee and Mark Villareel, Michelle Mary, Christa Jackson, and Wade "mutha-fucka" T. Jones for providing comedic relief during grad school. My twitterati have been there to discuss science at 3 a.m. when I am slogging through another draft. Thanks to @kate_clancy, @27andaPhD, @sciencegurl, @drrubidium, @DrJenGunter, @kejames, @drisis, @astrokatie, @gkygirlengineer, @mnmsplease, @GrrlScientist, @Dr24hours, and Neil deGrasse Tyson for always being there to discuss science.

Lastly, I would like to thank the Kansas Geological Survey for their personal and financial support during my PhD. I have grown to love so many people there and I am so grateful for all they taught me about Kansas' geology over the past 3 years. I'd like to give a special thank you to my boss, John Dunham, who gave me a happy place to work for 3 years and who has always been my favorite curmudgeonly supporter, along with Bob Sawin. I will sincerely miss all the fun we've had together. By far, working at the Survey was amongst my best experiences at KU.

Funding for this work was graciously provided by an NSF GK-12 Fellowship, an ExxonMobil Student Research Grant, a Kansas Geological Foundation Grant, a Geological Society of America Student Research Grant, an Association for Women Geoscientists Chevron Research Scholarship, an Association for Women Geoscientists Sean S. Thompson Service Research Scholarship, an University of Kansas

Dissertation Fellowship, a Joan S. Hollbrook Patton Military Spouse Scholarship, an Ernest Angino Geochemistry Scholarship and a Patterson Fellowship. This work would not be possible without this financial assistance.

Contents

Chapter 1. A Brief Introduction to Hydrothermal Systems and Their Significance in Understanding Early Earth and Other Planets

Introduction

The discovery, in the late 1970s, of microorganisms living in and around deep-sea hydrothermal vents off of dark energy, or energy derived from chemical oxidation and reduction reactions that are not dependent on solar energy, touched off the search for life in extreme environments that were previously considered uninhabitable (Edwards et al., 2005 and references therein; Janasch et al., 1979; Rau et al., 1979). Hydrothermal systems possess steep geochemical gradients that chemoautotrophic microorganisms could exploit and microorganisms cultured from these environments tend to be more deeply branching, or more closely related to the earliest life on Earth (Karl et al., 1980). Together, these data suggested that microorganisms in hydrothermal systems might hold keys to understanding the evolution of early life on Earth (Edwards et al., 2005).

Early Earth's history was dominated by volcanic and impact processes. Once the crust cooled and solidified, early volcanic processes, including island arc formation and seafloor spreading began. Volcanism allowed gases within the Earth's mantle, including H_2S, CO_2, H_2, CO, S^0, and water to vent to the surface and into the atmosphere (Canfield, 2005; Holland, 2002). Cooler temperatures driven by a weaker sun and significant volcanic particulates allowed water to condense on the Earth's surface (Feulner, 2012). Hydrothermal systems, including fumaroles, mud pits, and hot springs began to form from volatile escape and meteoric water circulation. These hot springs, therefore, provided warm, nutrient rich environments in which early life could evolve and thrive (Cady and Noffke, 2009). Textural and chemical biomarkers of life have been sought in modern hydrothermal systems so that we might be able to establish the presence of microbial biosignatures in Earth's rock record.

While thirty years of research in hydrothermal systems has provided substantial insights into life on early Earth and other rocky planets, and previous research has focused primarily on circum-neutral (pH 5-8) systems like Yellowstone. Circum-neutral hot spring systems provide strong evidence of microbial life,

because microbial cells are rapidly encased in siliceous sinters (Phoenix and Konhauser, 2003; 2008; Lalonde, et al., 2005). Microbial silicification is driven by the functional groups that comprise the cell's surfaces, which are negatively charged above ~pH 2-3 (Fein et al., 1997). This excess charge allows positively charge ions, including Fe, to bind to the cell's surface and create a "cation bridge" for negatively charged silica ions to bind (Konhauser et al., 2004). Silicification is a rapid process, and confers benefits to the cells by acting as a UV shield, which would have been important as the weak sun became stronger and early Earth's atmosphere allowed greater penetration of UV rays (Phoenix et al., 2001).

Circum-neutral pH hydrothermal systems comprise only a portion of the diversity of hydrothermal systems. Low pH (pH<4) or acidic hydrothermal systems have remained largely unexamined. This is partially driven by their lack of obvious exceptional preservation textures, like microbial silicification. However, these systems may provide unique clues to the evolution of early Earth and other rocky planets, and geochemical and textural biomarkers that microorganisms may leave outside of exceptionally preserved systems.

Study Significance

This study focuses on the Las Pailas acid-sulfate hydrothermal system, present on the SW flank of the Rincon de la Vieja volcano, Costa Rica. The Las Pailas hydrothermal system consists of fumaroles (gas vents), mudpots (water limited springs, dominated by clay-rich muds), and four hot springs. Three of the four springs, Laguna Fumarolica, Pailas de Agua I, and Pailas de Agua II, are acidic (pH 2.4-4), with temperatures ranging from 43-79^{o}C. Poza del Hongo, the fourth spring, is circum-neutral (pH 5.8) with a temperature of 96^{o}C. This study examines the influence of chemical and microbial weathering processes in this modern spring system and determines what influence microorganisms have on weathering processes in acid-sulfate systems. Ultimately, these data may be applied to similar systems in Earth's history and help us better discern the impact of microbial processes when obvious morphological indicators are not preserved.

Layout and Key Research Questions

The research presented in this dissertation is divided into three research chapters, a conclusions chapter, and appendices. The appendices include data from supporting experiments, produced over the course of this work. This data is currently unpublished but will form the backbone of at least one additional paper.

The main goal of this dissertation is to understand the contributions of microbial and chemical weathering in acid-sulfate hydrothermal systems. The research questions addressed include: 1) What role, if any, do microorganisms play in mineral dissolution at in acidic hot springs, where chemical reactions rates are predicted to be fast?, 2) What influence, if any, do microorganisms have on trace metal cycling in acid-sulfate hydrothermal systems?, 3) What role do microorganisms play in epithermal ore formation associated with high-sulfidation systems? and 4) What role do microorganisms play in authigenic clay formation in acid-sulfate systems?

The results of this dissertation have implications for both modern and ancient acid-pH settings. In particular, they suggest that although exceptional preservation of microbial morphologies may not exist, microbial influences on weathering and metals cycling may be detectable in the rock record. These geochemical indicators of life may be particularly important as we search for past indicators of life on Earth and other rocky planets.

Chapter 2: Microbially Induced Dissolution

Chapter 2 focuses on quantifying the rates of chemically- and microbially-induced dissolution of silicates in the various springs in the Las Pailas hydrothermal field. In modern, low temperature ($T \leq 25^{o}C$) circum-neutral pH waters, microorganisms have been shown to increase silicate dissolution rate by ~10x over abiotic chemical weathering reaction rates (Roberts, 2004). Textural evidence from modern and ancient oceanic crust suggests that microorganisms may weather basalt, in deep ocean, hydrothermal environments. *In situ* incubation studies and laboratory experiments have shown that microorganisms colonize silicates in hydrothermal systems; however it remains unclear what impact microorganisms have on dissolution of primary mineral phases (Templeton et al., 2009).

Chapter 3: Microbial Influences on Epithermal Ore Formation

In circum-neutral hydrothermal systems, microorganisms concentrate trace metals including Au, Ag, and Cu (Landrum et al., 2009; McKenzie et al., 2001; Simmons and Brown, 2007). These shallow hydrothermal systems are often surficial indicators of epithermal ore deposits at depth. This study examines whether microorganisms concentrate Au, Ag, and Cu in acid-sulfate systems in a similar fashion as has been observed in neutral-chloride systems. The results of this study shed light on the processes that shape shallow epithermal ore formation, and have implications for the formation of low temperature aureole around ore bodies throughout geologic time.

Chapter 4: Clay Mineral Formation in Acid-Sulfate Springs

Chapter 4 focuses on the formation of secondary minerals, particularly clay minerals, in acid-sulfate springs. In circum-neutral pH hot springs, silicification is driven by microorganisms, resulting in the rapid formation of siliceous sinters. In acid-sulfate springs, the dominant sediment mineralogy is nontronite and kaolinite (Marcucci et al., 2013). These clays are believed to form from acid-leaching of country rock; however, clay minerals form authigenically under a variety of Earth system conditions. Field and experimental studies of clay mineral formation yield often contradictory results, indicating high temperatures (Tosca et al., 2008), microorganisms (Konhauser and Urrutia, 1999) or Metal:Al ratios (Dekov et al., 2008) may be the dominant factor controlling clay mineral formation. For example, Dekov et al. (2008) suggested Mg:Al ratios control the type of clay mineral that forms in seafloor hydrothermal systems. In contrast, some experimental studies (Harder, 1976; 1978; Tosca et al., 2008) have shown that elevated temperature and reducing conditions are required to form nontronite and field-studies in low temperature, circum-neutral pH systems indicate that microbial processes appear to strongly influence clay mineral formation (Konhauser & Urrutia, 1999). Given these conflicting results, I examined the influence of temperature, an inorganic ligand (F-), and microbial surfaces on authigenic clay formation in a model hydrothermal solution whose chemistry was based on Pailas de Agua I. These data indicate that authigenic clays form in a variety of geochemical environments, which has important ramifications for our interpretation of clay minerals both in Earth's, as well as Mars' rock records.

Conclusion

Together, these data presented in my dissertation provide a broad survey of the processes that influence weathering in acid-sulfate hydrothermal systems. Each chapter seeks to differentiate chemical and microbial influences on weathering in the Las Pailas hot spring system. In sum, my dissertation research suggests microorganisms may play important roles in mineral dissolution and trace element cycling in acid-sulfate systems. However, they may play little to no role in authigenic mineral formation within the springs. Secondary mineral formation, in contrast, may be largely controlled by complexation chemistry within these springs.

In each chapter, I indicate the direct implications of my research on our interpretation of the rock record on Earth or Mars. In the conclusion, I discuss the importance of incorporating diverse data sets in order to best differentiate and interpret the roles and importance of chemical and microbial weathering in hydrothermal systems. This approach is particularly important as we search for analogs to early Earth and other planetary environments.

References

Cady, S., and Noffke, N. (2009). Geobiology: evidence for early life on Earth and the search for life on other planets. *GSA Today 19*, 4-10. doi: 10.1130/GSATG62A.1.

Canfield, D. E. (2005). The early history of atmospheric oxygen: homage to Robert M. Garrels. Annu. Rev. Earth Planet. Sci., 33, 1-36.

Dekov, V., Cuadros, J., Shanks, W., and Koski, R. (2008). Deposition of talc — kerolite–smectite — smectite at seafloor hydrothermal vent fields: Evidence from mineralogical, geochemical and oxygen isotope studies. *Chemical Geology*, *247*(1-2), 171-194. doi:10.1016/j.chemgeo.2007.10.022

Edwards, K. J., Bach, W., and McCollom, T. M. (2005). Geomicrobiology in oceanography: microbe–mineral interactions at and below the seafloor. *Trends In Microbiology*, *13*(9), 449-456. doi:10.1016/j.tim.2005.07.005

Fein, J., Daughney, C., Yee, N., and Davis, T. (1997). A chemical equilibrium model for metal adsorption onto bacterial surfaces. *Geochimica Et Cosmochimica 61,* 3319-3328.

Feulner, G.(2012). The faint young Sun problem. *Reviews of Geophysics 50*(2), 1-29. doi:10.1029/2011RG000375

Harder, H. (1976). Nontronite synthesis at low temperature. *Chemical Geology 18,* 169-180.

Harder, H. (1978). Synthesis of iron layer silicate minerals under natural conditions. *Clay and Clay Minerals 26,* 65-72.

Holland, H. D. (2002). Volcanic gases, black smokers, and the Great Oxidation Event. Geochimica et Cosmochimica Acta, 66(21), 3811-3826.

Jannasch, H. W., & Wirsen, C. O. (1979). Chemosynthetic primary production at East Pacific sea floor spreading centers. Bioscience, 29(10), 592-598.

Karl, D. M., Wirsen, C. O., & Jannasch, H. W. (1980). Deep-sea primary production at the Galapagos hydrothermal vents. Science, 207, 1345-1347.

Konhauser, K., and Urrutia, M. (1999). Bacterial clay authigenesis: a common biogeochemical process. *Chemical Geology 161*, 399-413.

Konhauser, K., Jones, B., Phoenix, V., and Ferris, G. (2004). The microbial role in hot spring silicification. *AMBIO: A Journal of the Human Environment 33,* 552-558.

Landrum, J. T., Bennett, P. C., Engel, A. S., Alsina, M. A., Pastén, P. A., and Milliken, K. (2009). Partitioning geochemistry of arsenic and antimony, El Tatio Geyser Field, Chile. *Applied Geochemistry*, *24*(4), 664-676. doi:10.1016/j.apgeochem.2008.12.024

Lalonde, S., Konhauser, K., Reysenbach, A., and Ferris, F. G. (2005). The experimental silicification of Aquificales and their role in hot spring sinter formation. *Geobiology 3,* 41-52.

Marcucci, E., Hynek, B., Kierein-Young, K., and Rogers, K. L. (2013). Visible-near-infrared reflectance spectroscopy of volcanic acid-sulfate alteration in Nicaragua: Analogs for early Mars. *Journal of Geophysical Research: Planets 118,* 1-21. doi:10.1002/jgre.20159

McKenzie, E., Brown, K., Cady, S., and Campbell, K. (2001). Trace metal chemistry and silicification of microorganisms in geothermal sinter, Taupo Volcanic Zone, New Zealand. *Geothermics, 30,* 483-502.

Phoenix, V., and Konhauser, K. (2003). Experimental study of iron and silica immobilization by bacteria in mixed Fe-Si systems: implications for microbial silicification in hot springs. *Canadian Journal of Earth Sciences 40,* 1669-1678.

Phoenix, V. and Konhauser, K. (2008). Benefits of bacterial biomineralization. *Geobiology 6,* 303-308.

Phoenix, V., Konhauser, K., Adams, D., and Bottrell, S. (2001). Role of biomineralization as an ultraviolet shield: Implications for Archean life. *Geology 29,*823-826.

Rau, G. H., & Hedges, J. I. (1979). Carbon-13 depletion in a hydrothermal vent mussel: suggestion of a chemosynthetic food source. Science, 203(4381), 648-649.

Roberts, J. (2004). Inhibition and enhancement of microbial surface colonization: the role of silicate composition. *Chemical Geology 212,* 313-327.

Simmons, S., & Brown, K. (2007). The flux of gold and related metals through a volcanic arc, Taupo Volcanic Zone, New Zealand. *Geology 35,* 1099-1102.

Templeton, A., Knowles, E., Eldridge, D., and Arey, B. (2009). A seafloor microbial biome hosted within incipient ferromanganese crusts. *Nature Geoscience 2,* 872-876.

Tosca, N. J., Milliken, R. J. and Michael, F. M. (2008). Smectite formation on early Mars: Experimental constraints, *in Workshop on Martian Phyllosilicates: Recorders of Aqueous Processes?,* Abstract 7030.

Chapter 2. Quantifying the Impact of Microbial Weathering in Acid-sulfate Hydrothermal Systems

Published as a separate article:
Phillips-Lander, C M, Fowle, D A, Taunton, A, Hernandez, W, Mora, M, Moore, D, Shinogle, H and Roberts, J A. (2014) Silicate dissolution in Las Pailas Thermal Field: Implications for microbial weathering in acidic volcanic hydrothermal spring systems. *Geomicrobiology Journal* **31**, 37-41.

Abstract

A longitudinal field microcosm study was conducted in the Las Pailas hot spring system located on the SW flank of Rincon de la Vieja, Costa Rica, in order to investigate initial microbial attachment and colonization, as well as chemical (abiotic) and biological silicate weathering under hydrothermal conditions. Solution chemistry was pH=2.42-3.96, T=43-89.3^{o}C, Si=4.45-8.19 mmol L^{-1}, Fe=1.50-6.95 mmol L^{-1} and PO_4^{3-}=bdl-4.9 μmol L^{-1}. Microcosms consisted of washed, sonicated primary silicate mineral samples in polycarbonate vessels. The vessels were enclosed either by mesh to observe water/rock/microbial interactions or by 0.2-0.45 μm filters to observe water/rock interactions. Microcosms were incubated for periods of six hours, 24 hours, or two months, fixed in the field, then analyzed in the laboratory. Scanning electron microscopy (SEM) analysis revealed that microbial attachment to mineral samples occurred in as little as six hours. Microbial colonization and the development of minor etch pits associated with microorganisms occurred within 24 hours. The most significant differences in chemical vs. biological weathering were observed after two months. SEM analysis of these incubated surfaces showed that volumetric losses to mineral samples were more than one order of magnitude greater for samples that had been colonized by microorganisms and thus weathered biologically. With time, preferential colonization of anorthoclase mineral samples with Fe-oxides and apatite inclusions occurred. Subsequent weathering, therefore, may be a metabolic strategy by microorganisms to access mineral-bound PO_4^{3-}, which is otherwise scarce in solution. Results

from this study suggest that microorganisms may play a significant role in weathering in some hydrothermal systems.

Introduction

Metabolically diverse microbial communities live in hydrothermal systems around the world (Dick and Tebo 2010; Vick et al. 2010; Jørgensen and Boetius 2007) with average cell counts of 10^5-10^6 cells cm^{-3} (Santelli et al. 2008; Einen et al. 2008). Moreover, there is a consensus in the scientific community that microorganisms play a critical role in weathering in many near surface Earth environments (Banfield et al. 1999). However, quantifying the role of microorganisms in dissolution reactions in hydrothermal systems remains an open question.

The earliest studies of microbial weathering in seafloor hydrothermal systems focused primarily on textural alteration evidence in basaltic glasses in association with mid-ocean ridge fluids that were pH <7 with temperatures ranging from 2-100^{o}C (Furnes et al. 1999; Fisk et al. 1998; Torsvik et al. 1998; Thorseth.et al. 1995). These studies incorporated petrography, electron microscopy, and geochemical and microbiological techniques to examine field collected samples of oceanic crust. Using petrographic thin-sections, Fisk et al. (1998) established the ubiquity of micron-sized inclusions and filamentous channels in basaltic glasses from the Atlantic, Pacific and Indian Oceans. Samples retrieved from 237 m below the top of the volcanic crust in ODP Hole 896A along the Costa Rica Rift contained spherulitic bodies in altered fractures within basaltic glass that fluoresced when stained with 4, 5-diamidino-2-phenylindol (DAPI; Thorseth et al. 1995), indicating the presence of DNA. Subsequently, fluorescent *in situ* hybridization (FISH) was used on the same samples to show that both Archaea and Bacteria were present in altered basaltic glass (Torsvik et al. 1998). Furnes et al. (2001) inferred activity of methanogens and bacteria within fractures in altered basaltic glasses from the Costa Rica Rift based on carbon isotope fractionation signatures. Recently, McLoughlin et al. (2011) observed rounded and elongated pores approximately the size of microorganisms within palagonite crystals retrieved from weathered basaltic glasses at the Mohns Ridge. Energy dispersive X-ray spectroscopy showed that these pores were

associated with carbon and nitrogen enrichments (McLoughlin et al. 2011). Similar borings and filamentous structures with depleted carbon isotopic signatures and elevated carbon, nitrogen and phosphorous concentrations were similarly reported for the Ontong Java Plateau (Banerjee and Muhlenbachs 2003). Despite the near ubiquity of these features in ophiolites and oceanic crust, microorganisms have been isolated from altered basaltic glasses in only a few instances (Templeton et al. 2005) and there is little known about the initial colonization process from these investigations.

In hot springs environments the influence of microorganisms on the lithology and geomorphology has been more clearly elucidated. For example, varied geomorphic features associated with hot springs in Yellowstone National Park have been associated with different microbial community structures using quantitative polymerase chain reaction (PCR; Havig et al. 2011; Martin et al. 2010). Integration of the observed aqueous chemistry and the phylogenetic surveys of microorganisms have been used to model the bioenergetics of some hot spring systems (Takai and Nakamura 2010; Spear et al. 2004). These studies demonstrate that potential energy resources are available to organisms in hydrothermal systems. As we become increasingly able to rapidly survey geologic systems to identify microbiology and potential metabolic impacts, weathering studies remain an important means of contextualizing the relationship between microorganisms and mineral surfaces.

Studies of microorganisms in hydrothermal systems have employed a diverse array of microbiological and geochemical techniques, including field and laboratory incubation studies and stable isotopes analyses (Glynn et al. 2006; Severmann et al. 2006) to determine the nature of microbial colonization and microbial influence on mineral equilibria, including field and laboratory incubation experiments (Toner et al. 2009; Templeton et al. 2009; Daughney et al. 2004; Edwards et al. 2003; Phoenix et al. 2001). Microcosm incubations of sulfide minerals in hydrothermal vents at the Juan de Fuca ridge showed that microorganisms rapidly (2 months) dissolve sulfide minerals and form iron-oxide coatings on biofilms (Toner et al. 2009; Edwards et al. 2003). This has been shown similarly through coupled geochemical and microbiological investigations of changes in sediment cores retrieved from the TAG (Trans-Atlantic

Geotraverse) hydrothermal vent field (Glynn et al. 2006; Severmann et al. 2006). Four month long laboratory experiments with Fe-oxidizing bacteria showed that microorganisms were involved in the off-axis dissolution of basalt and the precipitation of Fe-oxides associated with microbial surfaces (Daughney et al. 2004). In contrast, Templeton et al. (2009) showed that microorganisms rapidly (1 year) colonized a basalt slab incubated in the hydrothermal fluids at the Loihi seamount and microbial surfaces were covered in Fe-oxides, however it is unknown whether the presence of microbial biofilms enhanced dissolution of the basalt as controls were not available. Phoenix et al. (2001) used laboratory experiments to show that cyanobacteria facilitate the growth of siliceous sinters for UV protection. Microorganisms have also been shown to influence the precipitation of secondary mineral phases, including calcite at Angel Terrace, Yellowstone National Park (Kandianis et al. 2008; Fouke et al. 2000), siliceous sinters at El Tatio geothermal field (Phoenix et al, 2006) and Fe-oxides and jarosite from acid-sulfate Orange springs in Waiotaupo geothermal area, New Zealand and an acid-sulfate spring in Kyushu, Japan (Jones and Renaut 2007; Kawano and Tomita 2001). The formation of clays, particularly nontronite, has been observed in off-axis deep sea hydrothermal systems. Usually, its formation is attributed to alteration of sulfides (Dekov et al. 2008), although Masuda (1995) and Alt (1988) observed nontronite coating filamentous organisms in low-T alteration zones.

Chemical weathering processes are comprised of two components: dissolution of primary mineral phases and precipitation of mineral secondary phases. These processes have traditionally been treated separately in hydrothermal systems with most models presuming congruent dissolution of primary phases (Konhauser et al. 2002; Resing and Santone 2002). Using timed, *in situ* experiments in the Las Pailas hydrothermal system, this study seeks to characterize the initial attachment and colonization of microorganisms in an acidic volcanic hydrothermal system and determine the biological weathering effects on primary silicates from shorter (6 hours) to longer (2 month) time scales. This includes characterizing the nature of microbe-mineral interactions, the effect of extracellular polymers (EPS) on mineral surfaces, and factors that affect the formation of secondary mineral phases.

Geologic Setting

Rincón de la Vieja is an andesitic composite stratovolcano in northwestern Costa Rica formed by the subduction of the Cocos Plate beneath the Caribbean plate (Figure 1). The volcano last erupted in February 1998 (Kempter et al. 1995). Tephra deposits, ignimbrites, welded tuffs, and hornblende biotite lavas comprise this andesitic volcanic complex (Kempter et al. 1995). Current geologic processes at the Las Pailas hydrothermal field of Rincón de la Vieja National Park include fumaroles and hot spring activity along the volcano's southwestern flank. Geochemistry was evaluated as part of this study and compared with previous work completed by Tassi et al. (2005) who focused on the water chemistry of the system and Gehring et al. (1999) who described the mineralogy of the alteration products.

Las Pailas was chosen for the microbial metabolic guilds present at the site, including *Euglena pailasensis* (Sittenfeld et al. 2002), Cyanidium and Galderia-like algae, 15 different phylotypes of methanogenic Archaea, several strains of cyanobacteria (Finsinger et al. 2008) and the presence of *Acidothiobacillus caldus*, a moderately thermotolerant sulfur oxidizing bacterium (Semenez et al. 2002).

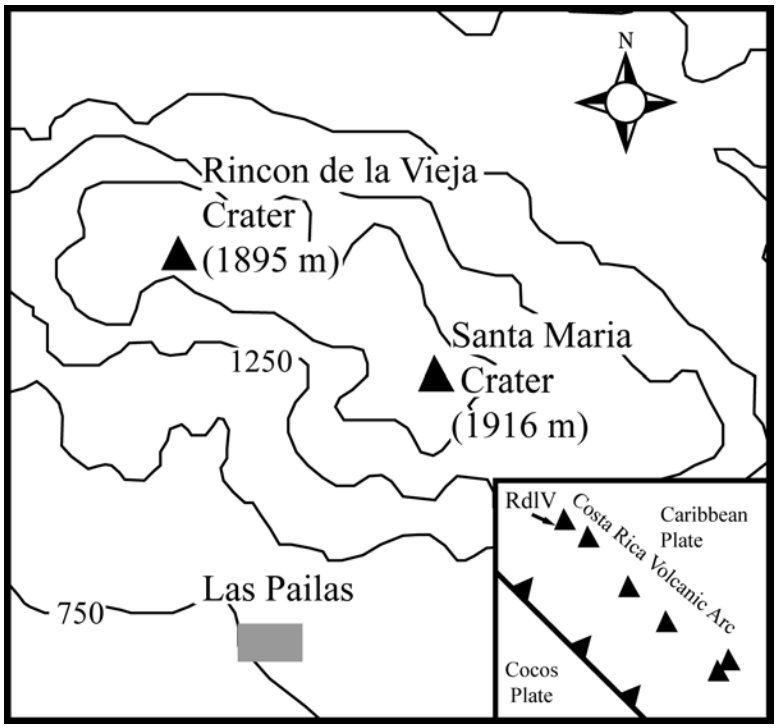

Figure 1: The Las Palias hydrothermal vent field (grey area) is located on the southwest flank of Rincón de la Vieja. Image is after the Costa Rica Travel and Tourism Bureau's Rincón de la Vieja National Park Map. Contour Interval ~250 m.

Methodology

Field and Laboratory Methods

Coupled field and laboratory methods were used to determine the degree of chemically and biologically induced weathering in the Las Pailas springs. Geochemical sampling of the Las Pailas area, along the southwest flank of the volcano was conducted in March 2009. In order to characterize the geochemical conditions of the sites, sediment and fluid samples were collected from four hot spring sites: Pailas de Agua I, Pailas de Agua II, Laguna Fumarólica, Poza del Hongo.

Spring pH and temperature were measured in the field. Because of the rapid cooling of water samples upon retrieval from the spring, temperatures were acquired using a Fisher Scientific Traceable Infrared thermometer. Water samples were filtered in the field using 0.45 μm polycarbonate filters, and samples for cation analysis were acidified with up to 2% high purity nitric acid. Major and trace cations were analyzed using inductively coupled plasma optical emission spectroscopy on a Perkin Elmer ICP-OES Optima 5300 DV at the University of Kansas. Anions were analyzed using a Microdrill ion chromatograph at the University of Kansas. Alkalinity was determined in the lab for Poza de Hongo, the only spring with a pH above 3. All samples were kept at kept at 4°C after collection and during transport to the laboratory. Sediment samples were collected, kept at 4°C during transport, freeze-dried in the laboratory to prevent significant alteration of the mineralogy, and then powdered and analyzed using a Bruker SMART APEX II X-ray Diffractometer with a copper charge coupled detector (CCD) at the University of Kansas X-ray Diffraction Laboratory.

Field Incubation Experiments

Chemical weathering as well as microbial colonization patterns and associated biological weathering were examined using field microcosm experiments. *In situ* field microcosms, a modification of the buried slide technique (Engel et al. 2004; Rogers and Bennett 2004; Rogers et al. 1998; Heibert and Bennett 1992), were composed of clear polycarbonate tubes with mesh-covered ends into which fresh mineral samples were placed. Each microcosm was filled with 12 g of crushed, sieved (2 mm size fraction), washed, and sonicated minerals designed to represent the general mineralogy of andesitic volcanic rocks. This

included 4 g each of amphibole (hornblende, $(Ca,Na)_{2-3}(Mg,Fe,Al)_5(Al,Si)_8O_{22}(OH,F)_2$; Wards Scientific #46V0392), pyroxene (augite, $(Ca,Na)(Mg,Fe,Al)(Si,Al)_2O_6$; Wards Scientific #46V6472), and anorthoclase feldspar ($(Na,K)AlSi_3O_8$; Wards Scientific #46V0578) with Fe-oxide and apatite inclusions obtained from Ward's Scientific. One aliquot of minerals was set aside as an unweathered control for comparison in order to address any effect on weathering rates caused by the dissolution of fines (e.g. Brantley et al. 2001). One control microcosm and one experimental microcosm were deployed in each spring. In addition to mesh on both ends, control microcosms had additional 0.2 μm polycarbonate filters for short-term experiments and 0.45 μm polycarbonate filters for long-term experiments. These additional filters served to prevent microbial contamination and therefore recorded strictly water/rock interactions (i.e. chemical weathering).

Microcosms were incubated in the hot springs for periods of six hours (6 h), 24 hours (24 h), and two months (2 mo). After each of these time frames, the microcosms were retrieved from the site and the contents were immediately placed into 15 mL falcon tubes with 2% glutaraldehyde solution to fix the samples while in the field to preserve fine-scale microbe-mineral surface interactions including pili and exopolymeric substances (EPS; Gorby et al. 2006). Details of experimental duration and retrieval for each hot spring are included in Table 1. Retrieved mineral samples were analyzed using scanning electron microscopy (SEM) to discern differences in colonization patterns and extracellular polymer development between minerals as well as differences in weathering textures observed for biological versus chemical incubations (Bennett et al. 2006). Thin sections and SEM images of the unreacted starting material were compared to weathered samples.

Microscopy

Microcosm samples were prepared for scanning electron microscope analysis using chemical fixation using glutaraldehyde and ethanol dehydration followed by critical point drying (e.g. Gorby et al. 2006). Mineral samples were then stub-mounted, gold-coated and analyzed on LEO 1550 field emission scanning electron microscope. Minerals from each time step were imaged to determine the differences in colonization by microorganisms, their association with primary and secondary mineral phases, and the

degree of weathering. Cell densities were determined by counting the number of microbial cells present using 5-10 fields of view with an area of 1000 μm^2 on average for each mineral type in each spring. A total cell count was calculated and divided by the total area of all fields of view counted.

Table 1: Field Experiment Parameters

Site	Incubation Time	Control Sample Filter Size (μm)	Notes
Poza del Hongo	6 h	0.2	Filters designed for pH< 4. Filters ruptured upon exposure to the spring. All samples colonized.*
Pailas de Agua II	6 h	0.2	
Pailas de Agua I	24 h	0.2	Long-term experiments lost. High T melted the anchor line.
Laguna Fumarólica	24 h	0.2	
	2 mo	0.45	

*Polycarbonate degrades above pH 4 at T>50^oC.

Because of the extensive clay formation associated with the microcosm samples, simply measuring the change in weight of the samples pre- and post-incubation was insufficient to determine the degree of dissolution. Similarly, atomic force microscopy (AFM) was attempted but abandoned as a reasonable method for determining weathering induced changes to the mineral surfaces because the surface roughness of the samples damaged the AFM tips.

In order to determine the volumetric losses caused by weathering, stereo images were captured, integrated, and analyzed to create digital elevation models (DEM) of mineral surfaces using MeX® 3-D image analysis software. These DEMs were used to determine the volume of etch pits resulting from weathering. An aliquot of samples were prepared for imaging using 10 minutes immersion in 5% Tween 20 to remove any attached biota and low-power sonication to remove fine material attached to the surface. These cleaned samples were then ultra-fine coated with gold-palladium before imaging. Pit volumes were

statistically analyzed to determine the quantitative difference in weathering between chemical and biological weathering reactions.

Results

Site Geochemistry

Field measurements revealed spring temperatures ranging from 43-90^{o}C and pH ranging from 2.4-5.7 (Table 2). With the exception of Poza del Hongo, the springs have high total iron and silica concentrations with a range of 1.50-6.95 mmol L^{-1} and 3.52-8.19 mmol L^{-1} respectively. Aluminum concentrations ranged from below detection limits in Poza del Hongo to 15.4 mmol L^{-1} in Pailas de Agua I. Sodium, calcium and magnesium concentrations were all lower than 1 mmol L^{-1} and potassium concentrations were below detection limits for all samples. Phosphate levels in the springs are low (below micromolar) with many springs containing no detectable phosphate and the highest value being 4.93 μmol L^{-1}. The aqueous geochemistry of the hydrothermal pools broadly correlates with the data collected previously; however chlorine and potassium concentrations were 1-2 orders of magnitude lower between the two studies and aluminum concentrations were 1-2 orders of magnitude greater between the two studies (Tassi et al. 2005; Table 3).

Previous studies of the Las Pailas vent field have shown that weathering products within the hydrothermal vents include kaolinite, quartz, α-cristobalite, anatase, rutile, hematite, and α-tridymite (Gehring et al. 1999). XRD analysis of collected sediment samples from this study contained secondary phases such as smectite, kaolinite, α-cristobalite quartz, alunite, 2-line ferrihydrite, 6-line ferrihydrite and hematite (Figure 2). No primary mineral phases were detected.

Previous studies of the Las Pailas vent field have shown that weathering products within the hydrothermal vents include kaolinite, quartz, α-cristobalite, anatase, rutile, hematite, and α-tridymite (Gehring et al. 1999). XRD analysis of collected sediment samples from this study contained secondary phases such as smectite, kaolinite, α-cristobalite quartz, alunite, 2-line ferrihydrite, 6-line ferrihydrite and hematite (Figure 2). No primary mineral phases were detected.

Table 2: Rincon de la Vieja Water Analyses Spring 2009					
	Site	**Laguna Fumarolica**	**Poza del Hongo**	**Pailas de Aguas II**	**Pailas de Aguas I**
Field data	**Elevation (m)**	759	756	727	749
	Sample Date	March 17	March 17	March 18	March 17
	T (° C)	43	90	83	80-89
	pH	2.42	5.75	2.77	2.60-3.96
	Ionic Strength	1.72E-01	2.10E-03	2.87E-01	4.69E-01
	Charge Balance	1.64E-01	-1.87E-03	2.70E-01	4.30E-01
Alkalinity	**meq/L HCO_3**	bdl	2.19E+00	bdl	bdl
Anions	**SO_4**	7.39E+00	1.72E-01	1.46E+01	3.84E+01
	F	1.76E-02	1.24E-02	2.00E-02	1.06E-01
	Cl	1.67E-01	8.70E-02	2.68E-02	5.35E-02
	Br	bdl	bdl	bdl	bdl
	NO_2	bdl	bdl	bdl	bdl
	NO_3	1.67E-02	3.87E-03	4.03E-03	7.10E-03
	PO_4 (µmol/l)	4.24E+00	4.93E+00	2.70E+00	bdl
Cations	**Na**	7.48E-01	1.32E-01	1.31E-01	3.91E-01
	K	bdl	bdl	bdl	bdl
	Ca	8.04E-01	1.69E-01	2.09E-01	6.88E-01
	Mg	5.60E-01	1.31E-01	1.85E-01	6.90E-01
	Sr	5.04E-04	1.50E-04	bdl	6.98E-04
	Ba	1.08E-04	1.49E-04	2.19E-04	2.87E-04
	FeT	1.50E+00	4.12E-04	2.48E+00	3.98E+00–6.95E+00
	Mn	1.29E-02	0.00E+00	4.34E-03	1.58E-02
	Ti	bdl	bdl	bdl	bdl
	Al	8.37E-01	bdl	2.58E+00	1.54E+01
	Si	4.45E+00	6.34E-01	4.29E+00	8.19E+00
	Zn	3.80E-04	bdl	5.72E-04	2.40E-03
	Pb	bdl	bdl	bdl	bdl
	Cd	bdl	bdl	bdl	1.44E-04
	Co	bdl	bdl	bdl	1.61E-04
	Cr	1.63E-03	bdl	3.40E-03	7.17E-03
	Cu	1.66E-03	2.58E-05	bdl	2.86E-03
	Ni	bdl	bdl	bdl	bdl
	V	2.43E-03	2.06E-05	1.20E-02	2.79E-02
	S	7.45E+00	2.12E-01	1.48E+01	3.94E+01

* All values in mM unless otherwise noted.

Table 3: Spring Field Analyses compared to Tassi et. al. (2005)					
		This Study		Tassi et. al.	
Field data	Site	Palias de Agua II	Palais de Agua I	Palais de Agua	Palais de Agua
	Elevation (m)	727	749	800	800
	Sample Date	Mar-09	Mar-09	Feb-98	Mar-99
	T (° C)	82.9	79.6	92.6	96
	pH	2.77	2.60	2.3	2.21
Anions	SO_4	1.46E+01	3.84E+01	1.11E+01	1.99E+01
	F	2.00E-02	1.06E-01	2.60E-01	2.50E-01
	Cl	2.68E-02	5.35E-02	6.00E+00	1.18E+02
	Br	bdl	bdl	bdl	1.50E-01
	NO_2	bdl	bdl	Not reported	Not reported
	NO_3	4.03E-03	7.10E-03	2.00E-02	bdl
Cations	Na	1.31E-01	3.91E-01	7.90E-02	1.22E-01
	K	bdl	bdl	4.00E-02	1.20E-01
	Ca	2.09E-01	6.88E-01	1.30E+00	2.74E-01
	Mg	1.85E-01	6.90E-01	2.00E-01	2.00E-01
	Mn	4.34E-03	1.58E-02	1.46E-03	bdl
	Al	2.58E+00	1.54E+01	bdl	bdl

*values in mmol/l unless otherwise noted

** bdl= below detection limits. Detection limits: Br=2.53×10^{-1} μmo/l, NO2 = 4.34×10^{-1} μmo/l; K= 2.56×10^{-2}-2.56×10^{-3} μmo/l

Field Incubation Experiments

Before use in the microcosm experiments, unreacted, starting mineral samples were characterized in petrographic thin-section and imaged using scanning electron microscopy. Pyroxene samples contained Fe-Ti oxide inclusions overgrown by biotite and quartz (Figure 3A). Amphibole samples contained large quartz inclusions as well as fractures filled with biotite that crosscut the sample surface (Figure 3B). These fractures were also observed under SEM in some samples. Anorthoclase mineral samples were previously described by Rogers et al. (1998). Thin sections of anorthoclase revealed prevalent apatite

inclusions that were frequently associated with large Fe-Ti oxides and biotite (Figure 3C). Trace element analysis of anorthoclase yielded a concentration of 1050 μg g^{-1} phosphate (Rogers et al. 1998).

Field incubations were conducted in four hydrothermal pools. Details regarding sample retrieval and timing are included in Table 1. Samples were imaged using scanning electron microscopy and analyzed to determine the nature and extent of chemical vs. biological weathering and microbial colonization. Polycarbonate filters manufactured by GE on microcosms incubated in Poza del Hongo ruptured due to pH conditions higher than 4 at temperatures greater than 50^{o}C, resulting in the colonization of all samples. Because weathering encompasses both dissolution of primary minerals and precipitation of secondary minerals, reacted mineral suites were examined for examples of both weathering factors. Etch pits and selective leaching along cleavage planes and mineral defects were used as indicators of primary mineral dissolution. The presence of minerals not originally found in the starting material (e.g. clays and silica spherules) was used as evidence of secondary mineral precipitation. As stated earlier, microorganisms can participate in both dissolution and precipitation weathering reactions. Therefore microbial colonization, defined by the number and type of individual cells attached to mineral surfaces, and the extent of EPS coverage associated with dissolution features and secondary mineralization were documented as indicators of biological weathering.

Starting Material

In order to most accurately represent the starting material for the present study, one set of mineral samples was carried to and from the field without reaction. The starting material was then examined using SEM upon return to the laboratory. Pyroxene mineral surfaces displayed well-defined cleavage at 90^{o}. Rarely, pyroxene mineral samples were cut by 1-2 μm wide fractures that were subparallel to cleavage planes (Figure 3D). Amphibole surfaces appeared fresh and unweathered and displayed characteristic pencil cleavage (Figure 3E). Anorthoclase samples appeared pristine with well-defined cleavage planes (Figure 3F). Some apatite crystals were exposed on the anorthoclase surfaces due to crushing of the mineral during sample preparation (Figure 3D). These apatite crystals were hexagonal and euhedral making them

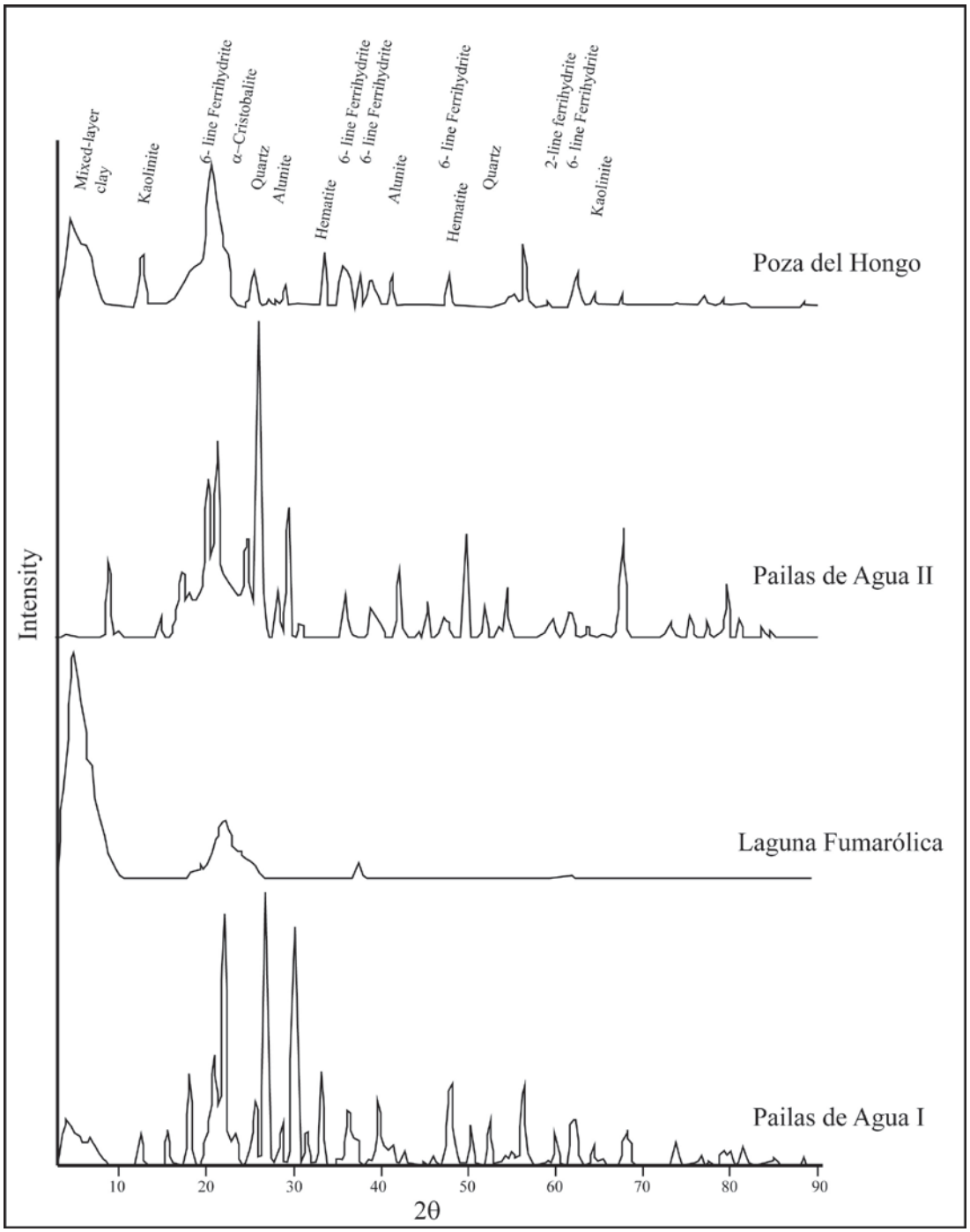

Figure 2: Mineralogy of the sediments collected from each hydrothermal pool were evaluated using XRD and show the presence of smectite, kaolinite, α-cristobalite quartz, alunite, 2-line ferrihydrite, 6-line ferrihydrite and hematite. The sample collected from Laguna Fumarólica displays only smectite and ferrihydrite.

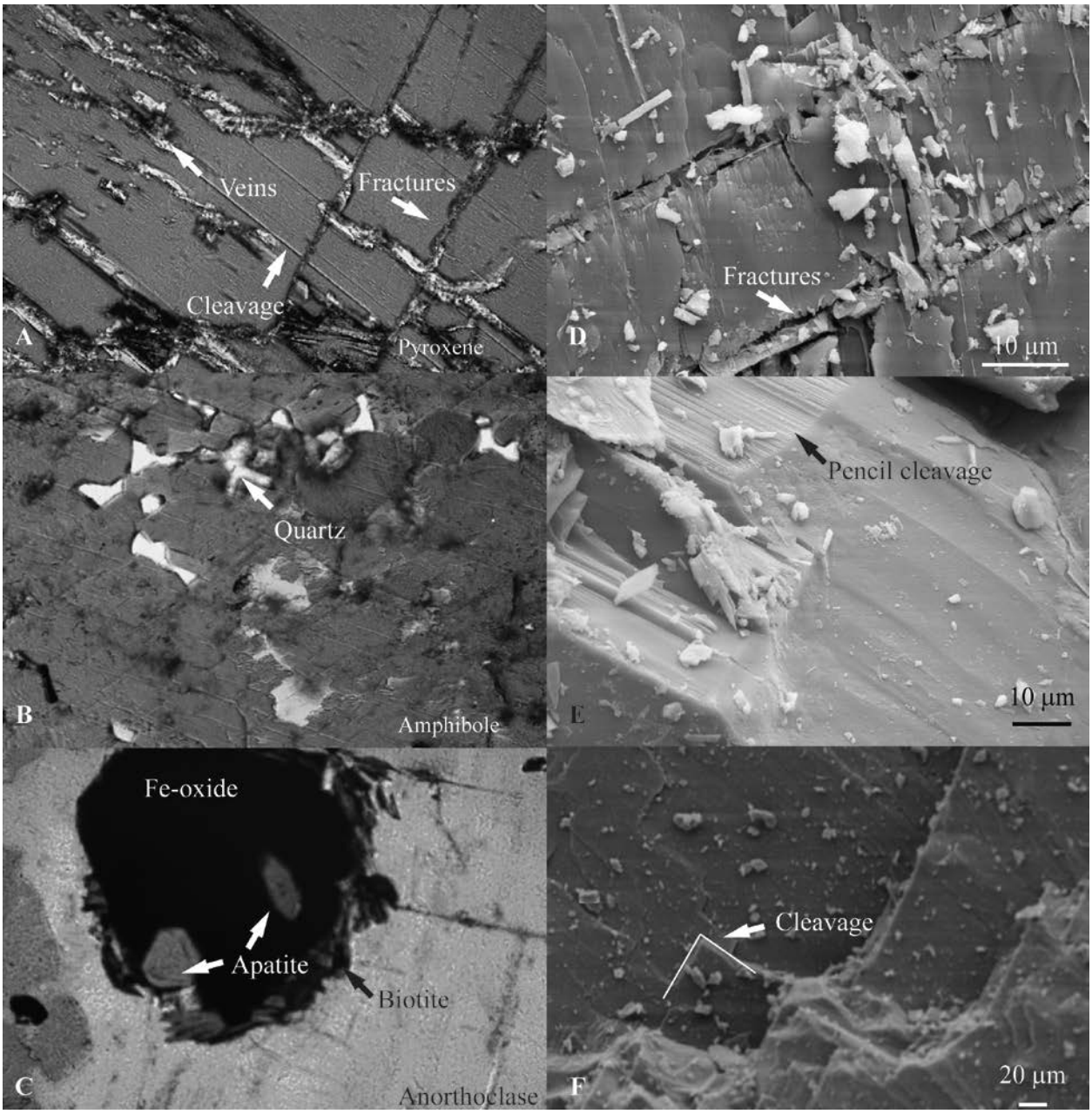

Figure 3: All samples were crushed, sieved, sonicated and washed prior to experimentation. The unweathered control samples have some attached fines to them because of breakage during transportation to and from the field. Petrographic Images: (A) Pyroxene surfaces are largely are heavily fractured. (B) Amphiboles are fresh and unweathered with quartz inclusions. (C) Anorthoclase samples contain large Fe-oxide and biotite inclusions which are commonly co-located with hexagonal apatite crystals. Some apatite crystals are distributed as inclusions throughout the mineral. SEM Analysis: (D) Pyroxenes are partially covered in fines and have 1-2 µm fractures that crisscross the surface in some locations. (E) Amphibole surfaces are euhedral and have characteristic pencil cleavage. (F) Anorthoclase samples are pristine with no obvious evidence of exsolution features.

easily definable features. Biotite/Fe-Ti oxide inclusions in anorthoclase were observed because they cross-cut the well-defined cleavage surfaces and had a blocky appearance. Some fines remained attached to mineral surfaces and were likely the result of mineral breakage while in transit to and from the field.

Pyroxene

Poza del Hongo (6h)

Due to filter rupturing in the control samples, all microcosms from Poza del Hongo were colonized and thus a comparison of chemical to biological weathering could not be performed on this suite of experiments. After six hours of exposure, all pyroxene samples from Poza del Hongo displayed minimally etched cleavage planes (Figure 4A & B). Small etch pits, averaging 27.7 μm^2, were observed (Table 4). Minor clay mineral attachment was observed (Figure 4B). Microbial attachment followed cleavage planes and surfaces (Figure 4A). The microorganisms within Poza del Hongo (6 h) had primarily a rod-shaped morphology ($4.02x10^{-4}$ cells μm^{-2}) though a few filamentous-shaped ($7.54x10^{-5}$ cells μm^{-2}) microorganisms were also observed. The average cell density after 6h was $4.78x10^{-4}$ cells μm^{-2} (Table 4).

Control microcosms retrieved from Pailas de Agua II (6 h) displayed etching along cleavage planes, however, substantial sorbed clay minerals and (Fe, Al) oxides were observed (Figure 4C and D). Some silica spherules were also present on mineral surfaces (4C). Small (1-10 μm^2) etch pits were observed (Table 4).

In biologically weathered pyroxene samples from this spring, small 1-10 μm long etch pits were documented (Table 4; Figure 4D). Microbial cell density in biological samples was $1.55x10^{-4}$ cells μm^{-2} (Table 4). Interestingly, the dominant feature observed in Pailas de Agua II (6 h) pyroxene samples, regardless of treatment, was the presence of substantial sorbed clays that almost completely coated the mineral surfaces (Figure 4D).

Pailas de Agua I (24 h)

Deeply etched cleavage planes were observed in all samples from Pailas de Agua I regardless of treatment (Figure 4E). Rod-shaped microorganisms were attached to pyroxene surfaces along cleavage planes and

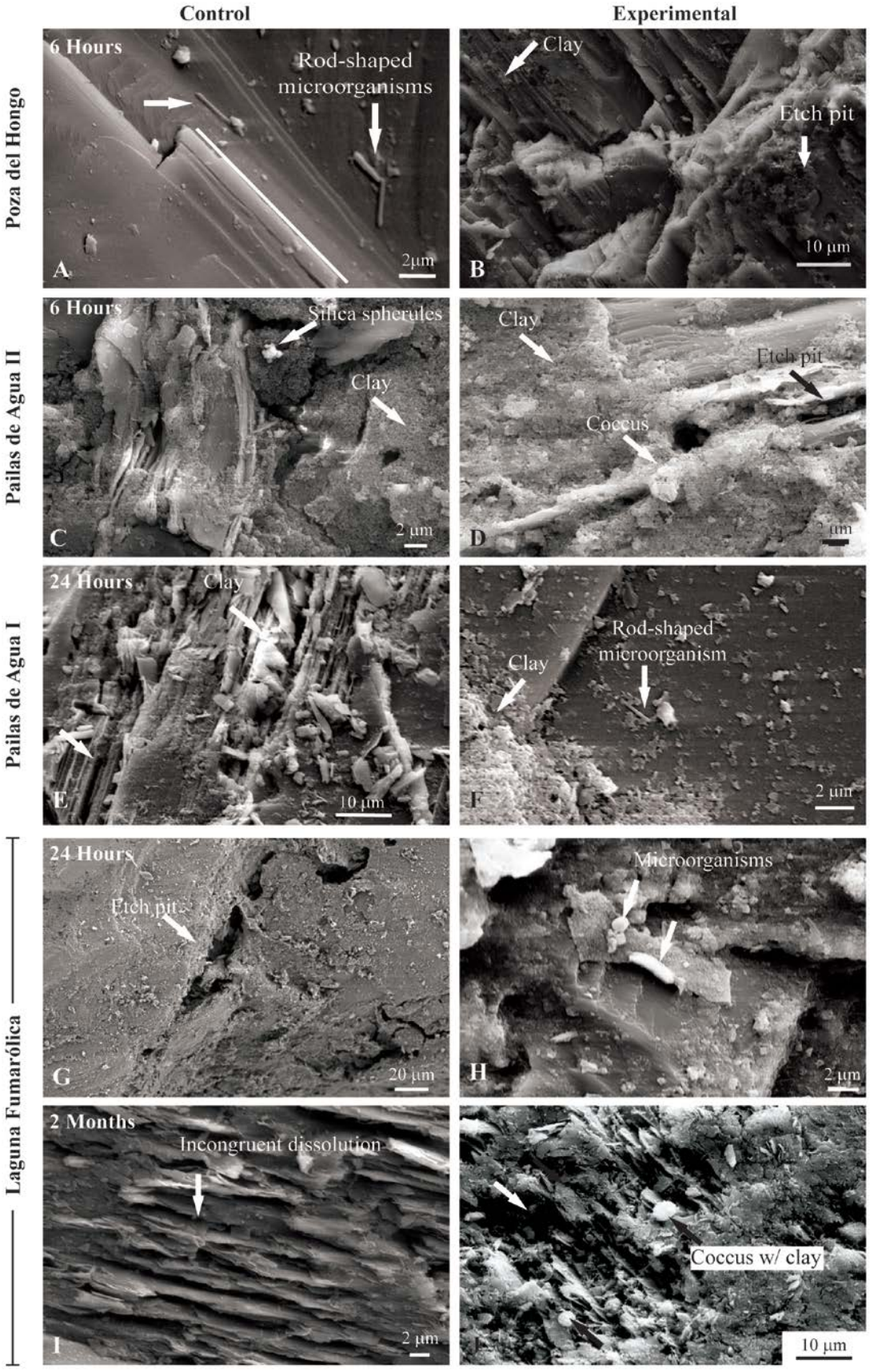
Control
Experimental
Poza del Hongo
Pailas de Agua II
Pailas de Agua I
Laguna Fumarólica
6 Hours
Rod-shaped microorganisms
2µm
A
Clay
Etch pit
10 µm
B
6 Hours
Silica spherules
Clay
2 µm
C
Clay
Etch pit
Coccus
D
24 Hours
Clay
10 µm
E
Clay
Rod-shaped microorganism
2 µm
F
24 Hours
Etch pit
20 µm
G
Microorganisms
2 µm
H
2 Months
Incongruent dissolution
2 µm
I
Coccus w/ clay
10 µm
J

Figure 4: Pyroxene weathering among treatments Poza del Hongo (6h) (A) Rod-shaped microorganisms attached parallel to cleavage planes; (B) Dissolution along cleavage planes, formation of nascent etch pits and clay formation; Pailas de Agua II (6 h) (C) Dissolution along cleavage planes, secondary silica spherules and clay minerals; (D) Dissolution along cleavage resulting in the formation of etch pits. Secondary clays and what appears to be ruptured Coccus; Pailas de Agua I (24 h) (E) Dissolution along cleavage planes, secondary clay minerals, (F) Attached secondary clay minerals, rod-shaped bacteria; Laguna Fumarólica (24h) (G) Etch pit developed along cleavage planes; (H) Rod-shaped microorganism near nascent etch pit; Laguna Fumarólica (2 mo) (I) Dissolution along cleavage planes; (J) Dissolution along cleavage planes leading to the development of etch pits, secondary clay minerals, cocci attached to nascent etch pits.

Table 4: Weathering and Colonization

Reaction Time	Poza del Hongo* 6h				
Mineral	**Colonized**	**Cell Density cells/μm²**	**Biofilm Coverage**	**Weathered**	**Pit Area μm²**
Control Pyroxene					
Control Amphibole					
Control Anorthoclase					
Pyroxene	+	4.78E-04	-	+	2.77E+01
Amphibole	++	7.20E-04	-	+	1.98E+01
Anorthoclase	++	2.76E-04	25%	+	5.80E+02
	Pailas de Aguas I 24 h				
Control Pyroxene	-			++	9.33E+02
Control Amphibole	-			++	2.08E+03
Control Anorthoclase	-			++	3.37E+03
Pyroxene	+	2.11E-04	-	++	1.79E+03
Amphibole	++	4.13E-04	-	+	2.13E+01
Anorthoclase	++	4.08E-04	-	++	3.99E+03
	Palais de Aquas II 6h				
Control Pyroxene	-			++	1.03E+01
Control Amphibole	-			++	6.63E+01
Control Anorthoclase	-			++	1.35E+02
Pyroxene	+	1.55E-04	-	++	2.50E+01
Amphibole	+	1.88E-04	-	++	1.10E+02
Anorthoclase	++	4.83E-04	20%	++	2.00E+02

Reaction Time	Palais de Aquas II 6h				
Mineral	**Colonized**	**Cell Density cells/μm²**	**Biofilm Coverage**	**Weathered**	**Pit Area μm²**
	Laguna Fumarolica 24 h				
Control Pyroxene	-			++	4.44E+03
Control Amphibole	-			++	6.56E+02
Control Anorthoclase	-			+	3.27E+02
Pyroxene	++	2.15E-04	40%	++	2.82E+02
Amphibole	+	2.66E-04	-	-	4.22E+00
Anorthoclase	++	2.87E-05	40%	+	2.87E+02
	Laguna Fumarolica 2 mo				
Control Pyroxene	-			++	1.07E+03
Control Amphibole	-			++	6.56E+02
Control Anorthoclase	-			++	9.42E+02
Pyroxene	+++	2.69E-03	40%	+++	3.82E+02
Amphibole	++	7.56E-04	40%	++	8.23E+02
Anorthoclase	+++	2.26E-03	40%	+++	9.98E+03

* + indicate relative intensity of weathering and colonization. – indicate no weathering or colonization was observed.

were associated with secondary clays in experimental samples (Figure 4F). The average biomass density was 2.11×10^{-4} cells μm^{-2} (Table 4). Clay minerals and Fe-oxides appeared to be nucleating proximal to zones of intense dissolution on the mineral surface (Figure 4E and F). This is indicative of rapid authigenic clay mineral formation (Michalopoulos and Aller, 1995).

Laguna Fumarólica (24 h)

Laguna Fumarólica (24 h) control samples were characterized by largely unweathered surfaces with few <10-100 μm long etch pits (Figure 4G). Minimal secondary clays were observed sorbed to the surface. In

biologically weathered samples, nascent etch pits (1-2 μm^2) were observed consistently associated with rod-shaped bacteria (Figure 4H; Table 4). Experimental sample surfaces were heavily coated in secondary clays minerals (Figure 4H). This may be partially due to sorption of secondary minerals onto EPS that covered approximately 40% of the surfaces. Cocci- and rod-shaped microorganisms were observed with an average cell density is $2.15x10^{-4}$ cells μm^{-2}.

Laguna Fumarólica (2 mo)

After two months, large etch pits (Table 4) were observed in all Laguna Fumarólica (2 mo) pyroxene samples. Etch pit areas were larger in experimental (LFB) samples than controls (LFC) (Figure 4 I & J; Table 4). Cocci and clay minerals were associated with etch pits in LFB samples. The average cell density for rod- and cocci-shaped microorganisms was $2.69x10^{-3}$ cells μm^{-2}. As with Pailas de Agua II site, clay minerals may prevent additional dissolution of the pyroxene surface.

Amphibole

Poza del Hongo (6 h)

Minimal clay minerals were observed associated with the surface (Figure 5A). Most amphibole surfaces displayed minimal dissolution features at this site including some small (19.98 μm^2) etch pits (Table 4) and dissolution along cleavage planes (Figure 5A). Filamentous ($3.37x10^{-4}$ cells μm^{-2}) and rod-shaped ($3.68x10^{-4}$ cells μm^{-2}) microorganisms were observed. Rod-shaped microorganisms were attached parallel to the amphibole cleavage planes (Figure 5B). Few cocci ($1.53x10^{-5}$ cells μm^{-2}) were also observed. The average cell density was $7.20x10^{-4}$ cells μm^{-2} (Table 4).

Pailas de Agua II (6 h)

Dissolution along amphibole cleavage planes was common, and minor 1-10 μm^2 etch pits were observed in control samples from Pailas de Agua II (Table 4; Figure 5C). In experimental samples, amphibole mineral grains were extensively weathered with preferential dissolution along cleavage planes in all treatments (similar to Figure 5C), and several surfaces were completely altered to thick clay layers in experimental samples (Figure 5D). Although uncommon, small (82.3 μm^2) etch pits were also observed in

experimental samples. Additionally, rod-shaped microorganisms ($1.88x10^{-4}$ cells μm^{-2}) were observed. Secondary clays, oxides and silica spherules were present on mineral surfaces regardless of treatment.

Pailas de Agua I (24 h)

In control samples, some amphibole surfaces were completely altered to thick clay layers (Figure 5E). Other amphibole control surfaces had a few etch pits that measured 10 μm by 5-10 μm (Table 4). Control and experimental samples retrieved from Pailas de Agua I (24 h) were dominated by etching along amphibole cleavage planes with minor sorption of clay minerals to the surface (Figure 5F). Etch pits in experimental amphibole surfaces were smaller than controls ($2.13x10^{1}$ μm^2 on average; Table 4). Microbial cell densities of $4.13x10^{-4}$ cells μm^{-2} were observed in the experimental samples.

Laguna Fumarólica (24 h)

In Laguna Fumarólica (24 h) control samples, minimal amphibole dissolution in the form of small etch pits (1-10 μm long by a few microns wide) was observed. Most surfaces remained unweathered with minor sorption of clays, silica spherules and oxides (Figure 5G). Experimental samples from this spring displayed small etch pits approximately 2 μm in diameter and minor sorbed clays and oxides (Figure 5H; Table 4). Microbial cell density of experimental samples averaged $2.66x10^{-4}$ cells μm^{-2}.

Laguna Fumarólica (2 mo)

After two months, experimental and control samples from Laguna Fumarólica displayed similar amphibole dissolution features to the 24 h control samples. Similar sized etch pits were observed in both control ($6.56x10^{2}$ μm^2) and biological samples ($8.23 x10^{2}$ μm^2) (Table 4). Minimally etched cleavage planes also were observed in both LFB (biological) and LFC (control) samples (Figure 5I). Secondary oxides and clays were observed in both LFB and LFC samples (Figure 5I). Discontinuous EPS covered approximately 40% of the LFB sample surfaces (Figure 5J). Rod-shaped and cocci microorganisms with an average cell density of $7.56x10^{-4}$ cells μm^{-2} were observed. To determine whether EPS formation may have enhanced or retarded weathering, LFB (2 mo) amphibole samples were washed to remove EPS.

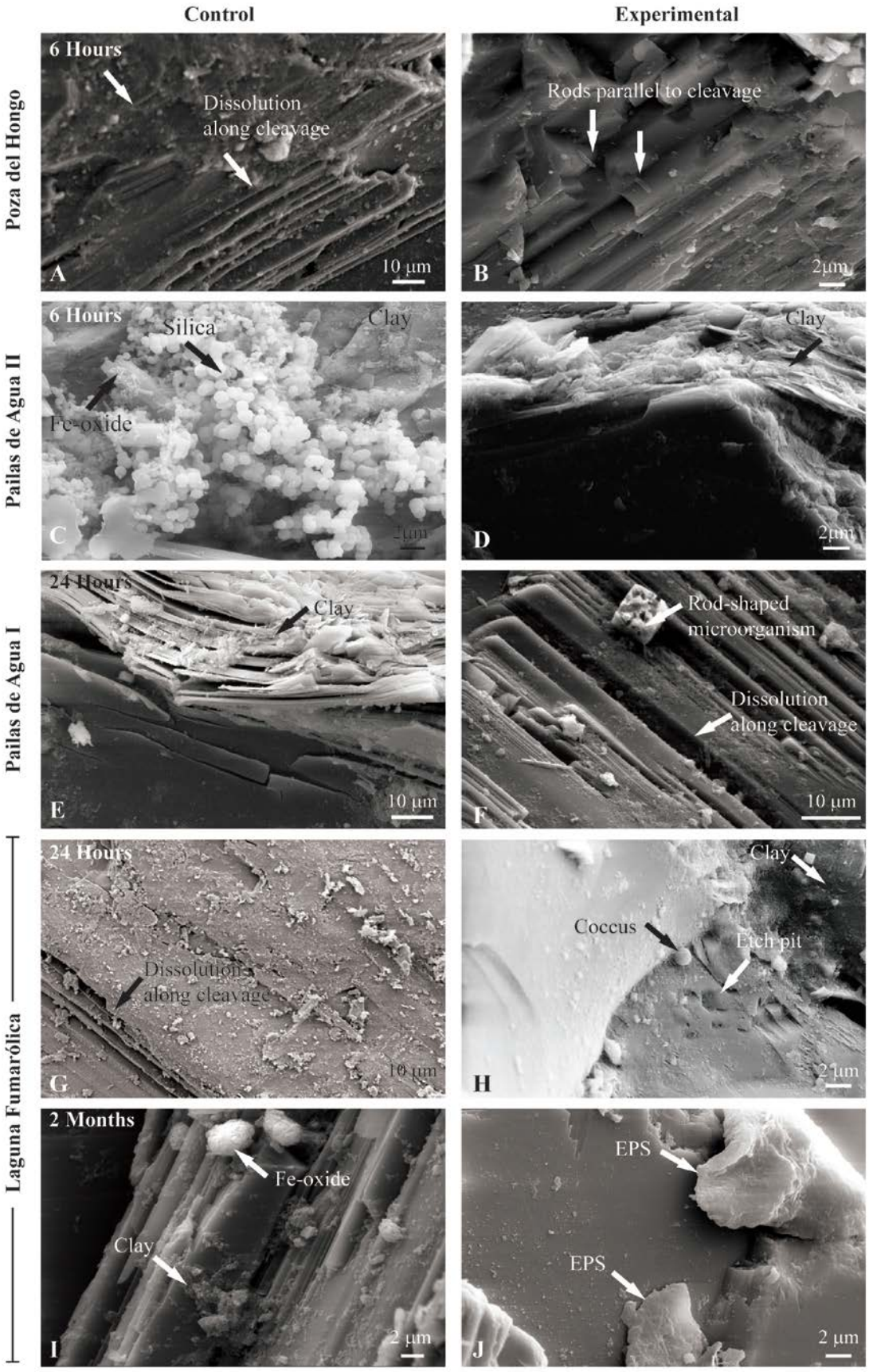
Control
Experimental
Poza del Hongo
Pailas de Agua II
Pailas de Agua I
Laguna Fumarólica
6 Hours
Dissolution along cleavage
A
10 µm
Rods parallel to cleavage
B
2µm
6 Hours
Silica
Clay
Fe-oxide
C
2µm
Clay
D
2µm
24 Hours
Clay
E
10 µm
Rod-shaped microorganism
Dissolution along cleavage
F
10 µm
24 Hours
Dissolution along cleavage
G
10 µm
Clay
Coccus
Etch pit
H
2 µm
2 Months
Fe-oxide
Clay
I
2 µm
EPS
EPS
J
2 µm

Figure 5: Amphibole weathering among treatments Poza del Hongo (6h) (A) Minor dissolution along cleavage planes, few attached clays; (B) Microorganisms attached parallel to cleavage. Pailas de Agua II (6h) (C) Attached clays and silica spherules with minor dissolution; (D) Conversion of amphibole to clay; no bacteria observed on rapidly dissolving surfaces. Pailas de Agua I (24 h) (E) Conversion of amphibole to clay in control sample. (F) Etch pit formation along cleavage and rod-shaped microorganism associated with Fe-oxide. Laguna Fumarólica (24 h) (G) Dissolution along cleavage; (H) Coccus-shaped microorganism near small etch pits and clay minerals; Laguna Fumarólica (2 mo) (I) Clay and Fe-oxide minerals; (J) Discontinuous EPS covers mineral surface.

Observations of washed samples did not show significant differences from unwashed control samples that were not covered in EPS suggesting EPS formation did not substantially influence dissolution processes.

Anorthoclase

Poza del Hongo (6 h)

Dissolution along cleavage planes and the formation of 1-2 μm diameter etch pits was observed in Poza del Hongo (6 h) anorthoclase samples (Figure 6A; Table 4). Nanoscale clay minerals were sorbed to anorthoclase surfaces (Figure 6A). Extensive biofilms developed over some surfaces, encapsulating up to 40% of the mineral surface in polymer (Figure 6B). The average cell density was 2.76×10^{-4} cells μm^{-2}.

Pailas de Agua II (6 h)

Pailas de Agua II (6 h) control and experimental anorthoclase samples were partially coated by secondary minerals, including clays and silica spherules that measured few hundred nanometers to 2 μm in size (similar to Figure 6C). Well-developed etch pits (~10 μm in diameter) covered in part by clay minerals were observed in control samples (Figure 6C; Table 4). The surfaces of the control samples were extensively covered by sorbed clay minerals. In the experimental samples, rods, filaments, and cocci were attached to mineral surfaces, leading to a cell density of 4.83×10^{-4} cells μm^{-2}. EPS covered approximately 20% of the mineral surface. The silica spherules, ranging from a few hundred nanometers to 2 μm in size, were typically associated with EPS on the surface (Figure 6D), whereas clays and oxides were associated with individual microorganisms (similar to Figure 4J). Etch pits in the experimental anorthoclase samples were more heterogeneous in their size distribution when compared to control samples. Most etch pits in the biological samples ranged from 5-10 μm in length, though several etch pits 10s of microns in length

by greater than 10 microns in width were also observed; however the average etch pit size was similar to control samples ($2.00x10^2$ μm^2; Table 4).

Pailas de Agua I (24 h)

Both control and experimental anorthoclase samples retrieved from Pailas de Agua I (24 h) were heavily coated in oxides and nanoscale clay minerals (similar to Figure 6F) with few large (~30 μm in diameter) etch pits observed (similar to 6E). Minor dissolution associated with cleavage planes was also observed in both experimental and control samples. Experimental surfaces had significant quantities of inorganic debris, including clays and oxides that completely coated the mineral surfaces (Figure 6F). This may result from transport to the surface of the high suspended load in the spring, which was composed in part of clays and Fe-oxides (Figure 2). Rod-shaped, cocci, filaments, and helical polymers typically attributed to the iron-oxidizing microorganism Gallionella were present on biologically weathered surfaces (Figure 6F). The average microbial cell density was $4.08x10^{-4}$ cells μm^{-2}.

Laguna Fumarólica (24 h)

After 24 h exposure in Laguna Fumarólica (24 h), crystallographically controlled dissolution was evident in both control and experimental weathered anorthoclase samples (Similar to Figure 6G). Etch pits measuring 1- >20 μm in diameter as well as sorbed clays were present in both treatments as well (Figure 6G; Table 4). Individual rods, cocci and putative fungal filaments (>246 μm long) were observed associated with anorthoclase surfaces in biologically weathered samples (Figure 6H). The average cell density was $2.87x10^{-5}$ cells μm^{-2}.

Laguna Fumarólica (2 mo)

After two months, LFC (controls) were characterized by deeply weathered cleavage planes and etch pits (diameters ranging from 50 to >1000 μm) typically associated with secondary clays (Figure 6I). Etch pits were crystallographically controlled. Individual microorganisms or clusters of microorganisms were associated with large (100- 200 μm long by 50-100 μm wide) etch pits in the biologically weathered

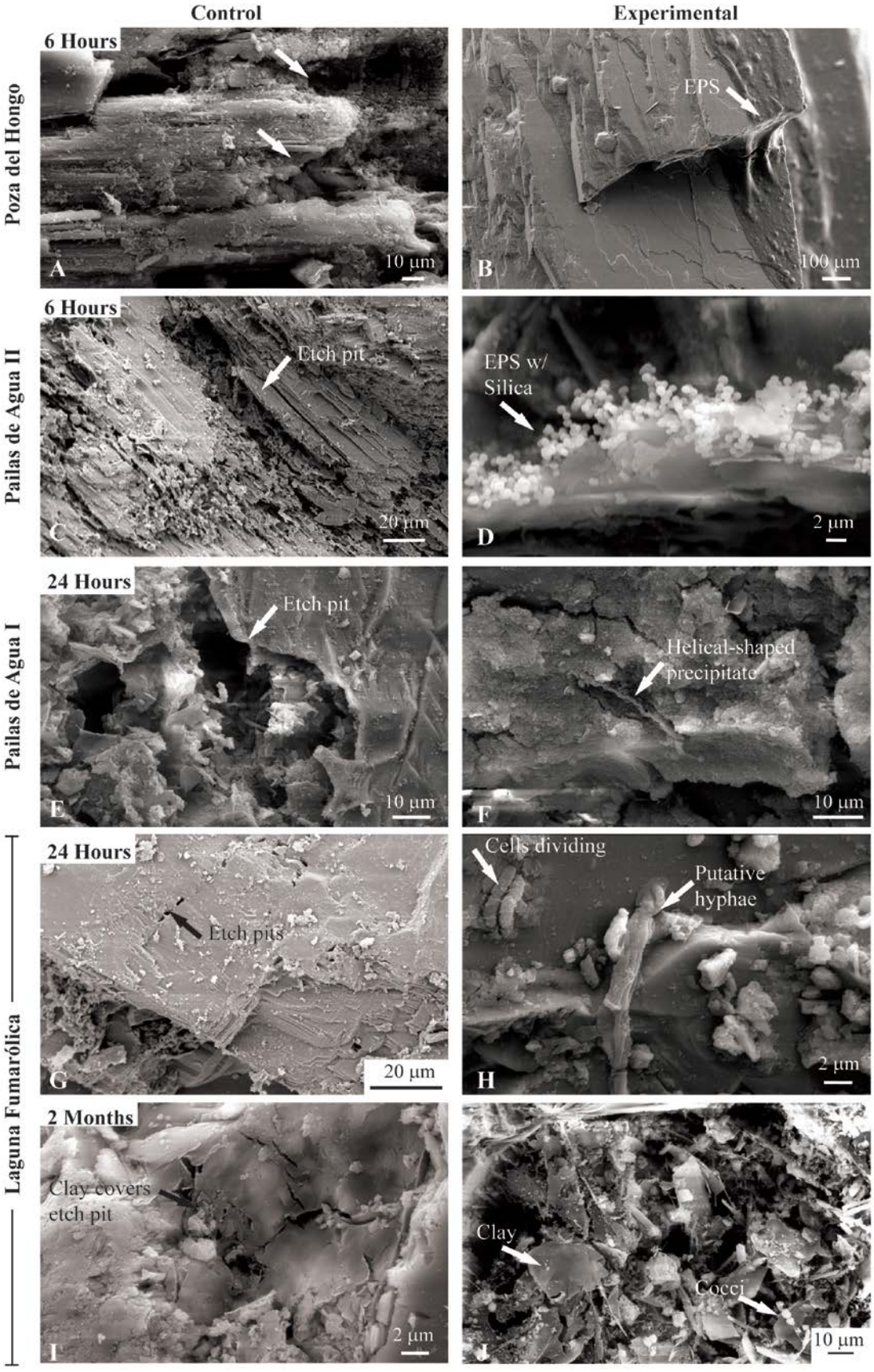
Control
Experimental
Poza del Hongo
Pailas de Agua II
Pailas de Agua I
Laguna Fumarólica
6 Hours
6 Hours
24 Hours
24 Hours
2 Months
EPS
Etch pit
EPS w/
Silica
Etch pit
Helical-shaped
precipitate
Etch pits
Cells dividing
Putative
hyphae
Clay covers
etch pit
Clay
Cocci
A
B
C
D
E
F
G
H
I
J
10 µm
100 µm
20 µm
2 µm
10 µm
10 µm
20 µm
2 µm
2 µm
10 µm

Figure 6: Anorthoclase weathering among treatments Poza del Hongo (6 h) (A) Development of etch pits and conversion of anorthoclase to clay (B) Extensive EPS covers parts of anorthoclase surface. Pailas de Agua II (6 h) (C) Dissolution and formation of etch pits; (D) EPS with silica spherules. Pailas de Agua I (24 h) (E) Etch pit in anorthoclase; (F) Helical-shaped precipitate resembling Gallionella with nanoparticulates. Laguna Fumarólica (24 h) (G) Minor etch pit formation along cleavage; (H) Rod-shaped microorganisms and putative fungal hyphae attached to anorthoclase surface. Laguna Fumarólica (2 mo) (I) Etch pit with clay; (J) Large etch pit w/ microorganisms attached via pili and abundant clays.

(LFB) anorthoclase samples. The average cell density was 2.26×10^{-3} cells μm^{-2} (Figure 6J; Table 4). The clusters of microorganisms were interconnected via pili and polymer within the large etch pits (Figure 6J). Many of these microorganisms were blanketed in nanoscale secondary clay minerals (Figure 6J). Small discontinuous EPS were observed covering approximately 40% of the surface (Table 4). Deep hexagonal

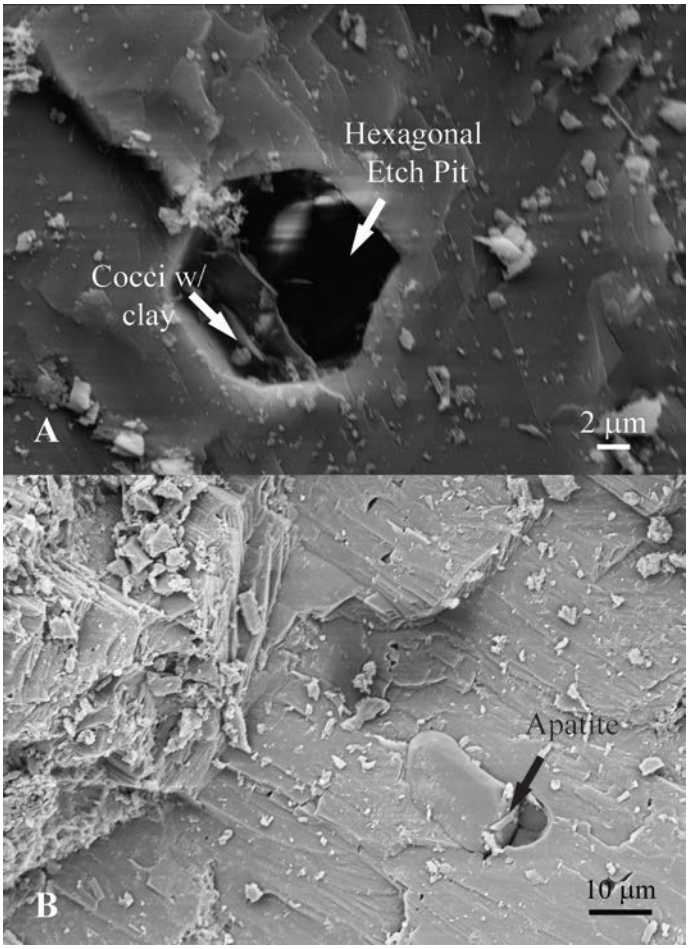

Figure 7: Differential weathering of apatite: (A) Euhedral apatite crystal exposed on LFC anorthoclase surface after 2 mo. (B) Hexagonal etch pit approximately 5 µm in diameter that has weathered out of LFB an anorthoclase sample after 2 mo.

etch pits were present in biologically weathered (LFB) samples and likely represent the preferential dissolution of apatite from the anorthoclase samples (Figure 7). This was not observed in the control experiments (Figure 7).

Quantification of Weathering

To quantify difference in etch pit size between the biological (LFB) and control (LFC) anorthoclase samples, three stereoimages were taken and integrated into a DEM using the MeX® software package. From the DEM, etch pit volumes were calculated. Results from this analysis are reported in Table 5.

In anorthoclase samples exposed to fluids in Laguna Fumarólica for 24 h, dissolution was an order of magnitude greater in control samples (3.6×10^5 μm^3) than in biological samples (4.6×10^4 μm^3). These values could serve as proxies for initial weathering rates. After two months, microbially weathered anorthoclase samples displayed broad, deep etch pits which ranged from 10 to $\geq$200 μm in length and up to 100 μm in width (Figure 8). In experimental samples, anorthoclase etch pits fell into two populations: a population with volumes that ranged from 10^3-10^4 μm^3 and one with volumes that ranged from 10^5-10^7 μm^3. Biologically weathered systems had significantly greater dissolution (4.7×10^6 μm^3) than controls

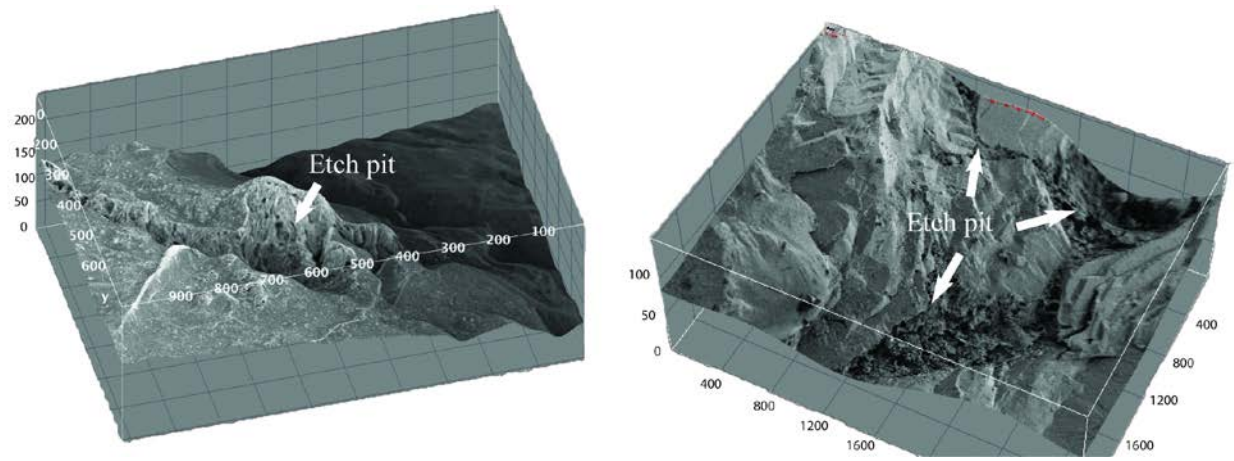

Figure 8: Digital elevation models of anorthoclase control and experimental samples retrieved from Laguna Fumarólica after 2 months. (A) Control samples consistently show etch pit volumes of 104-105 μm^3, similar to the DEM shown here. (B) Experimental sample etch pits are highly variable in size, shape, and depth, and range in volume from from 10^4-10^7 μm^3. This is a weathered Fe-oxide inclusion. Some clays remained cemented to the surface which may mask the true depth of the pit and thus potentially underestimate the volume.

($5.0x10^5$ μm^3) (Table 5; Figure 9). Utilizing volumetric loss and experimental duration, we have calculated long-term weathering rates for these samples. Biological samples showed volume losses of $7.8x10^4$ μm^3 day^{-1}, which was an order of magnitude faster than controls ($7.8x10^3$ μm^3 day^{-1}) (Table 5). This is the opposite of short-term (24 h) weathering rates.

Table 5: Weathering Volumes and Rates
Laguna Fumarólica Anorthoclase

	Experimental		Control	
Duration	24 h	2 mo	24 h	2 mo
Volume (μm^3)	4.63E+04	4.67E+06	3.53E+05	4.95E+05
Standard Deviation	4.05E+04	8.68E+06	3.51E+05	2.57E+05
Weathering Rate (μm^3 day^{-1})	4.63E+04	7.71E+04	3.53E+05	7.48E+03

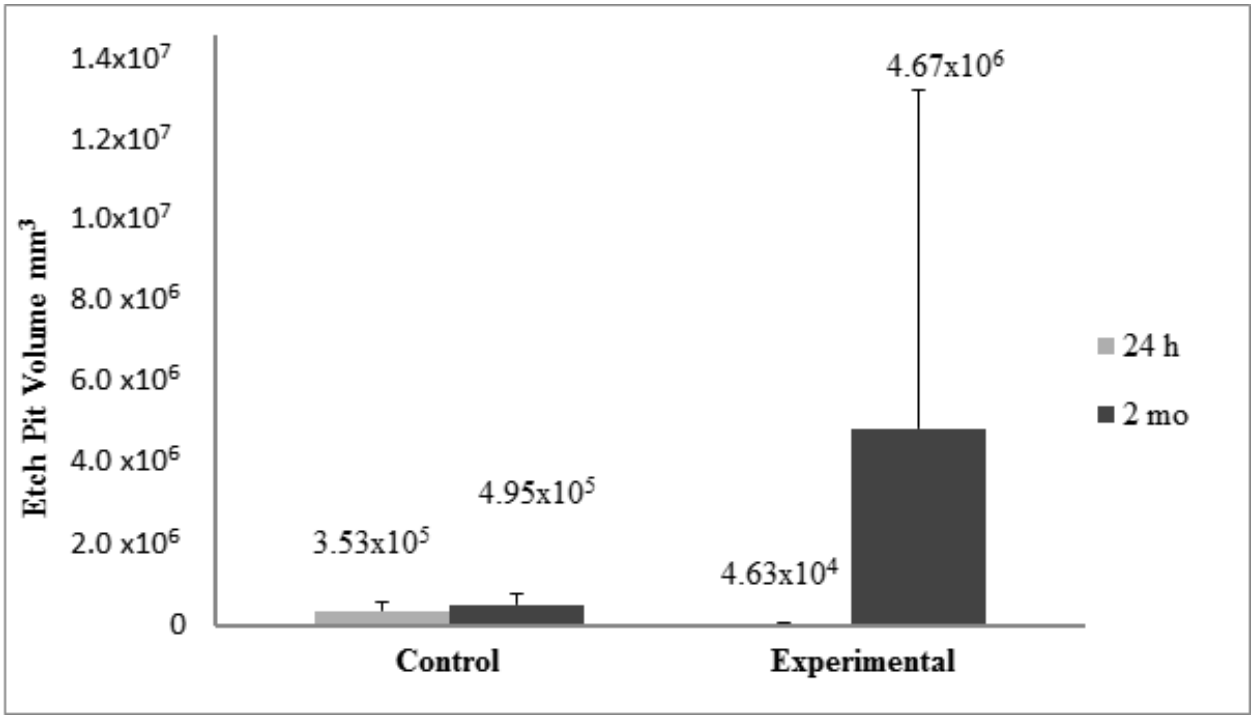

Figure 9: Quantification of etch pit volume with time and experimental treatment. Initially control samples are more significantly weathered than experimental samples; however, after 2 mo, experimental samples have etch pit volumes that are approximately an order of magnitude greater than control samples. Error represents the standard deviation from the average for all measurements.

Discussion

While many studies have investigated microorganisms in hydrothermal systems as well as their role in mineral alteration, this is the first study to document *initial* microbial attachment and colonization of silicate minerals in an acidic (pH 2.6-5) volcanic hydrothermal (T 43-80^{o}C) system. These data give us insight into the factors that influence microbial weathering and secondary mineral formation in acid-sulfate hydrothermal systems over short time scales and quantify the importance of microbial weathering in acidic hydrothermal systems.

Mineral Dissolution

Factors affecting mineral dissolution include pH, temperature, ionic strength, and microbial processes. For the short-term (6 h) biologically weathered experiments, both temperature (90°C vs. 83°C, Table 2) and ionic strength (0.210 vs. 0.281, Table 2) were similar for Poza del Hongo and Pailas de Agua II, respectively. Thus, these two factors were not likely responsible for differences in dissolution features in samples from the two springs. Additionally, microbial contributions to weathering could not be examined due to contamination of control samples. However, pH did seem to play a role in these short-term weathering reactions. Samples from Poza del Hongo (pH 5.8) appeared to show less dissolution along cleavage planes, fewer and less well-developed etch pits, and fewer sorbed secondary minerals than samples from Pailas de Agua II (pH 2.8). Chemical weathering studies at similar temperature ranges (25-90^{o}C) have shown that pyroxene, amphibole and feldspar dissolution rates increase with decreasing pH (Schott et al. 2009; Oelkers and Schott 2001; Chen and Brantley 1998; Frogner and Schweda 1998). As such, the present study suggests that pH played a primary role in mineral dissolution rates in hot spring systems over short time spans (e.g. 6-24 hours).

When comparing spring characteristics of samples weathered over 24 hours, the temperature of the Laguna Fumarólica spring was substantially lower than the Pailas de Agua I spring (43^{o}C vs. 80-89^{o}C, Table 2). Additionally, the pH of Laguna Fumarólica was lower than that of Pailas de Agua I (2.42 vs. 2.60-3.96, Table 2). Despite the temperature and pH differences, pyroxene dissolution features appeared similar between these springs' control samples after 24 hours. Oelkers and Schott (2001) showed that

abiotic pyroxene dissolution was largely temperature independent over the range of 22-90^{o}C. In contrast, anorthoclase dissolution in the control samples was greater at Pailas de Agua I than at Laguna Fumarólica, suggesting increased abiotic dissolution rates for anorthoclase at higher temperatures. Chen and Brantley (1997) observed that the complex nature of abiotic feldspar dissolution was linked to both pH and temperature, with increased dissolution observed at higher temperature. Ionic strengths of the two springs were similar (0.172 for Laguna Fumarólica vs. 0.470 for Pailas de Agua I, Table 2) and therefore not considered a factor when examining the differences between chemical and biological dissolution characteristics of the two springs. In experimental (biologically active) microcosms reacted over 24 hours, etch pits were much larger in amphibole samples from Pailas de Agua I than those from Laguna Fumarólica. It is possible that the presence of EPS development in Laguna Fumarólica (24 h) samples retarded mineral dissolution (e.g. Welch et al. 1999) and thus smaller and fewer dissolution features formed.

Within as little as two months, the importance of microorganisms in silicate mineral dissolution becomes more evident. While all of the LFB experimental samples were colonized, dissolution did not appear to be significantly enhanced (Table 4) on pyroxene or amphibole surfaces. In contrast, dissolution was significantly enhanced by microorganisms on anorthoclase feldspar grains. Microorganisms may, therefore, preferentially enhance weathering of select silicate minerals in acid-sulfate hydrothermal systems.

Microbe-Mineral Interactions

SEM observations of Las Pailas acid-sulfate hot spring system samples indicated that microbial attachment to silicate mineral surfaces occurred rapidly. Microbial attachment to *in situ* microcosm samples occurred within as little as six hours of incubation. This may be due to van der Waals interactions between the mineral grains and the microorganisms at the low pHs observed in this system (Yee 2000). However, initial attachment is primarily crystallographically controlled due to high energy and unsatisfied charge of these sites and the formation of pili or other polymeric attachments between the bacteria and

mineral surface after contact in a high ionic strength solution (Lower et al. 2000). These interactions have been shown to be largely pH independent (Cail and Hochella 2005). Filaments, cocci, rods, and helical microorganisms as well as putative fungal hyphae were observed in biologically weathered samples within 24 hours. Fungal hyphae have been observed in other hydrothermal systems including the Lost City hydrothermal vent field (López-García et al. 2006). Development of EPS was also observed on Poza del Hongo and Pailas de Agua II experimental samples within six hours, and within Palias de Agua I and Laguna Fumarólica within 24 hours. These observations suggest that mineral and rock surfaces in volcanic systems may be colonized as soon as they cool below ~113^{o}C (the upper limit for life; Kashefi and Lovely 2003).

In all springs, microorganisms preferentially colonized anorthoclase samples as shown by the combination of cell count and EPS coverage data. Amphibole minerals were more heavily colonized than pyroxene samples. All experimental (biologically weathered) samples were partially covered by sorbed minerals. Silica spherules and (Fe, Al) oxides were associated with EPS and mineral surfaces. Silica spherules were not observed sorbed to individual cells. In contrast, clay minerals were sorbed to mineral surfaces and cells, but not to EPS. The difference in secondary mineral sorption may be intrinsically related to charge characteristics of the minerals, microorganisms, and EPS present. Both microbial cells zero point of charge (ZPC 1-4.5; Yee and Fein 2001; He and Tebo, 1998; Crist et al. 1992) and polymeric silica (ZPC 2-3; Dietrich, 1997) are neutrally to slightly negatively charged charged at the pH values of our study. This should result in minimal interaction between the cells and silica spherules in Pailas de Agua II (pH 2.77; Table 2) where silica spherules were observed. Interactions between EPS and silica are more difficult to predict due to the variability in ZPCs of organic acids; however, Konhauser and Ferris (1996) observed sorption of silica onto biofilms and microbial cells in acidic Krusívík hydrothermal pools in Iceland. In Krusívík, silica bound to cell surfaces included Fe that acted as a cation bridge between the cell surface and silicic acid in solution (Konhauser and Ferris, 1996). The variability in organic ZPCs may account for the sorption of silica onto mineral surfaces and EPS, however it is likely that dehydration

reactions may also account for this result. It is possible that the high concentrations of Al, Fe, and Si in the spring solutions resulted in the transformation of adsorbed silica to clay minerals on microbial cell surfaces upon aging (Kawano and Tomito, 2002; Konhauser and Uttria, 1999).

In addition to sorption of minerals, authigenic clay formation was observed associated with etch pit formation in experimental and control samples. These clays were also associated with and potentially nucleating on microbial cell surfaces. Kennedy et al. (2006) suggested that organic matter was critical to inception of the clay mineral factory in the Proterozoic, and microorganisms have been shown to mediate clay formation in natural systems (Michalopoulos and Aller 2004; Konhauser et al. 2002; Tazaki 1997). Microorganisms covered in nontronite are observed in the sediments of low-temperature alteration zones, though these clays were attributed to alteration of Fe-oxides sorbed to microbial surfaces (Masuda 1995; Alt, 1988). The association between clays and microbial surfaces in the present study raises interesting questions about the role of microorganisms in authigenic clay formation in hydrothermal systems. It remains unclear whether microorganisms are directly implicated in clay formation in these systems, or if adsorption of clays to their cell surfaces. Pailas de Agua I and Pailas de Agua II are both oversaturated (SI of 3.92 for Pailas de Agua I and 3.73 for Pailas de Agua II) with respect to nontronite, however Laguna Fumarólica and Poza del Hongo are undersaturated with respect to nontronite (SI -0.73 for Laguna Fumarólica and -0.57 for Poza del Hongo). Despite this, in Laguna Fumarólica substantial clays are observed in the spring and clay minerals coat microbial cells. This suggests that microorganisms may play a role in clay formation in hydrothermal systems.

Pyroxene samples experienced significant dissolution, which was predominantly crystallographically controlled. Initial etch pit development was observed in all short-term (6 and 24 h) experiments regardless of treatment. After two months incubation in Laguna Fumarólica, microorganisms were attached to pits that appeared broadly similar in size, shape and frequency as etch pits in control samples indicating that microorganisms had no significant (less than an order of magnitude) effect on etch pit formation. Research has shown that pyroxene dissolution is only weakly affected by organic acids

(Golubev and Porovsky 2006; Grandstaff 1977), which may explain these results. Alternatively, the significant sorbed clays observed associated with mineral surfaces may provide a diffusive barrier to pyroxene dissolution. These results demonstrate that even significant microbial colonization of pyroxene minerals over two months may not affect pyroxene dissolution in acidic hot springs.

Substantial dissolution of amphibole mineral samples and complete conversion of some amphiboles to clays were observed in Pailas de Agua II (6 h) biological and Pailas de Agua I (24h) control samples. In contrast, the amphibole surfaces of Laguna Fumarólica and Poza del Hongo displayed EPS, which appear to protect parts of the surface from dissolution.

A primary function of EPS is to protect microorganisms from hostile environmental conditions including high T and low pH, toxic metal concentration, and UV exposure (Decho 2000). EPS formation may either serve to enhance or inhibit dissolution of mineral surfaces (Welch et al. 1999; Welch and Vandevivere 1994). By decreasing diffusion rates, EPS may concentrate nutrients required for growth and effectively protect the mineral surface from dissolution (Decho 2000). Additionally EPS may chelate metals, locally decrease pH by up to 1 pH unit, and displays an adhesive effect that increases microbial contact time with the surface (Decho 2000; Liermann et al., 2000; Welch et al. 1999). Welch et al. (1999) experimentally showed that each of these processes may enhance microbial impacts on dissolution, even under acidic (pH~3) conditions when the solution was saturated with respect to Si and Al.

Both the protective and destructive effects of EPS are observed in this study. Experimental samples retrieved from Laguna Fumarólica (24 h) were partially encapsulated by EPS and had smaller etch pit sizes than those measured in experimental samples retrieved from Pailas de Agua I (24 h) Additionally, amphibole mineral grain surfaces from Laguna Fumarólica (2 mo) were extensively covered with EPS after two months; however experimental amphibole surfaces from which EPS had been removed appeared similar to control samples, indicating that EPS effectively protect mineral surfaces in this spring. This compares well with Buss et al. (2007) in which hornblende surfaces showed no substantial weathering beneath the EPS surface. After two months exposure, LFB (2 mo) anorthoclase surfaces colonized by

microorganisms experienced an order of magnitude greater dissolution rate than control samples. Similarly, Barker et al.'s (1998) cross-sections through EPS covering weathered feldspar surfaces showed substantial etching beneath EPS. Therefore the impact of EPS on weathering in Las Pailas is related to both the incubation time and mineralogy.

After two months, apatite grains were preferentially dissolved from LFB (biological weathering) samples leaving hexagonal etch pits similar to those observed in Taunton et al. (2000a and b). In contrast, apatite crystals remained pristine in LFC (chemical weathering) samples. The PO_4^{3-} concentration of this spring was 4.24 μmol $^{-1}$, which is only slightly higher than the 3.2 μmol L^{-1} phosphate concentration reported in Wolfe-Simon et al. (2011) experiments with phosphate-limited microorganisms from Mono Lake. Apatite inclusions may act as a source for phosphate in this study's phosphate-limited system. Mineral-bound phosphate, present as apatite inclusions, is an apparently available phosphate source that drives microbial colonization and subsequent dissolution of the anorthoclase mineral surface. Microorganisms have been shown to preferential colonize and weather minerals that contain phosphate grains and inclusions in minerals in a variety of circum-neutral to acidic pH systems (Mauck and Roberts 2007; Rogers and Bennett 2004; Bennett et al. 2001; Taunton et al. 2000a; Taunton et al. 2000b; Rogers et al. 1998). Moreover, Welch et al. (2002) experimentally showed that organic acids could increase the dissolution of apatite by up to an order of magnitude by decreasing the bulk pH of the system. Therefore, phosphate or other nutrient limitations may be an important driver for microbial weathering in hydrothermal systems.

Chemical vs. Biological Weathering

AFM has been previously used to define differences in biologically induced weathering (Gorbushima et al. 2011). However, AFM is unsuitable for the rough topography presented by most mineral surfaces in the environment, and this has limited our ability to quantify weathering in natural systems. The value of the MeX® software package is that it allows us to conduct 3-D analysis of large etch pits with variable topography, which may be beyond the scope of AFM. Volumetric analysis of etch pits in anorthoclase at two time steps indicates that initial dissolution is primarily the result of chemical interactions. In long-

term (i.e. two month) incubations, this trend is reversed. After two months, microbial weathering results in an order of magnitude greater volumetric loss when compared with control samples. These results indicate that geochemical factors may control weathering in the short-term (6-24 h). However, microorganisms and specifically EPS play an important role in mineral dissolution over longer time scales (2 mo). This result was unexpected as microbial weathering at Iron Mountain, an AMD site (pH 3.5 and T 18-50^{o}C) did not show increased metal release (used as a proxy for sulfide mineral weathering) in association with microorganisms (Edwards et al. 2000).

EPS in the short-term (i.e. < 2 mo) appears to retard weathering relative to control samples. Microorganisms may initially secrete EPS, which functions specifically to protect the cells from the surrounding environment. This has the effect of similarly protecting the mineral surface. However, the opposite trend is observed in LFB (2 mo) samples. This indicates that the nature of the EPS-mineral surface interface changes with time and may be a result of the changing chemical conditions within the EPS or the changing structure of the EPS with time.

Weathering in acidic hydrothermal systems is the result of a complex interplay of geochemical and biological drivers. Microbial attachment and subsequent colonization occurs almost instantaneously within hydrothermal systems. Geochemically driven mineral dissolution reactions proceed quickly at high T and low pH in acid-sulfate hydrothermal systems and chemical weathering initially predominates over biological weathering. Despite this, the impact of microbial activity is evident even on short time (2 mo) scales. Preferential microbial colonization may initially serve to protect some mineral surfaces from dissolution. Nevertheless, the net effect of microbial activity in acidic volcanic hydrothermal systems is significant enhancement dissolution of mineral surfaces by approximately an order of magnitude. Microbially enhanced dissolution appears to be tied to metabolic requirements and nutrient limitation within the system. This result may have important implications for microbial enhancement of elemental cycling in acid-sulfate hydrothermal systems.

Acknowledgements

We would like to thank the two anonymous reviewers whose careful revisions improved this work. This work would not be possible without the financial support of the Costa Rica/United States of America Foundation for Cooperation (CRUSA) to (awarded to Jennifer Roberts and Marielos Mora), and KU Geology Associates Grant (awarded to David Fowle), as well as the support of the Costa Rica National Parks Service, which provided access to the site. Microscopy and fieldwork support were provided by a Geological Society of America Student Research Grant, an Ernest Angino Geochemistry Scholarship, and an ExxonMobil Student Research Grant (awarded to Charity Phillips Lander). We thank Victor Day for his technical assistance with XRD analyses and Annette Summers Engel and Geoffrey Lander for consulting on microcosm construction.

References

Alt, J. 1988. Hydrothermal oxide and nontronite deposits on the seamounts of the Eastern Pacific. Marine Geology 81: 227-239.

Barker, W W, Welch, S A, Chu, S, and Banfield, J F. 1998. Experimental observations of the effects of bacteria on aluminosilicate weathering. American Mineralogist 83:1551-1563.

Banfield, J F, Barker, W W, Welch, S A, and Taunton, A. 1999. Biological impact on mineral dissolution: application of the lichen model to understanding mineral weathering in the rhizosphere. Proceedings of the National Academy of Sciences of the United States of America 96: 3404-11.

Banerjee, N R, and Muhlenbachs, K. 2003. Tuff life: Bioalteration in volcaniclastic rocks from the Ontong Java Plateau. Geochemistry, Geophysics, Geosystems 4: 1037-1059. doi:10.1029/2002GC000470

Bennett, P C, Rogers, J R, Choi, W J, and Hiebert, F K. 2001. Silicates, silicate weathering, and microbial ecology. Geomicrobiology Journal 18: 3-19. doi:10.1080/01490450151079734

Bennett, PC, Engel, A S, and Roberts, J A. 2006. Counting and imaging bacteria on mineral surfaces. In: Maurice J P and Waen L A editors. Methods of Investigating Microbial-Mineral Interactions, CMS Workshop Lectures, Vol, 14, The Clay Mineral Society, P. 37-78.

Brantley, S L, Liermann, L, Bau, M and Wu, S. 2001. Uptake of trace metals and rare earth elements from hornblende by a soil bacterium. Geomicrobiology Journal 18: 37-61.

Buss, H L, Lüttge, A, and Brantley, S L. 2007. Etch pit formation on iron silicate surfaces during siderophore-promoted dissolution. Chemical Geology 240: 326-342. doi:10.1016/j.chemgeo.2007.03.003

Cail, T. and Hochella, M F. 2005. The effects of solution chemistry on the sticking efficiencies of viable Enterococcus faecalis: An atomic force microscopy and modeling study. Geochimica et Cosmochimica Acta 69: 2959-2969. doi:10.1016/j.gca.2005.01.017

Chen, Y and Brantley, S L. 1998. Diopside and anthrophyllite dissolution at 25^{o} and 90^{o}C and acid pH. Chemical Geology 147: 233-248.

Chen, Y, and Brantley, S L. 1997. Temperature- and pH-dependence of albite dissolution rate at acid pH. Chemical Geology 135: 275-290.

Crist, R H, Oberholser, K, McGarrity, J, Crist, D R, Johnson, J K, and Brittsan, J M. 1992. Interaction of metals and protons with algae. 3. Marine algae, with emphasis on lead and aluminum. Environmental Science and Technology 26:496-502.

Daughney, C, Rioux, J, Fortin, D, and Pilcher, T. 2004. Laboratory investigation of the role of bacteria in the weathering of basalt near deep sea hydrothermal vents. Geomicrobiology Journal 21: 21-31.

Decho, A. 2000. Microbial biofilms in intertidal systems: an overview. Continental Shelf Research 20: 1257-1273. doi:10.1016/S0278-4343(00)00022-4

Dekov, V. M., Cuadros, J., Shanks, W. C., & Koski, R. A. (2008). Deposition of talc—kerolite–smectite—smectite at seafloor hydrothermal vent fields: Evidence from mineralogical, geochemical and oxygen isotope studies. Chemical Geology, 247(1), 171-194.

Dietrich, P G, Lerche, K –H, Reusch J, and Nitzsche, R. 1997. The characterization of silica nanoparticles by electrophoretic mobility measurements. Chromatographia 44: 362-366. doi:10.1007/BF02466311Dekov, V M, Cuadros, J, Shanks, W C, and Koski, R A. 2008. Deposition of talc, kerolite-smectite, smectite at seafloor hydrothermal vent fields: Evidence from mineralogical, geochemical and oxygen isotope studies. Chemical Geology 247: 171-194.

Dick, G J, and Tebo, B M. 2010. Microbial diversity and biogeochemistry of the Guaymas Basin deep-sea hydrothermal plume. Environmental Microbiology 12: 1334-1347. doi:10.1111/j.1462-2920.2010.02177.x

Edwards, K J, Bond, P L, Druschel, G K, McGuire, M M, Hamers, R J, and Banfield J F. 2000. Geochemical and biological aspects of sulfide mineral dissolution: lessons from Iron Mountain, California. Chemical Geology 169: 383-397.

Edwards, K J, McCollum, T M, Konishi, H, and Buseck, P R. 2003. Seafloor bioalteration of sulfide minerals: Results from in situ incubation studies. Geochimica et Cosmochimica Acta 67: 2843-2856. doi:10.1016/S0016-7037(00)00089-9

Einen, J, Thorseth, I H, and Ovreås, L. 2008. Enumeration of Archaea and Bacteria in seafloor basalt using real-time quantitative PCR and fluorescence microscopy. FEMS Microbiology Letters 282:182-7. doi:10.1111/j.1574-6968.2008.01119.x

Engel A S, Stern, L A, and Bennett, PC. 2004. Microbial contributions to cave formation: New insights into sulfuric acid speleogenesis. Geology 32: 369-372.

Finsinger, K, Scholz, I, Serrano, A, Morales, S, Uribe-Lorio, L, Mora, M, Sittenfeld, A, Weckesser J, and Hess W R. 2008. Characterization of true-branching cyanobacteria from geothermal sites and hot springs of Costa Rica. Environmental Microbiology 10: 460-473.

Fisk, M, Giovannoni S J, and Thorseth, I H. 1998. Alteration of Oceanic Volcanic Glass: Textural Evidence of Microbial Activity. Science 281: 978-980.

Fouke, B W, Farmer, J D, Des Marais, D J, Pratt, L, Sturchio, N C, Burns, P C, and Discipulo, M K. 2000. Depositional facies and aqueous-solid geochemistry of travertine-depositing hot springs (Angel Terrace, Mammoth Hot Springs, Yellowstone National Park, U.S.A.). Journal of Sedimentary Research 70: 565-585.

Frogner, P. and Schweda, P. 1998. Hornblende dissolution kinetics at 25^{o}C. Chemical Geology 151: 169-179.

Furnes, H, Muehlenbachs, K, Tumyr, O, Torsvik, T and Thorseth, I. 1999. Depth of the active bio-alteration in ocean crust: Costa Rica Rift (Hole 504B). Terra Nova 11: 228-233.

Furnes, H, Muehlenbachs, K, Torsvik, T, Thorseth, I H, and Tumyr, O. 2001. Microbial fractionation of carbon isotopes in altered basaltic glass from the Atlantic Ocean, Lau Basin and Costa Rica Rift. Chemical Geology 173: 313-330. doi:10.1016/S0009-2541(00)00285-0

Gehring, A U, Schosseler, P M, and Weidler, P G. 1999. Mineral formation and redox sensitive trace elements in a near-surface hydrothermal alteration system. Geochimica et Cosmochimica Acta 63: 2061-2069.

Glynn, S, Mills, R A, Palmer, M R, Pancost, R D, Severmann, S, and Boyce, A J. 2006. The role of prokaryotes in supergene alteration of hydrothermal sulfides. Earth and Planetary Science Letters 244: 170-185.

Golubev, S, and Pokrovsky, O. 2006. Experimental study of the effect of organic ligands on diopside dissolution kinetics. Chemical Geology 235: 377-389. doi:10.1016/j.chemgeo.2006.08.004

Gorbushima, A A, Kempe, A, Rodenacker, K, Jutting, U, Altermann, W, Stark, R W, Heckl, W M, and Krumbein, W E. 2011. Quantitative 3-dimensional image analysis of mineral surface modifications- chemical, mechanical and biological. Geomicrobiology Journal 28:172-184.

Gorby, Y A, Yanina, S , McLean, J S, Rosso, K M, Moyles, D, Dohnalkova, A, Beveridge, T J, Chang, I S, Kim, B H, Kim, K S, Culley, D E, Reed, S B, Romine, M F, Saffarini, D A, Hill, E A, Shi, L, Elias, D A, Kennedy, D W, Pinchuk, G, Watanabe, K, Ishii, S, Logan, B, Nealson, K H, and Fredrickson, J K. 2006. Electrically conductive bacterial nanowires produced by Shewanella oneidensis strain MR-1 and other microorganisms. Proceedings of the National Academy of Sciences of the United States of America 103: 11358-11363.

Grandstaff, D E. 1977. Some kinetics of bronzite orthopyroxene dissolution. Geochimica et Cosmochimica Acta 41: 1097-1103.

Havig, J R., Raymond, J, Meyer-Dombard, D R, Zolotova, N and Shock, E L. 2011. Merging isotopes and community genomics in a siliceous sinter-depositing hot spring. Journal of Geophysical Research 116, G01005: 1-15. doi: 10.1029/2010JG001415

He, L M, and Tebo, B M. 1998. Surface charge properties of and Cu(II) adsorption by spores of the marine Bacillus sp. strain SG-1. Applied and Environmental Microbiology 64: 1123-1129.

Hiebert F K, and Bennett, P C. 1992. Microbial control of silicate weathering in organic-rich ground water. Science 258: 278–281.

Jones, B, and Renaut, R W. 2007. Selective mineralization of microbes in Fe-rich precipitates (jarosite , hydrous ferric oxides) from acid hot springs in the Waiotapu geothermal area , North Island , New Zealand. Sedimentary Geology 194: 77 - 98. doi:10.1016/j.sedgeo.2006.05.025

Jørgensen, B B, and Boetius, A. 2007. Feast and famine--microbial life in the deep-sea bed. Nature Reviews Microbiology 5:770-781. doi:10.1038/nrmicro1745

Kandianis, M T, Fouke, B W, Johnson, R W, Veysey, J and Inskeep, W P. 2008. Microbial biomass: A catalyst for CaCO3 precipitation in advection-dominated transport regimes. Geological Society of America Bulletin 120: 442–450. doi: 10.1130/B26188.1

Kashefi, K, and Lovely, D R. 2003. Extending the upper temperature limit for life. Science 301: 934. doi:10.1126/science.1086823

Kawano, M, and Tomita, K. 2002. Microbiotic Formation of Silicate Minerals in the Weathering Environment of a Pyroclastic Deposit. Clays and Clay Minerals 50: 99–110.

Kawano, M, and Tomita, K. 2001. Geochemical modeling of bacterially induced mineralization of schwertmannite and jarosite in sulfuric acid spring water. American Mineralogist 86:1156-1165.

Kempter K, Benner, S G, and Williams, S N. 1995. Rincon de la Vieja volcano, Guanacaste province, Costa Rica: geology of the southwestern flank and hazards implications. Journal of Volcanology and Geothermal Research 71: 109-127.

Kennedy, M, Droser, M, Mayer, L M, Pevear, D, and Mrofka, D. 2006. Late Precambrian oxygenation; inception of the clay mineral factory. Science 311:1446-1449. doi:10.1126/science.1118929

Konhauser, K O, Schiffman, P, and Fisher, Q J. 2002. Microbial mediation of authigenic clays during hydrothermal alteration of basaltic tephra, Kilauea Volcano. Geochemistry Geophysics Geosystems 3: 1-13. doi:10.1029/2002GC000317

Konhauser, K O, and Urrutia, M M. (1999) Bacterial clay authigenesis : a common biogeochemical process. Chemical Geology 161: 399–413.

Konhauser, K O, and Ferris, F G. 1996. Diversity of iron and silica precipitation by microbial mats in hydrothermal waters, Iceland: Implications for Precambrian iron formations. Geology 24: 323-326. doi: 10.1130/0091-7613(1996)024<0323:DOIASP>2.3.CO;2

Liermann, L J, Barnes, A S, Kalinowski, B E, Zhou, X, and Brantley, S L. 2000. Microenvironments of pH in biofilms grown on dissolving silicate surfaces. Chemical Geology 171: 1-16. doi:10.1016/S0009-2541(00)00202-3

López-García, P, Vereshchaka, A, and Moreira, D. 2006. Eukaryotic diversity associated with carbonates and the fluid-seawater interface in the Lost City hydrothermal field. Environmental Microbiology 9: 546-554. doi:10.1111/j.1462-2920.2006.01158.x

Lower, S K, Tadanier, C J, and Hochella, M F. 2000. Measuring interfacial and adhesion forces between bacteria and mineral surfaces with biological force microscopy. Geochimica et Cosmochimica Acta 64: 3133–3139.

Martín, H G, Veysey, J, Bonheyo, G T, Goldenfeld, N, and Fouke, B W. 2010. Statistical Evaluation of Bacterial 16S rRNA Gene Sequences in Relation to Travertine Mineral Precipitation and Water Chemistry at Mammoth Hot Springs, Yellowstone National Park, US. In: Barton, L L, Mandll, M, and Loy, A, editors. Geomicrobiology: Molecular and Environmental Perspective. New York: Springer P. 239-249.

Masuda, H. 1995. Iron-rich smectite formation in the hydrothermal sediment of the Iheya Basin, Okinawa Trough. In: Sakai, H. and Nozaki, Y. editors. Biogeochemical Processes and Ocean Flux in the Western Pacific. Terra Scientific Publishing Company, P. 509-521

Mauck, B S, Roberts, J. 2007. Mineralogic control on abundance and diversity of surface-adherent microbial communities. Geomicrobiology Journal 24: 167–177.

Michalopoulos, P, and Aller, R C. 2004. Early diagenesis of biogenic silica in the Amazon delta: alteration, authigenic clay formation, and storage. Geochimica et Cosmochimica Acta 68: 1061-1085. doi:10.1016/j.gca.2003.07.018

Michalopoulos, P, and Aller, R C. 1995. Rapid clay mineral formation in Amazon Delta sediments: reverse weathering and oceanic elemental cycles. Science 270: 614-617. doi:10.1126/science.270.5236.614

McLoughlin, N, Wacey, D, Kruber, C, Kilburn, M R, Thorseth, I H, and Pedersen, R B. 2011. A combined TEM and NanoSIMS study of endolithic microfossils in altered seafloor basalt. Chemical Geology. 289: 154-162. doi:10.1016/j.chemgeo.2011.07.022

Oelkers, E H, and Schott, J. 2001. An experimental study of enstatite dissolution rates as a function of pH, temperature, and aqueous Mg and Si concentration, and the mechanism of pyroxene/pyroxenoid dissolution. Geochimica et Cosmochimica Acta 65: 1219-1231. doi:10.1016/S0016-7037(00)00564-0

Phoenix, V R, Bennett, P C, Engel, A S, Tyler, S W, and Ferris, F G. 2006. Chilean high-altitude hot-spring sinters : a model system for UV screening mechanisms by early Precambrian cyanobacteria. Geobiology 4: 15-28.

Phoenix, V R, Konhauser, K O, Adams, D G, and Bottrell, S H. 2001. Role of biomineralization as an ultraviolet shield: Implications for Archean life. Geology 29: 823-826.

Resing, J, and Sansone, F. 2002. The chemistry of lava-seawater interactions II: the elemental signature. Geochimica et Cosmochimica Acta 66: 1925–1941.

Rogers JR, Bennett PC, and Choi WJ. 1998. Feldspars as a source of nutrients for microorganisms. American Mineralologist 83: 1532–1540.

Rogers, J R and Bennett, P C. 2004. Mineral stimulation of subsurface microorganisms: Release of limiting nutrients from silicates. Chemical Geology 203: 98-108.

Santelli, C M, Orcutt, B N, Banning, E, Bach, W, Moyer, C L, Sogin, M L, Staudigel, H. 2008. Abundance and diversity of microbial life in ocean crust. Nature 453: 653-6. doi:10.1038/nature06899

Schott, J, Pokrovsky, O S, and Oelkers, E H. 2009. The link between mineral dissolution/precipitation kinetics and solution chemistry. Reviews in Mineralogy and Geochemistry 70: 207-258. doi:10.2138/rmg.2009.70.6

Semenez, M, Viera, M , Curutchet, G, and Donati, E. 2002. The role of *Acidithiobacillus caldus* in the bioleaching of metal sulfides. Latin American Applied Research 32: 303-306.

Severmann, S. Mills, R A, Palmer, M R, Telling, J P, Cragg, B, and Parkes, R J. 2006. The role of prokaryotes in subsurface weathering of hydrothermal sediments: A combined geochemical and microbiological investigation. Geochimica et Cosmochimica Acta 70: 1677-1694.

Sittenfeld, A, Mora, M, Ortega, J M, Albertazzi, F, Cordero, A, Roncel, M, Sanchez, E, Vargas, M, Fernandez, M, Weckesser, J, and Serrano, A. 2002. Characterization of a photosynthetic Euglena strain isolated from an acidic hot mud pool of a volcanic area of Costa Rica. FEMS Microbiology Ecology 42: 151-161.

Spear, J R, Walker, J J, Mccollom, T M, and Pace, N R. 2004. Hydrogen and bioenergetics in the Yellowstone geothermal ecosystem. Proceedings of the National Academy of Sciences of the United States of America 102: 2555-2560.

Takai, K and Nakamura, K. 2010. Compositional, physiological and metabolic variability in microbial communities associated with geochemically divers, deep-sea hydrothermal vent fluids. In: Barton, L L, Mandll, M, and Loy, A. editors. Geomicrobiology: Molecular and Environmental Perspective. New York: Springer, P. 251-283.

Tassi, F, Vaselli, O, Capaccioni, B, Giolito, C, Duarte, E, Fernandez, E, Minissale, A, and Magro, G. 2005. The hydrothermal-volcanic system of Rincon de la Vieja volcano (Costa Rica): A combined (inorganic and organic) geochemical approach to understanding the origin of fluid discharges and its possible application to volcanic surveillance. Journal of Volcanology and Geothermal Research 148: 315-333.

Taunton, A E, Welch, S A, and Banfield, J F. 2000a. Geomicrobiological controls on light rare earth element, Y and Ba distributions during granite weathering and soil formation. Journal of Alloys and Compounds 304: 30-36.

Taunton, A E, Welch, S A, and Banfield, J F. 2000b. Microbial controls on phosphate and lanthanide distributions during granite weathering and soil formation. Chemical Geology 203: 371-382.

Tazaki, K. 1997. Biomineralization of layer silicates and hydrated Fe/Mn oxides in microbial mats; an electron microscopical study. Clay and Clay Minerals 45: 203-212.

Templeton, A S, Knowles, E J, Eldridge, D L, Arey, B W, Dohnalkova, A C, Webb, S M, Bailey, B E, et al. 2009. A seafloor microbial biome hosted within incipient ferromanganese crusts. Nature Geoscience 2: 872-876. Nature Publishing Group. doi:10.1038/ngeo696

Templeton, A S, Staudigel, H, and Tebo, B E. 2005. Diverse Mn(II)-oxidizing bacteria isolated from submarine basalts at Loihi Seamount. Geomicrobiology Journal 22:127-139. doi:10.1080/01490450590945951

Thorseth, I H, Torsvik, T, Furnes H, and Mulenbachs, K. 1995. Microbes play an important role in the alteration of oceanic crust. Chemical Geology 126: 137-146.

Toner, B M, Santelli, C M, Marcus, M A, Wirth, R, Chan, C S, McCollom, T, Bach, W, and Edwards, K J. 2009. Biogenic iron oxyhydroxide formation at mid-ocean ridge hydrothermal vents: Juan de Fuca Ridge. Geochimica et Cosmochimica Acta 73: 388–403.

Torsvik, T, Furnes, H, Muehlenbachs, K, Thorseth, I H, and Tumyr, O. 1998. Evidence for microbial activity at the glass-alteration interface in oceanic basalts. Earth and Planetary Science Letters 162: 165-176.

Vick, T J, Dodsworth, J A, Costa, K C, Shock, E L, and Hedlund, B P. 2010. Microbiology and geochemistry of Little Hot Creek, a hot spring environment in the Long Valley Caldera. Geobiology 8: 140-154. doi:10.1111/j.1472-4669.2009.00228.x

Welch, S A, Taunton, A E, and Banfield, J F 2002. Effect of microorganisms and microbial metabolites on apatite dissolution. Geomicrobiology Journal 19: 343-367.

Welch, S, Barker, W W, and Banfield, J F. 1999. Microbial extracellular polysaccharides and plagioclase dissolution. Geochimica et Cosmochimica Acta 63: 1405-1419. doi:10.1016/S0016-7037(99)00031-9

Welch, S A, and Vandevivere, P. 1994. Effect of microbial and other naturally occurring polymers on mineral dissolution. Geomicrobiology Journal 12: 227-238.

Wolfe-Simon, F, Switzer Blum, J, Kulp, T R, Gordon, G W, Hoeft, S E, Pett-Ridge, J, Stolz, J F, Web, S M, Weber, P K, Davies, P C W, Anbar, A D, Oremland, R S. 2011. A bacterium that can grow by using arsenic instead of phosphorus. Science 332: 1163-6. doi:10.1126/science.1197258

Yee, N and Fein, J. 2001. Cd adsorption to bacterial surfaces: a universal adsorption edge? Geochimica et Cosmochimica Acta 65: 2037-2042.

Yee, N. 2000. Experimental study of the pH, ionic strength, and reversibility behavior of bacteria–mineral adsorption. Geochimica et Cosmochimica Acta 64: 609-617. DOI:10.1016/S0016-7037(99)00342-7.

Chapter 3. Microbial processes facilitate shallow epithermal Au-Ag ore formation

Submitted as a separate article:
Phillips-Lander, C M, Fowle, D A, Hernandez, W, Mora, M, and Roberts, J A. (2014) Micobial processes facilitate shallow epithermal Au-Ag formation. *(to be submitted to Applied Geochemistry).*

Abstract

Epithermal ore deposits are classified into high- and low-sulfidation systems based on the mineralogy and geochemical characteristics of the hydrothermal fluids from which they form. In low-sulfidation, or circum-neutral pH (pH 5-8) hot springs, siliceous sinters and Fe-oxides dominate the mineralogy. Microbial metabolic processes are often associated with the formation of Fe-oxyhydroxides, which co-precipitate and sorb Ag, Au, As, and Sb. In sum, these processes have been implicated previously in epithermal Au and Ag ore formation, however, the influence of microorganisms in high-sulfidation systems has yet to be established.

Here we assessed the role of microbial processes in trace metal partitioning in high-sulfidation systems, using sediments collected from two acid (pH=2.6-4) sulfate springs in Las Pailas, Costa Rica. Sediments, that included visual evidence of microbial biofilms, were characterized for mineralogy, using transmission electron microscopy and x-ray diffraction, and trace metal concentration and distribution, using a modified Tessier sequential extraction. With the exception of Au (1.4-2.3mg kg^{-1}), which is exclusively associated with Fe-oxyhydroxides, Cu (3.6-563mg kg^{-1}), Ni (2.4-7.4 mg kg^{-1}), As (0.2-16 mg kg^{-1}), and Ag (3.8-13 mg kg^{-1}) preferentially adsorb to organic matter, comprised principally of exopolymeric substances (EPS), microbial cell surfaces, and Fe-oxides precipitated within EPS. We hypothesize trace metal sorption is facilitated by the development of pH microenvironments. These microenvironments are observed in both low- (neutral-chloride) and high-sulfidation (acid-sulfate) hydrothermal systems and increase charge differentials between metals and surfaces within EPS, resulting in trace metal sequestration. Consequently, higher concentrations (~10x) of metals are captured by microbial processes in neutral chloride springs, owing to the increased charge differential between positively charged metal cations and negatively charged Fe-oxides and microbial surfaces. While acid-

sulfate systems possess smaller charge differences, Au, Ag, and As concentrations in Las Pailas spring sediments are enriched by ~10x relative to average crustal abundances. Results from this study support a model in which microbial processes concentrate trace metals in both types of modern hydrothermal systems and may provide an indicator for actively forming epithermal Au-Ag-Cu deposits in stockwork veins at depth.

Introduction

Microorganisms, their metabolic processes and exudates are closely associated with the cycling of trace metals in both modern and ancient sedimentary environments (Kabata-Pendias, 2004). Microorganisms influence element cycling by influencing solution pH and redox, which may result in the mobilization or mineral sequestration of trace metals depending on mineral equilibria (Konhauser, 2006). Depending on pH conditions, microbial cell- and biofilm- surfaces may adsorb metals, effectively removing them from solution and concentrating them in microbial biomass. Microorganisms have been specifically linked to trace metal enrichments in ancient ore deposits (e.g. Brocks et al., 2005; Rainbow et al., 2006; Nelson et al., 2007). For example, the oldest well-preserved microbial biomarkers, indicative of Chlorobiaceae, green sulfur bacteria, Chromitaceae, purple sulfur bacteria, and other biomarkers suggestive of a diverse microbial community, are found in association with the Proterozoic (1.6 Ga) MacArthur River HYC Cu-Zn-Ag deposit (Brocks et al., 2005). Carbon, oxygen, and sulfur isotopes indicative of microbial metabolic processes further support the role of microorganisms in economic enrichment of trace metals, including Cu, Au, and Ag in ore deposits (Rainbow et al., 2006; Nelson et al., 2007). Ores collected from the Cenozoic Huinquintipa and Mina Sur porphyry copper deposits in the central Andes display isotopically light $\delta^{13}C$ values $\leq$ -47 $‰$ in carbonates (Nelson et al., 2007), consistent with a depleted dissolved inorganic carbon (DIC) pool resulting from carbon cycling by methanogens and methanotrophs (Nelson et al., 2007). Because some methanotrophs require high concentrations of Cu to support enzyme activity (Semrau et al., 2010) methanotrophic metabolic activity may influence the cycling and concentration of Cu (Leslie et al., 2013).

Epithermal ore deposits also display biomarkers, which suggests microbial processes may be involved in trace metal accumulation. Rainbow et al. (2006) examined the evolution of S- and O-isotopes up-section through the Miocene Pierina high-sulfidation epithermal Au-Ag deposit. The enrichment of S- and O-isotopes in near-surface (<100 m depth) barite associated with the deposits is inferred to reflect the activity of sulfur oxidizing bacteria (SOB; Rainbow et al., 2006). Epithermal ore deposits are enriched in Au, Ag, Pb, Zn, Cu, Sn, Sb, U, and Hg and typically sourced from two primary compositional end members: low- and high-sulfidation systems, which are classified by their aqueous geochemistry and mineralogy (Arribas, 1995; White and Hedenquist, 1995). Low-sulfidation spring systems are silica dominated, and connected to siliceous ore veins in the subsurface (Heald et al., 1987). Ore deposits associated with these systems are thought to form at low-temperatures (~100^{o}C), in near-neutral pH (6-8) solutions with fluid compositions predominately composed of sodium chloride, bicarbonate and hydrogen sulfide (White and Poizat, 1995). In contrast, high-sulfidation systems are dominated by vuggy quartz and disseminated Au- and Cu-rich ore in the subsurface (Heald et al., 1987). High-sulfidation epithermal deposits are associated with high temperature (100-300^{o}C), low pH (<1 to >3) solutions rich in hydrochloric and sulfuric acid (White and Poizat, 1995; White and Hedenquist, 1995). The major difference between these two end- member fluids may be the degree to which these fluids have equilibrated with the host rock (White and Poizat, 1995). The presence of active microbial populations in modern epithermal environments paired with ancient evidence for their activity in these systems suggests microorganisms may be an additional variable that contributes to trace element distribution once hydrothermal fluids cool below the upper limit of life (~121^{o}C, Kashefi et al., 2007).

Modern hydrothermal systems provide surficial access to actively forming epithermal deposits and opportunities to identify and elucidate operative processes in ore formation. Simmons and Brown (2006) reported Ag and Au bearing hydrothermal fluids at Ladolam, Papua New Guinea, an actively forming gold low-sulfidation deposit. Simmons and Brown (2006) reported similar Au-Ag rich hydrothermal fluids at depth in the Taupo Volcanic Zone, New Zealand. Siliceous sinters, precipitated from these low-

sulfidation metal-rich waters are enriched in Ag, Au, and Cu and are associated with microorganisms and microbial biofilms (Simmons and Brown, 2007). Low-sulfidation hydrothermal fluids in Yellowstone have also shown anomalously high Cu (16 mmol L^{-1}) and As (13 mmol L^{-1}) concentrations (Walker et al., 2005) indicating potential ore formation at depth. Arsenic and Sb enrichments occur also in the El Tatio hydrothermal field in Chile (Landrum et al., 2009) and in the Champagne Pool in New Zealand (Simmons and Brown, 2007).

Although microbial contributions to metal enrichment in low-sulfidation systems have been well-studied, less is known about microbial processes in high-sulfidation systems. Acid-sulfate-chloride springs in Yellowstone contain As-oxidizing microorganisms and microbial mats rich in Fe-oxides to which As adsorbs (Donahoe-Christiansen et al., 2004; Inskeep et al., 2004). One analog to high-sulfidation systems are low temperature ($\leq 25^{o}$C), low pH (typically ≤ 3) acid mine drainage systems, which also display trace metal enrichments (Torres and Auleda, 2013; Torres et al., 2013; Harris and Lottermoser, 2003). Despite differences in pH, Eh, and T conditions, the similarity in metal partitioning between acid mine drainage (AMD) systems and neutral-chloride hydrothermal systems, suggests microorganisms may sequester trace metals (Zn, Ni, Cu, As) in acid-sulfate hydrothermal systems by binding them to Fe-oxide/-oxyhydroxide minerals, including ferrihydrite, goethite, lepidocrocite, and hematite. In both cases, enrichments in Cu, Zn, Ni, As, and Sb are associated with the mineral oxide sediment fraction, operatively defined by different sequential extractions methods (Torres and Auleda, 2013; Harris and Lottermoser, 2003; Tessier et al., 1979), and interpreted as trace metal adsorption onto or co-precipitation with goethite, lepidocrocite, and hematite within the sediments (Landrum et al., 2009). Partitioning of these metals into the oxide minerals is inferred to be a microbially-driven process, where iron oxidizing bacteria (IOB) mediate Fe-oxide precipitation, followed by trace metal adsorption to the mineral precipitates from spring solutions (Landrum et al., 2009).

IOB including *Acidothiobacillus ferrooxidans*, can also form Fe-oxyhydroxysulfates such as jarosite and schwertmannite from AMD solutions (Egal et al., 2009), to which trace metals may sorb. Moreover,

sulfate reducing bacteria (SRB) reduce sulfate to sulfide, producing sulfide minerals that effectively remove trace metals including As, Cd, Cu, Fe^{2+}, Pb, Ni, and Zn from solution (Leblanc et al., 1996). Because trace metal sorption is strongly pH dependent, the minerals precipitated from AMD solutions may not adsorb significant trace metals concentrations, except where EPS influences local pH (Egal et al., 2009). The purpose of this study is to evaluate the geochemical and biological factors that influence trace metal distributions (Cu, Zn, Ag, and Au) in acid-sulfate hydrothermal system sediments and to determine whether acid-sulfate hydrothermal systems provide valuable indicators of epithermal ore deposits.

Geologic Setting

Rincón de la Vieja is an active, andesitic stratovolcano in northwestern Costa Rica formed by the subduction of the Cocos Plate beneath the Caribbean Plate (Kempter et al., 1996). The southwest flank of the volcano includes the Las Pailas hydrothermal field consisting of the fumaroles (steam vents), mudpots (water limited, clay dominated springs), and hot springs of Rincón de la Vieja National Park. Giggenbach and Soto (1992) demonstrated that spring waters in Las Pailas were derived from a single large hydrothermal reservoir that is variably mixed with meteoric fluids. As a result, fluid composition within the springs remains relatively constant throughout the dry season as indicated by the similarity between our analyses and Giggenbach's results (Phillips-Lander et al., 2014). This report will focus on two of these springs, Pailas de Agua I and II, which are high temperature (80-89^{o}C), low pH (2.6-4.0), sulfate-(15 -38mmol L^{-1}) dominated hot springs (Phillips-Lander et al., 2014). While there is very little Mg present (0.1-0.7 mmol L^{-1}), Fe (2.5-7.0 mmol L^{-1}), Al (0.1-15 mmol L^{-1}), and Si (3.5-8.2 mmol L^{-1}) are abundant (Phillips-Lander et al., 2014).

The Las Pailas system is microbially-active, with documentation of microorganisms and microbial metabolic guilds including *Euglena pailasensis* (Sittenfeld et al., 2006), Cyanidium, Galderia-like algae, 15 different phylotypes of methanogenic Archaea (Hernandez, 2012), several strains of cyanobacteria (Finsinger et al., 2008) and the presence of *Acidothiobacillus caldus*, a moderately thermotolerant sulfur oxidizing bacterium (Semenez et al., 2002).

Previous studies of Pailas de Barro, a mudpot within the Las Pailas vent field, have shown that weathering products include kaolinite, quartz, α-cristobalite, anatase, rutile, hematite, and α-tridymite (Gehring et al., 1999). Electron paramagnetic resonance spectroscopy of Pailas de Barro sediments indicated that Fe and V were found in association with Fe-oxides and clay minerals. Copper, in contrast, was observed to be structurally bound to opal-C (Gehring et al., 1999). Previous reports of Cu and V in the spring sediments and previous characterization of some of the microbial ecology of Las Pailas makes this hydrothermal system ideal for investigating trace metal enrichment and potential microbial mechanisms involved in active epithermal systems.

Methods

Samples were collected from two springs, Pailas de Agua I (PDA I) and Pailas de Agua II (PDA II) in March 2009. Sediment samples were collected in sterile bags, from multiple locations within each hot spring, including evaporative crusts, as well as sediments associated with microbial biofilms and each spring basin and source. These samples were kept at 4°C during transport. Upon return to the laboratory, sediment subsamples were freeze-dried to prevent significant alteration of the mineralogy, powdered to clay-sized particles (0.0039 mm) and homogenized for all analyses. Mineralogy was determined using a Bruker SMART APEX II X-ray Diffractometer with a copper charge coupled detector (CCD). Subsamples were epoxy impregnated and sectioned for transmission electron microscopy analysis using an FEI Tacnai F20 XT field emission transmission electron microscope (TEM) to determine the metals distribution and association with mineralogy within the sediments. Additional subsamples of the freeze-dried sediments were powdered, homogenized, and weighed into 100 mg aliquots. The concentrations and operationally-defined availability of trace metals in Las Pailas hydrothermal sediments were determined using a modified Tessier et al. (1979) sequential extraction. The selective extraction of the sediment was conducted as follows (Suppl. Table 1):

(a) Exchangable fraction (operationally defined as weakly-sorbed metal species, including ion exchange species and metals bound through weak electrostatic interactions)- 1 M Ammonia Acetate solution adjusted to pH 8.2 was reacted for 30 minutes at 25^{o}C with continuous agitation;

(b) Acid-soluble fraction (typically considered to be metals specifically bound to carbonates; however, Gleyzes et al. (2002) noted metals recovered in this fraction are specifically bound to minerals that are sensitive to pH changes, including clays, Fe-oxyhydroxides, some sulfide and sulfate minerals)- 1 ml of 4% Acetic acid (HAc) was reacted for 2 hours at 25^{o}C;

(c) Fe/Mn-oxyhydroxide fraction (defined as metals specifically bound to redox sensitive minerals, including Fe-oxide and -oxyhydroxide minerals, though some sulfide minerals may also be included in this fraction (Peltier et al., 2005)- 0.04 M NH_2OH-HCl in 25% v/v HAc 12 hours at 96^{o}C under constant agitation. Samples were then cooled for 1 hour before the supernatant was removed;

(d) Organic fraction (metals are bound to fulvic and humic acids, living organisms, EPS, and possibly some carbohydrates, proteins, and amino acids; Gleyzes et al., 2002)- 0.02 M HNO_3 and 30% H_2O_2 adjusted to pH 2 followed by 3.2 M Ammonia Acetate in 20% v/v HNO_3 for 5 hours at 85^{o}C and then 1 hour at room temperature;

(e) Residual fraction (metals structurally bound in silicate minerals)- 1:1 HF and distilled HNO_3 for 24 hours at 85-95^{o}C;

Sediments were washed three times with distilled deionized water between each step and the supernatant was removed and added to the associated fraction. Each extract was resuspended in high purity, concentrated nitric acid and analyzed on Perkin Elmer ICP-OES Optima 5300 DV ICP-OES to determine major and trace metal concentrations bound in each operationally defined fraction.

Results

Mineralogy

Sediment mineralogy and trace element geochemistry were characterized using XRD (Figures 1 and 2) and analyzed using ICP-OES (Table 1), respectively. Green biofilms exist beneath the surface of the

sediments in Pailas de Agua I (PDA I-1) mat sediments, as shown in the inset image (Figure 1A). These biofilm associated sediments were sampled by scraping away surficial sediments until the biofilm was visible (highlighted in the black box of Figure 1A). PDA I samples 2-4 were collected from sediments associated with a series of closely spaced (~2-3 cm) tri-colored pools, which are distinguished in the field by their color (gray=PDA I-2, red=PDA I-3, and brown=PDA I-4 respectively; Figure 1B). XRD analysis of samples collected from PDA I (1-4) indicates the mineralogy is dominantly smectite, kaolinite, ferrihydrite, jarosite, and quartz (Figure 1C and D). The mat sediment in PDA I-1 also contains bandylite (a Cu-borate) and uvanite (a U-V hydrated oxide phase; Figure 1C), which are not present in the other sample locations.

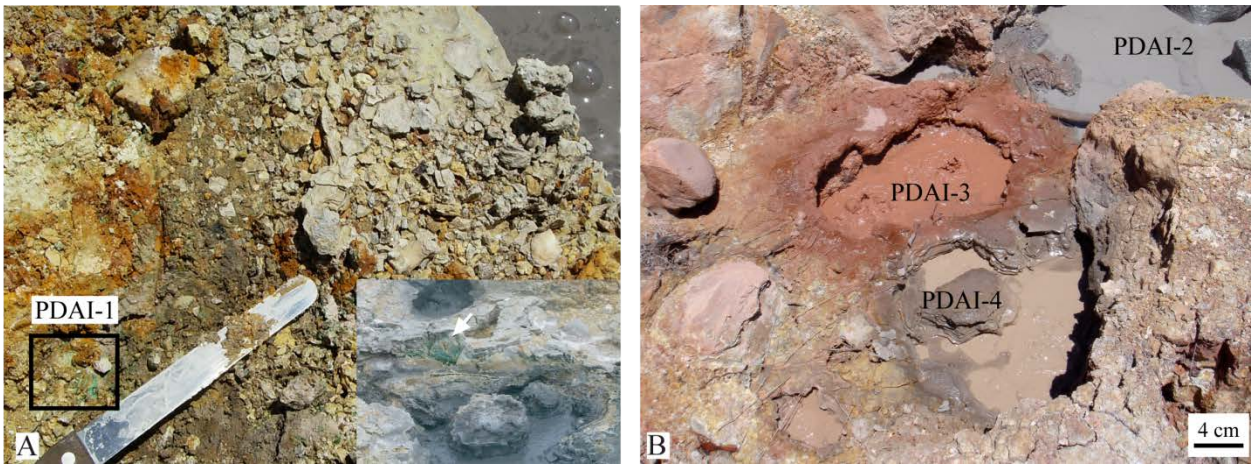

Figure 1A/B: Location and Mineralogy of Samples collected from Pailas de Agua I: (A) Sample location for PDA I mat sediments (PDA I-1) with a spatula for scale. Samples were taken from the green endolithic biofilm is present just below the surface (inset image; PDA I-1) and is highlighted by the black box (main image). Microbiology described for the Las Pailas system was largely cultured from this sample location, unless otherwise noted. (B) Tri-colored pools within Pailas de Agua I, representing samples PDA I-2-4. The red and brown pools are small (~0.5 m in diameter), while the gray pool is part of the main spring body and encompasses an area of ~10 m by 15m.

In Pailas de Agua II (PDA II), samples were collected from sediment associated with a green biofilm near the edge of the spring (biofilm sediments= PDA II-1; Figure 2A) and from the sediment crusts present over the solution in the pool (mineral crust=PDA II-2; Figure 2B). Both samples collected from PDA II

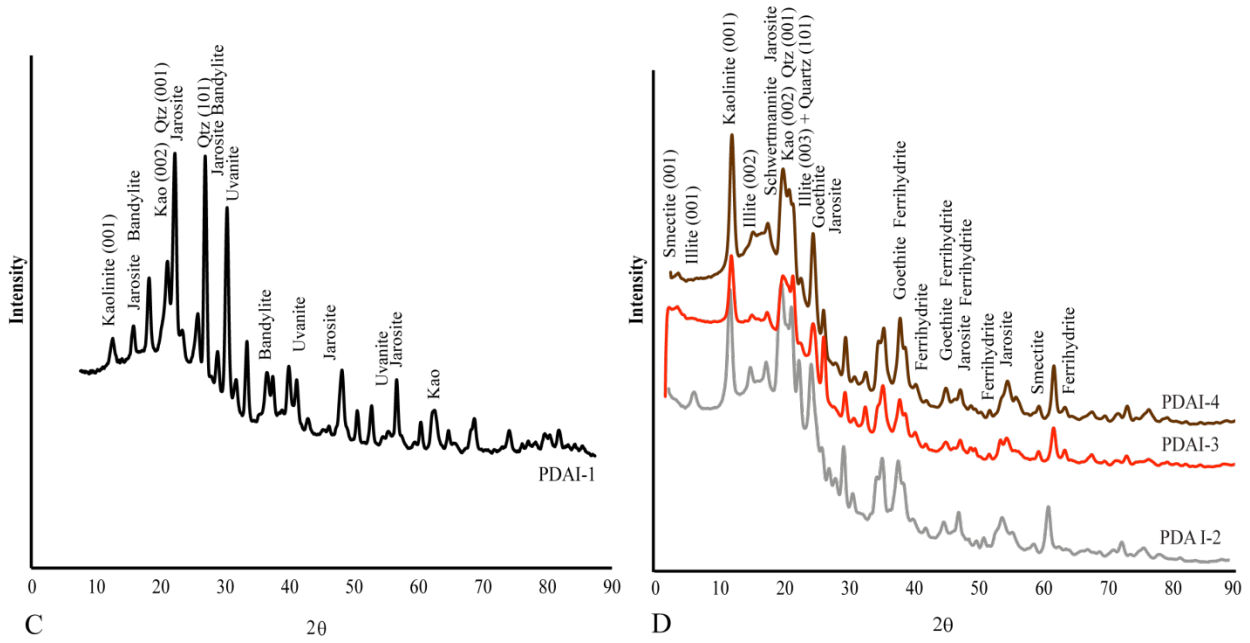

Figure 1C/D: (C) XRD of PDA I-1 indicates the presence of bandylite and uvanite associated with the biofilm, in addition to mixed layer smectite, ferrihydrite, and jarosite. (D) X-ray diffraction analysis (XRD) of tri-colored pools (PDA I-2-4). Lines are color coded to match spring solutions. Despite changes in color, the mineralogy between the pools is similar.

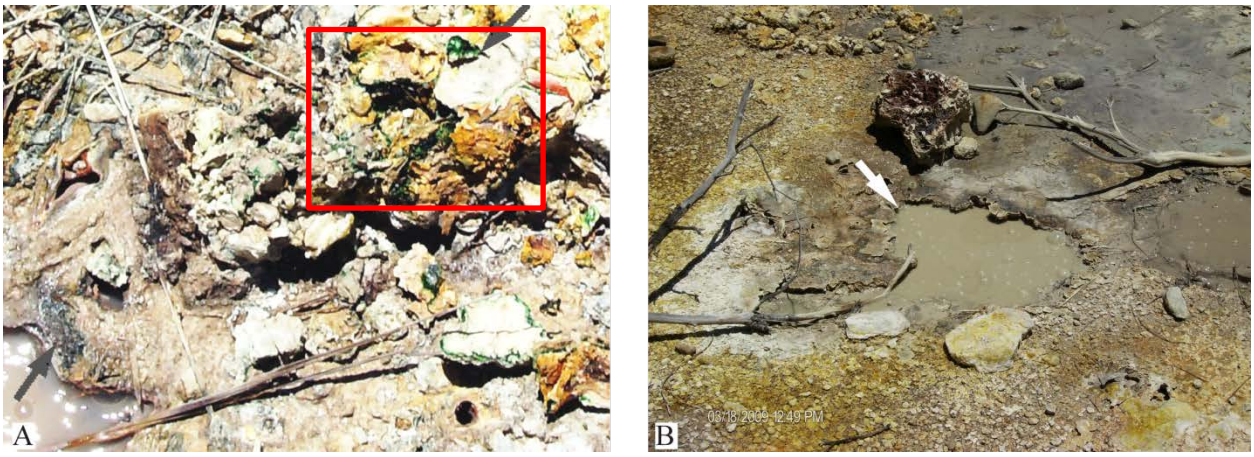

Figure 2A/B: Location and Mineralogy of Samples collected from Pailas de Agua II: (A) Green endolithic biofilm associated sediments sampled and recorded as PDA II-1. Red box indicates the sampling location. (B) PDA II's mineral crust, sample PDA II-1, were taken from the crusts that cover the edges of the pool.

contain mixed-layer smectites, kaolinite, and jarosite (Figure 2C and D). Schwertmannite is present in the biofilm sediments of PDA II-1(Figure 2C), while gypsum is present in PDA II-2 mineral crusts (Figure 2D).

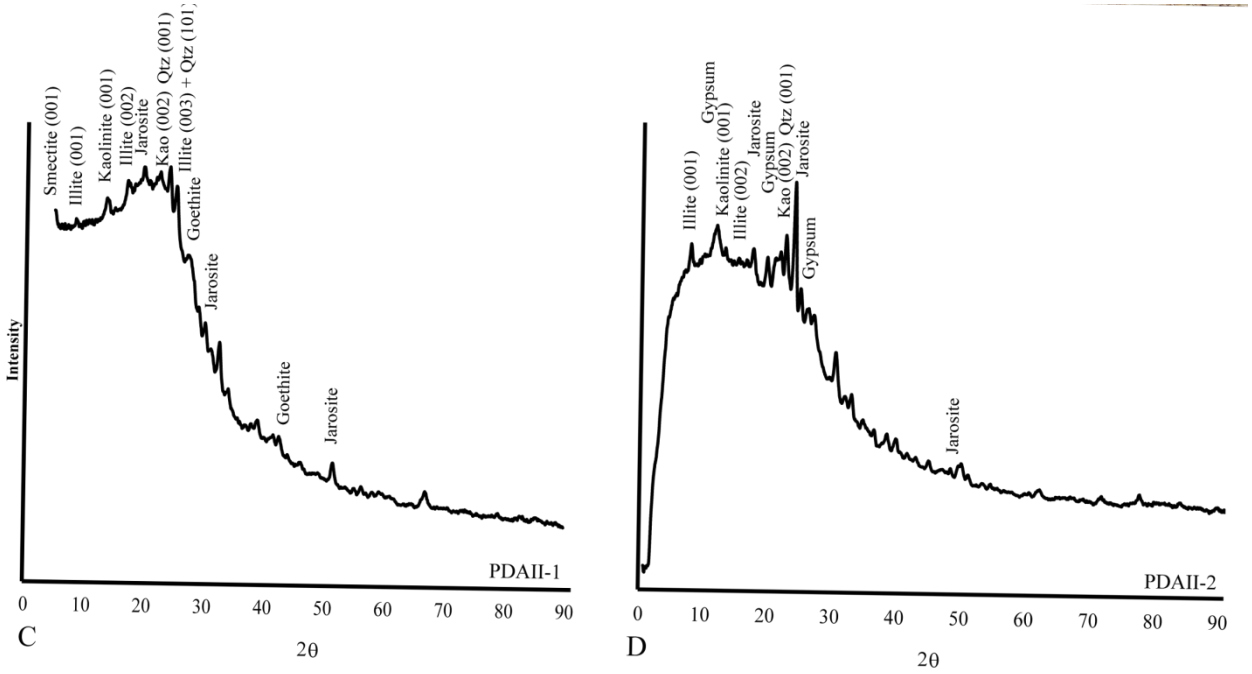

Figure 2C/D: Mineralogy of Samples collected from Pailas de Agua II: (C) XRD analysis of PDA II-1, showing a diversity of clay, sulfate and oxide minerals. (D) XRD of PDA II-1 indicates the presence of clays and sulfate minerals.

Metal Partitioning in Las Pailas

Selected trace metal concentrations from PDA I and II sediments are summarized in Table 1. Sulfur concentrations in these sediments are 280-370 mmol kg^{-1} (S=8,800-12,000 mg kg^{-1}). Although phosphate concentrations are below detection limits in PDA I and II spring waters, ample P is present in the sediments of PDA I and II, ranging from 3-4 mmol kg^{-1} (P=93-120 mg kg^{-1}). Vanadium and Cu sediment concentrations range from 6.2-87 mg kg^{-1} and 3.6-38 mg kg^{-1}, respectively. Arsenic and Sb sediment concentrations range from 0.2 mg kg^{-1} and Sb 1.7-3.0 mg kg^{-1}, respectively (Table 1). Silver and gold are also present in low concentrations, ranging from 0-0.1 mmol kg^{-1} (Ag=0-13 mg kg^{-1}) and 0-2.3 mg kg^{-1} Au, respectively. Bulk partition coefficients between the sediments and hydrothermal solutions in PDA I and II were calculated and trace metals, with the exception of Zn, preferentially partition from the

solution into the sediment at all sites (Figure 3). Copper tends to more strongly complex with organic matter than Zn, which may explain Zn's weaker sorption (McBride and Blasiak, 1979).

Table 1: Total Metals in Sediment

	B	S	V	Fe	P	Au	Cu	Zn	As	Ni	Ag	Sb	Pb
Pailas de Aguas II													
Sample 1	bdl	11687.57	86.66	940.71	123.06	bdl	10.51	5.91	15.62	2.77	4.41	2.64	27.10
Sample 2	0.11	10505.79	9.02	360.41	110.62	1.37	3.56	bdl	14.02	2.41	4.53	1.69	30.05
Pailas de Aguas I													
Sample 3	bdl	9594.74	6.22	2354.17	101.02	1.67	38.43	12.07	0.15	7.42	12.64	2.57	29.16
Sample 4	0.18	9413.90	35.05	1903.19	99.12	2.33	56.33	5.49	13.29	5.27	4.53	3.57	25.39
Sample 5	bdl	8791.77	21.95	507.18	92.57	bdl	44.97	bdl	10.92	3.55	3.87	2.65	25.49
Sample 6	bdl	11445.90	16.30	1346.78	120.51	bdl	18.24	3.12	14.41	3.15	3.84	2.98	26.53

*values in $mgkg^{-1}$

*bdl= below detection limits; Detection limits for B= $1.0x10^{-1}$-$1.0x10^{-2}$ mg kg^{-1}; Au=$1.0x10^{-2}$-$1.0x10^{-3}$ mg kg^{-1}; Zn= $1.0x10^{-1}$-$1.0x10^{-2}$ mg kg^{-1}

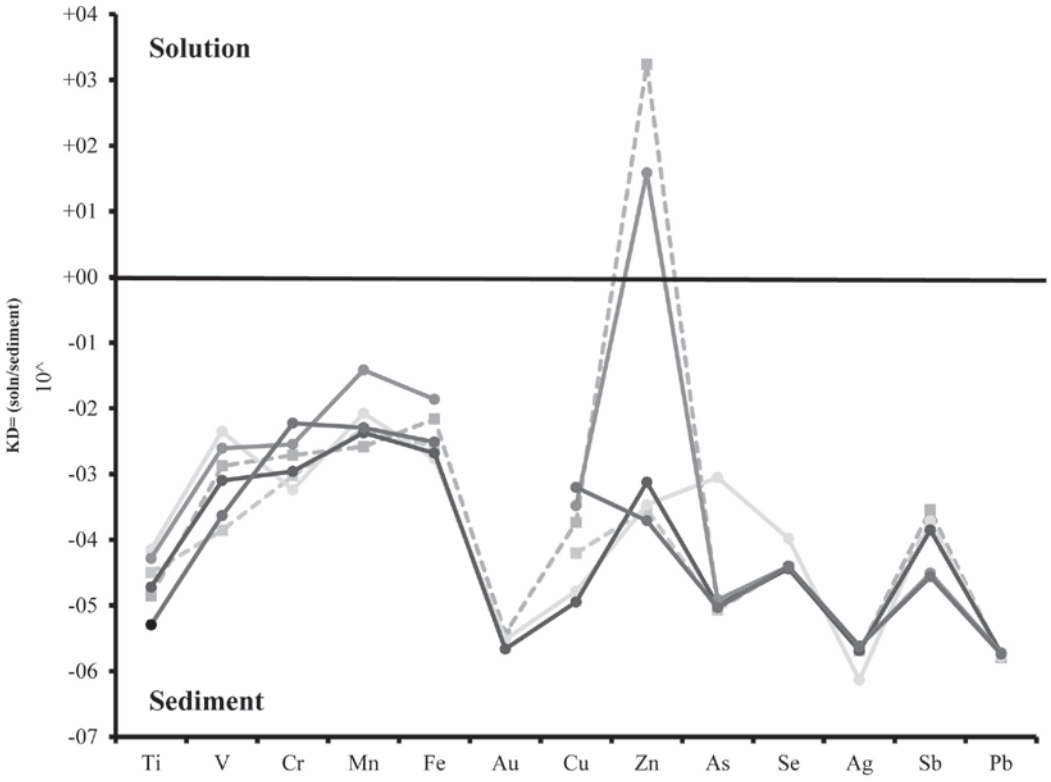

Figure 3: Trace Element Partitioning between Water and Sediments in PDA I and II: Trace elements, with the exception of Zn, partition into the sediment fraction. Dashed lines are data from PDA II. Solid lines are based on data from PDA I.

Metal Distribution in Sediments

Sequential extraction has been extensively used to quantify the mobility of trace metals within sediments. Traditionally sequential extraction techniques have been used to determine the mobility of toxic metals in environmentally contaminated soils (Tessier et al., 1979; Gleyzes, et al., 2002), however the application has been extended to understand the distribution of trace elements in AMD and hydrothermal systems (Gleyzes et al., 2002; Torres and Auleda, 2013). Sequential extraction results for PDA I and II are presented in Table 2.

Major Element Distribution

Sulfur and Fe are present in both the hot spring solutions and sediments in PDA I and II (Figure 2; Phillips-Lander et al., 2014) and therefore, may represent major components within the carbonate/sulfate and Fe-oxide sediment fractions. Therefore, the distribution of Fe and S in the sediments was characterized using sequential extraction.

Table 2: Sequential Extraction of Las Pailas Sediments (mg/kg)

Sample	Fe					S				
	Exchangeable	Carbonate	Oxide	Organic	Residual	Exchangeable	Carbonate	Oxide	Organic	Residual
Pailas de Aguas II										
Sample 1	20.61	2.98	287.52	1.23	5.32	3609.47	7.01	317.19	88.83	0.64
Sample 2	62.88	7.28	1.97	0.18	0.00	12011.61	485.74	62.51	bdl	0.01
Pailas de Aguas I										
Sample 3	21.74	7.19	12.86	455.74	1.91	2477.88	33.06	121.12	11536.55	2.29
Sample 4	119.38	8.09	11.64	15.31	0.24	18014.41	4.71	147.30	1074.31	63.37
Sample 5	9.34	7.42	65.21	27.30	4.12	bdl	bdl	28.60	703.56	0.02
Sample 6	17.16	6.88	38.62	29.47	0.06	1248.80	399.35	bdl	674.22	0.05

*Dectection limits for Fe<$1x10^{-4}$ mg kg-1; S=$1x10^{-2}$-$1x10^{-3}$ mg kg^{-1}

Sulfur. Sulfur is abundant within Las Pailas spring system sediments. Sulfur is weakly adsorbed within the exchangeable fraction in the PDA I-2 (93%; 18,000 mg kg^{-1}) and the PDA I-4 (54%; 1,300 mg kg^{-1}) sediments (Table 2; Figure 4A). In PDA I-4, 29% (670 mg kg^{-1}) of S is bound to organic matter and 21% (400 mg kg^{-1}) is bound to sulfates. Organic matter binds the majority of S in PDA I-1 (81%; 12,000 mg kg^{-1}) and PDA I-3 (96%; 700 mg kg^{-1}). In PDA II (1-2), $\geq$90% of the total S in the sediments is sorbed to the exchangeable fraction (Table 2; Figure 4A).

Iron. Iron is found in all sediment fractions of PDA I and II (Table 2; Figure 4B). In PDA I-1, 91% (460 mg kg^{-1}) of the total Fe in the sediments is bound in the organic fraction (Table 2; Figure 4B). The remaining 9% is distributed between the exchangeable (4.4%; 22 mg kg^{-1}), carbonate/sulfate (1.4%; 7.2 mg kg^{-1}), oxide (2.6%; 13 mg kg^{-1}), and residual/silicate (0.4%; 1.9 mg kg^{-1}) fractions. In contrast, 77% (120 mg kg^{-1}) of the total Fe weakly sorbed to mineral surfaces in the PDA I-2 sediments (Table 2; Figure 4B). Organic matter binds 10% (15 mg kg^{-1}) and Fe-oxides/-oxyhydroxides bind 7.5% (12 mg kg^{-1}). The remaining 0.5% of Fe in PDA I-2 is bound to sulfate minerals. Approximately half of the Fe in PDA I-3 sediments (58%; 65 mg kg^{-1}) is bound to Fe-oxides/oxyhydroxides and organic matter present binds 24% (27 mg kg^{-1}) of the total Fe (Table 2; Figure 4B). In PDA I-2, ~8% (9.3 mg kg^{-1}) is sorbed in the exchangeable fraction, 6.5% (6.9 mg kg^{-1}) is bound to sulfates, and 3.5% (4.1 mg kg^{-1}) is bound to silicates. In PDA I-4, 42% (39 mg kg^{-1}) is bound to Fe-oxides/-oxyhydroxides and 32% (30 mg kg^{-1}) is bound to organic matter. Of the remaining 26%, the majority of Fe is present in the exchangeable fraction (19%; 17 mg kg^{-1}), while the remaining 7% (6.9 mg kg^{-1}) is bound to sulfates.

In PDA II-1, Fe-oxides/-oxyhydroxides binds 91% (290 mg kg^{-1}) of the total Fe (Table 2; Figure 4B). Of the remaining 9% Fe in PDA II-1sediments, 6% (21 mg kg^{-1}) is weakly sorbed to the sediment exchangeable fraction, 2% (5.3 mg kg^{-1}) is bound to silicates, and 1% (3.0 mg kg^{-1}) is bound to sulfate minerals. Less than 1% of the Fe in PDA II-1 is bound in the organic fraction. Ten percent (7.3 mg kg^{-1}) of the Fe in PDA II-1 sediments is bound as Fe-oxides/-oxyhydroxides. In contrast, Fe in PDA II-1, partitions primarily into the exchangeable fraction (86%; 63 mg kg^{-1}). The remaining Fe in PDA II-2 is bound to (3%; 2.0 mg kg^{-1}) organic matter, and ($7.2x10^{-4}$ mg kg^{-1}) silicates (Table 2; Figure 4B).

Weakly sorbed trace metals

Zinc. The total concentration of Zn present in the springs is 3.1-12 mg kg^{-1} (Table 1). No Zn was detected in PDA I-3 and PDA II-2 (Table 3; Figure 5A). In contrast, nearly 100% (5.5 mg kg^{-1}) of the total Zn present in PDA I-2 sediments was observed in the exchangeable fraction, with minor Zn ($5.3x10^{-2}$ mg kg^{-1}) bound within the residual fraction. Similarly, 74% (2.3 mg kg^{-1}) of the 3.1 mg kg^{-1} of Zn present in

PDA I-4 sediments partition into the exchangeable fraction, while 26% (0.8 mg kg^{-1}) is bound to Fe-oxides. In PDA I-1, the majority of Zn (86%; 11 mg kg^{-1}) is bound to Fe-oxides, while 14% (1.7 mg kg^{-1})

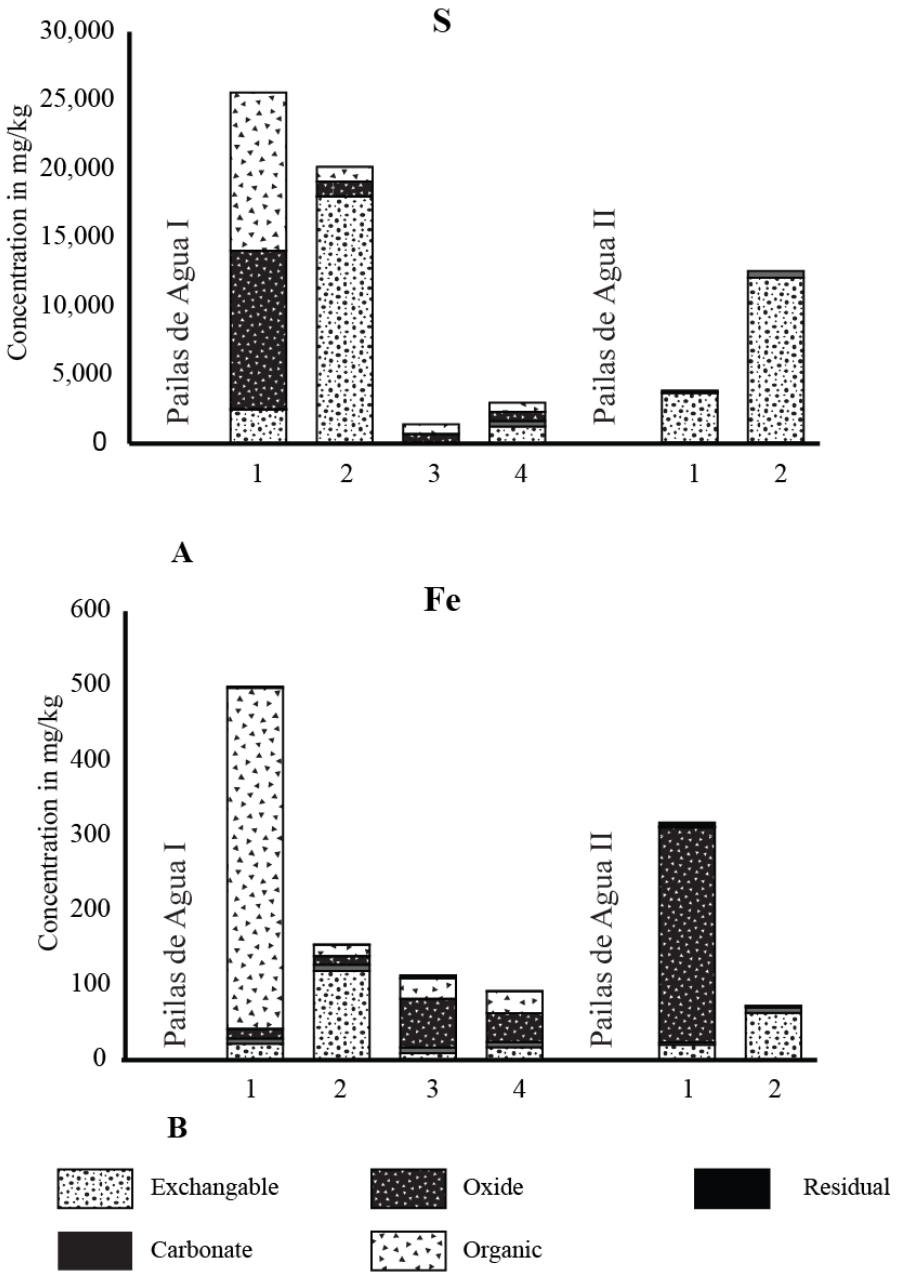

Fig. 4.

Figure 4: Elemental partitioning between fractions: (A) Sulfur primarily partitions into the exchangeable fraction, with the exception of PDA I mat sediments where sulfur is primarily present in the oxide and organic fractions. (B) Iron partitions primarily into the oxide fraction, with the exception of PDA I mat sediments, where iron is primarily in the organic fraction.

is weakly adsorbed within the exchangeable fraction. Less than 1% (1.3x10-3 mg kg^{-1}) of Zn is structurally bound in silicates present in PDA I-1. In PDA II-1, nearly 100% (6.0 mg kg^{-1}) of total Zn in the sediments is bound to Fe-oxides in the spring, with minor Zn ($1.2x10^{-3}$ mg kg^{-1}) bound within silicates.

Trace metals bound to oxides

Gold. In PDA I and II, Au concentrations range from bdl-2.4 mg kg^{-1} (Table 1). Gold is exclusively found in association with oxide minerals in these springs, where it is present (Table 3; Figure 5B).

Table 3: Sequential Extraction of Las Pailas Sediments (mg/kg)

Sample	Zn					Au				
	Exchangeable	Carbonate	Oxide	Organic	Residual	Exchangeable	Carbonate	Oxide	Organic	Residual
Pailas de Aguas II										
Sample 1	bdl	bdl	5.94	bdl	0.00	bdl	bdl	bdl	bdl	bdl
Sample 2	bdl	bdl	bdl	bdl	bdl	bdl	bdl	1.37	bdl	bdl
Pailas de Aguas I										
Sample 3	1.69	bdl	10.46	bdl	0.00	bdl	bdl	1.67	bdl	bdl
Sample 4	5.47	bdl	bdl	bdl	0.05	bdl	bdl	2.34	bdl	bdl
Sample 5	bdl	bdl	bdl	bdl	bdl	bdl	bdl	bdl	bdl	bdl
Sample 6	2.33	bdl	0.80	bdl	bdl	bdl	bdl	bdl	bdl	bdl

*Dectection limits for Zn detection limits=$1x10^{-4}$-$1x10^{-3}$ mg kg^{-1}, Au detection limits=$1x10^{-4}$-$1x10^{-3}$ $mgkg^{-1}$.

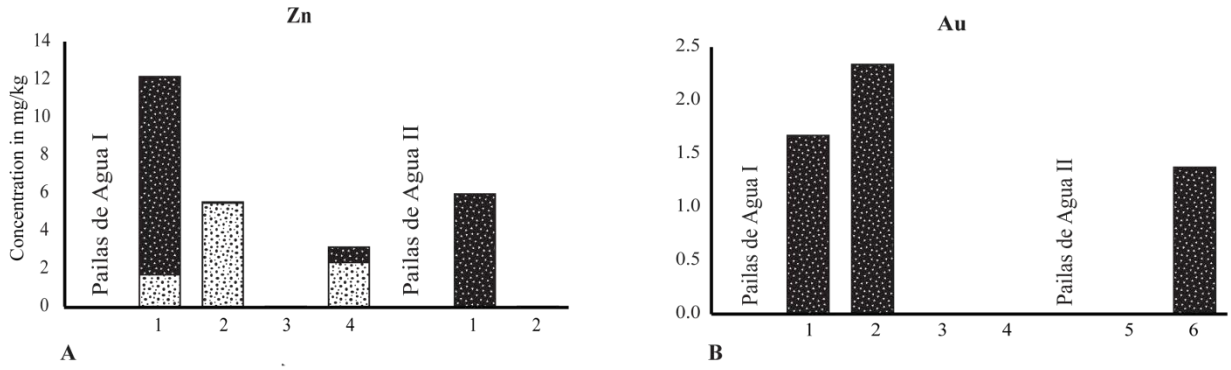

Figure 5A/B: Distribution of trace metals in Pailas de Agua fractions: (A) Zinc primarily partitions into the exchangeable and oxide fractions. (B) Gold partitions into the oxide fraction.

Trace metals bound within organic matter

Copper. In PDA I and II's sediments, Cu is observed in each fraction. The majority of Cu is present in the organic fraction and lesser concentrations are observed in the exchangeable, carbonate/sulfate, oxide, and residual fractions. The majority (74%; 28 mg kg^{-1}) of Cu present in PDA I-1 is bound in the organic matter. The remaining 26% is divided between Cu weakly adsorbed in the exchangeable fraction (15.5%;

6.0 mg kg^{-1}) and Cu bound to Fe-oxides (11%; 4.0 mg kg^{-1}). Less than 1% of Cu present in PDA I-1 sediments is structurally bound to silicates in the residual fraction (Table 4; Figure 5C). A similar distribution of Cu is observed in PDA I-2 with 69% (39 mg kg^{-1}) of the Cu bound to organic matter, 20% (11 mg kg^{-1}) weakly adsorbed in the exchangeable fraction, and 12% (6.4 mg kg^{-1}) bound to Fe-oxides/-oxyhydroxides (Table 4; Figure 5C). The organic fraction of the red sediments of PDA I-3 sediments bound 69% (31 mg kg^{-1}) of Cu, while 31% (14 mg kg^{-1}) is bound to Fe-oxides/-oxyhydroxides (Table 4; Figure 5C). In PDA I-4 sediments, 79% (15 mg kg^{-1}) of the Cu is bound to organic matter, 13% (2.4 mg kg^{-1}) of the Cu is weakly adsorbed in the exchangeable fraction, and 12% (6.4 mg kg^{-1}) of the Cu is bound to Fe-oxides/-oxyhydroxides.

Copper is nearly evenly distributed between the exchangeable (2.2 mg kg^{-1}; ~22% of total Cu), oxide (4.3 mg kg^{-1}; ~40% of total Cu), and organic fractions (4.0 mg kg^{-1}; ~38% of total Cu) in PDA II-1 sediments (Table 4; Figure 5C). In PDA II-2, 83% (3.0 mg kg^{-1}) of the total Cu in the sediment is bound in the organics. Copper weakly adsorbed in the PDA II-2 exchangeable fraction constitutes 12% (0.4 mg kg^{-1}), while 4% (0.2 mg kg^{-1}) is bound to Fe-oxides/-oxyhydroxides.

Table 4: Sequential Extraction of Las Pailas Sediments (mg/kg)

Sample	Cu					As				
	Exchangeable	Carbonate	Oxide	Organic	Residual	Exchangeable	Carbonate	Oxide	Organic	Residual
Pailas de Aguas II										
Sample 1	2.24	bdl	4.29	3.96	0.02	bdl	bdl	2.88	12.74	bdl
Sample 2	0.44	bdl	0.15	2.97	bdl	bdl	bdl	bdl	14.02	bdl
Pailas de Aguas I										
Sample 3	5.97	bdl	4.02	28.43	0.00	bdl	bdl	0.15	bdl	bdl
Sample 4	10.73	bdl	6.73	38.67	0.19	bdl	bdl	bdl	13.29	bdl
Sample 5	bdl	bdl	13.88	31.09	0.00	bdl	bdl	bdl	10.92	bdl
Sample 6	2.36	1.04	0.37	14.48	0.00	bdl	bdl	0.54	13.88	bdl

*Detection limits for Cu=$1x10^{-4}$-$1x10^{-3}$ mg kg^{-1}; As=$1x10^{-3}$-$1x10^{-2}$ mg kg^{-1}

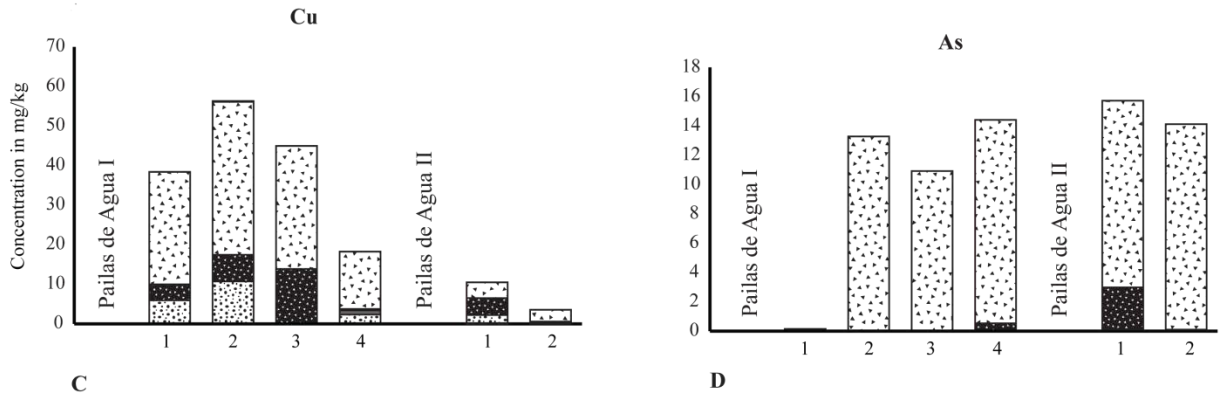

Figure 5C/D: Distribution of trace metals in Pailas de Agua fractions: (C) Cu is primarily distributed in the organic fraction of the sediments, although some Cu is present in oxide and exchangeable fractions. (D) In contrast, As is almost exclusively present in the organic fraction, with only minor As in the oxide fraction.

Sectioned subsamples from PDA I-1 and PDA II-1 mat sediments were examined using TEM in order to observe associations between trace metals, minerals, and native biological materials in Las Pailas. These analyses revealed Cu bound to individual cells, as well as within heavily mineralized biofilms. Mat sediments from PDA I-2 show clay minerals and nanoscale Fe-oxides present (Figure 6A). EDS point spectra of the nanoscale Fe-oxides associated with the mineralized biofilm are composed of are Fe and Cu

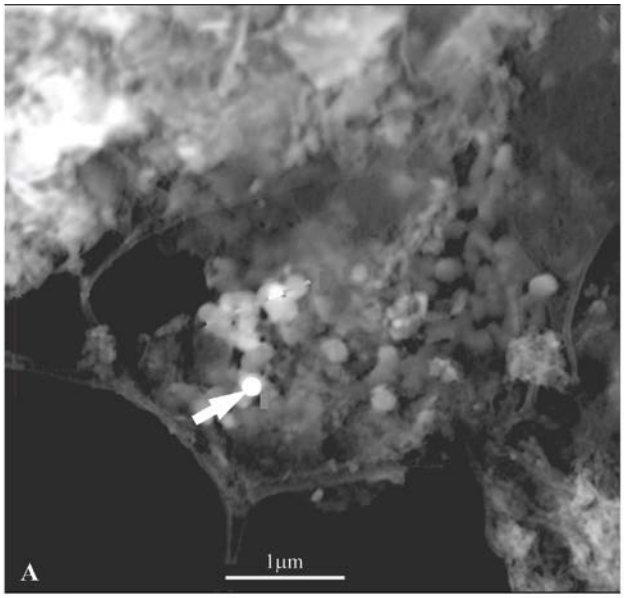

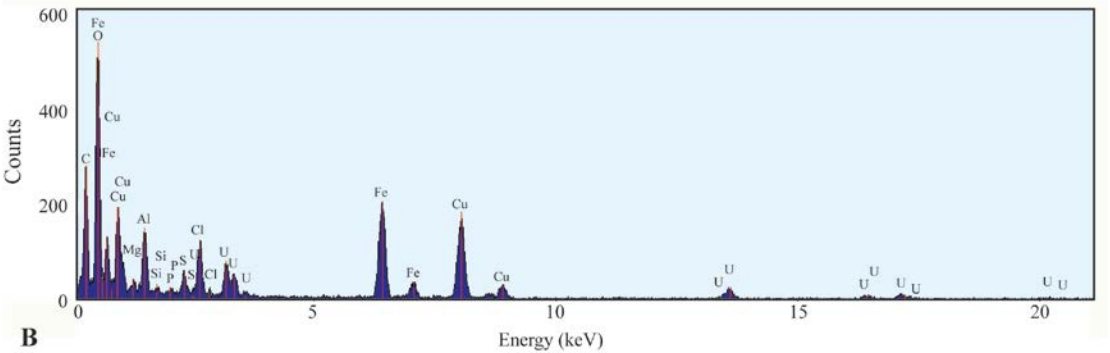

Figure 6: Transmission electron microscopy image of trace metals bound to Fe-oxides/-oxyhydroxides within microbial EPS in PDA I mat sediments: (A) EPS associated with mixed-layer smectites and iron, copper, and uranium oxides. Arrow indicates the location of the EDS point spectra obtained for the sample. (B) EDS point spectrum of A, showing the elemental distribution.

(Figure 6B). Microorganisms were observed as individual cells and filaments, associated with mineralized biofilms in PDA II-2 (Figure 7A). Copper concentrations are elevated in association with the coccus and filamentous microorganisms as shown by the bright areas in C (red) and Cu (blue) on X-ray dispersive spectra maps (Figure 7B). The copper concentration in the sample is 3.4% by weight after background and instrument corrections. Aluminum and Si are primarily associated with clay minerals present near the edges of the sample (Figure 7B).

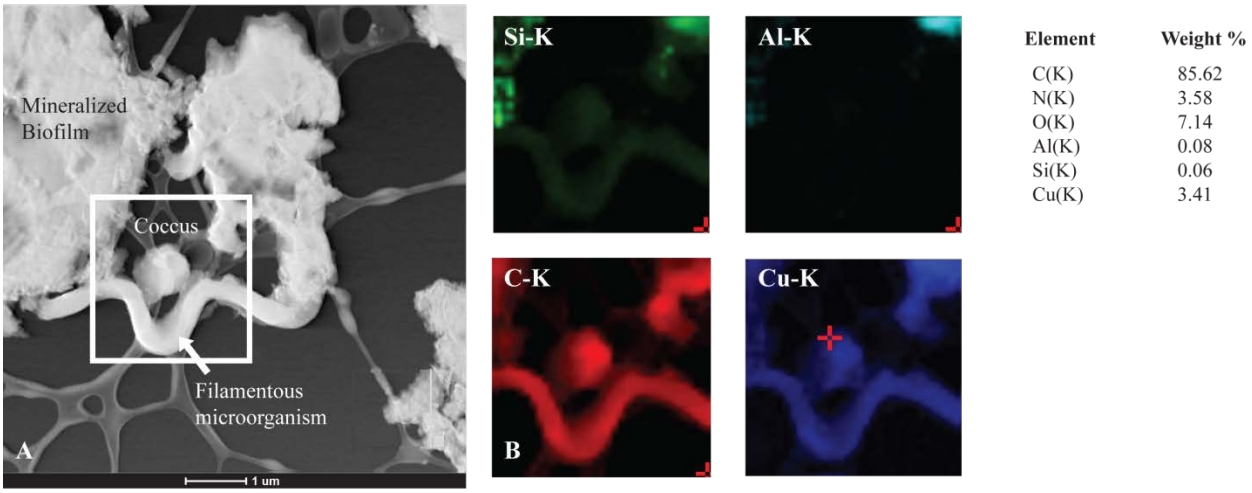

Figure 7: Transmission electron microscopy image of microorganisms in PDAII. The white box indicates the location of EDS mapping of trace elements. Each image is background subtracted to help determine enrichment over background. Microorganisms bind trace metals to cellular surfaces in PDA II mat sediments. Microbial cells, in this case a filament and cocci, bind Cu in PDA II (A). The red box in A indicates the location of the EDS maps shown in (B), while the white box indicates the area selected for background subtraction from the obtained EDS spectra acquired. These maps (B) shows microbial cell surfaces and biofilms, indicated by C and N signals, binds 3.41% weight percent Cu.

Arsenic. Total concentrations of As range from 0.2-16 mg kg^{-1} in PDA I and II (Table 1; Figure 5D). Arsenic is only present in the oxide and organic fractions of PDA I and II (Table 4). In PDA I-1, 100% of the total As (0.2 mg kg^{-1}) is bound to Fe-oxides and –oxyhydroxides. In PDA I-4, ~4% (0.5 mg kg^{-1}) of the total As is bound to Fe-oxides, while the majority (96%; 14 mg kg^{-1}) of the total As is bound within the organic fraction. All As present in PDA I-2, I-3, and PDA II-1 sediments is bound to organic matter present in the sediments. In Pailas de Agua II-1, 17.5% (2.9 mg kg^{-1}) of the 16 mg kg^{-1} total As is bound

to Fe-oxides and -oxyhydroxides, while the remaining 13 mg kg^{-1} (81.5%) is bound within the organic fraction. (Table 4; Figure 5D). The remaining 82% (13 mg kg^{-1}) is bound within the organic fraction.

Silver. The concentration of Ag in PDA I and II ranges from 4-13 mg kg^{-1}. The majority (>90%) of Ag in PDA I and II is bound to organic matter, with 100% of Ag in PDA I-1, -3 and -4 sediments and PDA II-1 is bound to organic matter. In PDA I-2, 92% (4.18 mg kg^{-1}) of Ag present in the sediment is bound to organic matter with ~8% (0.35 mg kg^{-1}) of the total Ag bound to Fe-oxides/-oxyhydroxides and <1% ($4.10x10^{-4}$ mg kg^{-1}) of total Ag structurally bound within silicates (Table 2; Figure 5E). In PDA II-2 minor concentrations (~5% of total Ag; 0.25 mg kg^{-1}) are bound to Fe-oxide/-oxyhydroxide minerals and <1% ($2.97x10^{-5}$ mg kg^{-1}) are structurally bound within silicates (Table 2; Figure 5E); 95% (4.29 mg kg^{-1}) are bound to organics.

Table 5: Sequential Extraction of Las Pailas Sediments (mg/kg)

Sample	Ag					Ni				
	Exchangeable	Carbonate	Oxide	Organic	Residual	Exchangeable	Carbonate	Oxide	Organic	Residual
Pailas de Aguas II										
Sample 1	bdl	bdl	bdl	4.41	bdl	bdl	bdl	0.33	2.43	bdl
Sample 2	bdl	bdl	0.24	4.29	0.00	0.15	bdl	0.04	2.22	bdl
Pailas de Aguas I										
Sample 3	bdl	bdl	bdl	12.64	bdl	1.61	bdl	0.11	5.70	bdl
Sample 4	bdl	bdl	0.35	4.18	0.00	2.22	bdl	0.28	2.77	0.00
Sample 5	bdl	bdl	bdl	3.87	bdl	0.14	bdl	0.22	3.19	bdl
Sample 6	bdl	bdl	bdl	3.84	bdl	0.21	bdl	0.11	2.83	bdl

*Detection limits for Ag=$1x10^{-4}$-$1x10^{-3}$ mg kg^{-1}

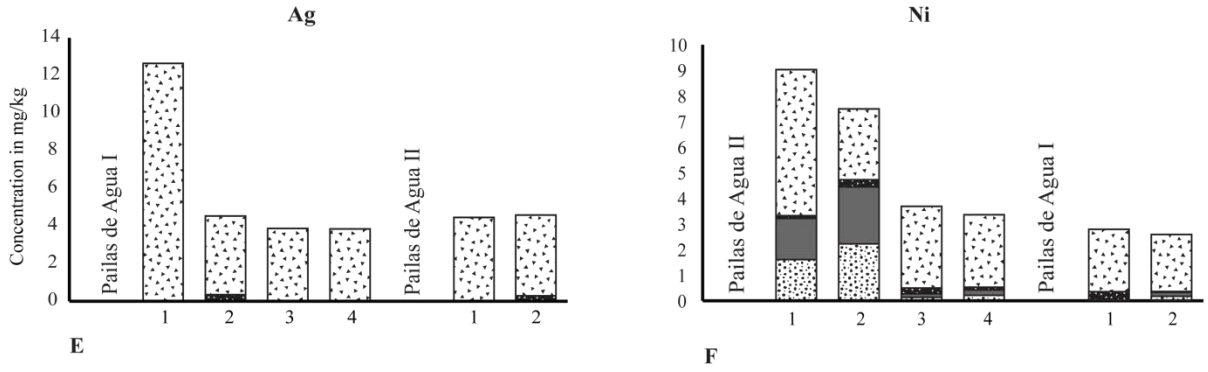

Figure 5E/F: Distribution of trace metals in Pailas de Agua sediment fractions: (E) Silver is almost exclusively present in the organic fraction. Ag detection limits=$1x10^{-3}$-$1x10^{-2}$ mgkg^{-1} (F) The distribution of Ni is more variable. While the majority of Ni is present in the organic fraction, some Ni is also present in the exchangeable and carbonate/sulfate fractions. Ag detection limits=$1x10^{-3}$-$1x10^{-2}$ mgkg^{-1}.

Nickel. Nickel concentrations in the sediments of PDA I and II range from 2.4-7.4 mg kg^{-1} of sediment (Table 5). In PDA I-1, the majority of Ni (76%; 5.7 mg kg^{-1}) is bound to organic matter, while 22% (1.6 mg kg^{-1}) is found in the exchangeable fraction and ~7% (0.1 mg kg^{-1}) is bound to Fe-oxides/-oxyhydroxides. Nickel is nearly evenly distributed between the organic (52.4%; 2.8 mg kg^{-1}) and exchangeable (42.3%; 2.2 mg kg^{-1}) fractions in PDA I-2 sediments (Table 5; Figure 5F). Approximately 5.3% (0.3 mg kg^{-1}) of Ni is bound to Fe-oxides/-oxyhydroxides in PDA I-2, with less than 1% ($4.0x10^{-3}$ mg kg^{-1}) Ni structurally bound to silicates. In PDA I-3 sediments, 90% (3.2 mg kg^{-1}) of Ni partitions into the organic fraction (Table 5; Figure 5F). The remaining 10% is approximately evenly distributed between the exchangeable (4%; 0.1 mg kg^{-1}) and oxide (6%; 0.2 mg kg^{-1}) fractions. The distribution of Ni in PDA I-4 sediments is similar to PDA I-3. The majority (90%; 2.8 mg kg^{-1}) of Ni is bound in the organic fraction; the remaining 10% is split between the exchangeable (7%; 0.2 mg kg^{-1}) and oxide (3%; 0.1 mg kg^{-1}) fractions (Table 5; Figure 5F).

In PDAII (1-2), the majority of Ni in the sediments is bound within the organic fraction. Eighty-eight percent of the Ni in PDA II-1(2.4 mg kg^{-1}) and 92% (2.2 mg kg^{-1}) in PDA II-2 is bound in the organic fraction. Fe-oxides/oxyhydroxides present in PDA II-1 bind the remaining 12% (0.3 mg kg^{-1}) of Ni in the sample. In PDA II-1, 6.3 % (0.2 mg kg^{-1}) of the Ni is weakly adsorbed to the sediment exchangeable fraction and the remaining 1.7% ($4.0x10^{-2}$ mg kg^{-1}) is bound to Fe-oxides/-oxyhydroxides.

Discussion

Previous sequential extraction studies of sediments associated with circum-neutral hot spring sediments indicate trace metals, including Cu, Ni, Zn, As, Ag, Au, and Sb, primarily bind to Fe-oxides (Simmons and Brown, 2007; Landrum et al., 2009). Our sequential extraction results, in contrast, show microbial influences on trace metal enrichments including binding to microbial cells and EPS, and potentially adsorption to microbially-mediated minerals in acid-sulfate hydrothermal systems. The partitioning of the majority of metals studied (As, Ni, Cu, and Ag) are influenced by microbial processes within the spring system.

Abiotic Influences on Spring Geochemistry and Mineralogy

Magmatic and meteoric water mixing in Pailas de Agua I and Pailas de Agua II creates oxidizing spring waters dominated by sulfate (Giggenbach and Soto, 1992), that ascend to the surface to form spring pools. As these metal-rich waters reach the surface, steep geochemical gradients, boiling, and evaporation, facilitate the rapid precipitation of minerals from solution, leading to the preferential partitioning of trace metals into the sediment (Figure 3). Of the trace metals examined in this study, only Cu was detectable in solution in low concentrations ($1.2x10^{-2}$-$6.6x10^{-4}$ mM; Phillips-Lander et al., 2014). PhreeqC modeling of PDA I spring water chemistry indicates that Fe-, Al-, and Zn-oxides, elemental sulfur, pyrite, and clay minerals are supersaturated and should precipitate from solution, while barite, bornite, pyrite, elemental sulfur, amorphous silica, and iron oxides are supersaturated and should precipitate from PDA II spring solution. X-ray diffraction of the sediments from these locations confirms PDA I and II are dominated by clays, Fe-oxyhydroxides, Fe-hydroxysulfate minerals, accessory oxides, and sulfate minerals. PDA I sediments also contain bandylite and uvanite. Sequential extraction data indicates Fe and S are primarily found within the most chemically accessible fractions (exchangeable, carbonate/sulfate, and oxide), which is expected considering the oxidizing conditions present in the spring sediments and the mineralogy observed via XRD (Tessier et al., 1979; Giggenbach and Soto, 1992; Gehring et al., 1999; Gleyzes et al., 2002).

Sulfur is found primarily within the exchangeable fraction and may represent either sulfate or sulfide ions (as our analysis did not identify elemental speciation) weakly adsorbed to positive cations associated with the cation exchange capacity of clay minerals present in each of the springs (Gleyzes et al., 2002). However, previous work by Giggenbach and Soto (1992) and Gehring et al. (1999) indicates that sulfur is mainly present as the sulfate species and some sulfate minerals, including gypsum and jarosite, are susceptible to acid attack (Gleyzes et al., 2002; Dold, 2003; Torres and Auleda, 2013). Therefore, some of the sulfur observed in the exchangeable and carbonate/sulfate fractions is likely related to dissolution of these minerals, particularly PDA II-2 (Table 2; Figure 4B). Sulfur sorption to Fe-oxide surfaces and the

formation of schwertmannite ($Fe_{16}O_{16}(OH)_{12}(SO_4)_2$) likely account for sulfur present in the oxide fraction (Brady et al., 1986; Webster and Swedlund, 1998).

While the adsorption of sulfur does not appear to be biologically influenced, the partitioning of Fe and Zn reflect both abiotic and biological influences. Zinc is primarily associated with the exchangeable fraction in PDA I. This weak adsorption to mineral surfaces in the sediment is not expected to be biologically mediated. In contrast, Zn in PDA II-1 is structurally bound in oxide minerals. PhreeqC modeling of PDA-I predicts the formation of Zn-oxides, which may account for Zn partitioning into the oxide fraction. However, the total concentration of Zn-oxides is expected to be low and these oxides may not have been present in the small sample analyzed via XRD. In PDA I-1 Zn is common in the oxide fraction and may be structurally bound to Fe-oxides, which could reflect the influence of biological processes. Overall Zn in spring sediments is 3.1-12.1 mg kg^{-1} reflects decreased adsorption to organic matter and depletion of Zn in the sediment relative to average crustal abundance (79 mg kg^{-1}; McBride and Blasiak, 1979).

Biological Influences on Metal Partitioning

PDA I and II sediments, Au, As, Cu, Ni, and Ag preferentially partition into the organic fraction of the sediments. This organic fraction is comprised of cells, organic acids that make up biofilm, and minerals precipitated within the biofilm. Each of these components has the capacity to adsorb trace metals and together these components account for the distribution of trace metals within the organic fraction.

In PDA I and II, Fe is primarily bound to Fe-oxides, although minor adsorption within the exchangeable (representing cation exchange capacity), sulfate (representing jarosite) and silicate fraction occurs. Fe-oxides/-oxyhydroxides are common minerals in both acid-sulfate springs and acid-mine drainage (Harris and Lottermoser, 2003; Donahoe-Christiansen et al., 2004; Inskeep et al., 2004; Torres and Auleda, 2013; Torres et al., 2013). PhreeqC modeling of PDA I and II solutions and experimental work (data presented in Chapter 4) indicates that Fe-oxides precipitate abiotically from these acid-sulfate waters and these Fe-oxides represent Fe bound within the oxide fractions of these sediments. With the exception of PDA II-1, oxides do not bind the majority of Fe in the sediments. Instead, Fe is primarily found within the organic

fraction. This Fe may represent microbial metabolic processes, adsorption to microbial cell surfaces and EPS, or to Fe-oxides precipitates within the biofilms. Metabolic activities of IOB, including Galderia-like algae present in the spring, may enhance Fe-oxidation and Fe-oxide/-oxyhydroxide formation in PDA I and II (Hernandez, 2012; Phillips-Lander et al., 2014).

Microbial metabolic processes and organic acids have been implicated in the concentration of Au in a number of ore deposits, including the Ladolam epithermal deposit, Papua New Guinea (Dexter-Dyer et al., 1984; Lengke and Southam, 2006). SRBs often drive Au bioaccumulation by reducing Au-thiosulfate complexes producing Fe-sulfides and elemental gold (Lengke and Southam, 2006). This elemental gold is released from microbial cells upon cell death (Lengke and Southam, 2006). However, gold produced by microbial processes is indistinguishable from gold produced by inorganic processes, making it unclear what role, if any, microorganisms play in the concentration and distribution of Au in hydrothermal sediments.

Biofilm mediated trace metal partitioning

In addition to metabolic effects, microorganisms may passively adsorb metals to cell walls and sheaths. For example, *Thiobacillus sp.* have been implicated in As immobilization by co-precipitation with Fe^{3+} onto microbial sheaths and within biofilms in AMD sediments (Leblanc et al., 1996). However, total metal adsorption to cellular surfaces within acidic pH springs is expected to be minimal as most microorganisms' functional groups are positively charged below their zero point of charge (zpc= 1-4.5; Yee and Fein 2001; He and Tebo, 1998; Crist et al. 1992). Therefore, trace metal adsorption to cellular surfaces in Pailas de Agua I and II should be minimized due to prevailing low pH (2.4-2.6). Despite PDA I and II's acidic pH, Ni, As, Cu, Ag preferentially partition into the sediment organic fraction.

The presence of microbial EPS can limit diffusion and create pH microenvironments, which can influence pH by $\pm$1 pH unit (Decho, 2000; Liermann et al., 2000). Localized pH increase could facilitate the adsorption of metals on cellular surfaces. In PDA II, Cu preferentially binds to cell surfaces within biofilms (Figure7). Ultimately, increased metal sorption would facilitate the formation of nanoscale

minerals, including Fe-oxides/-oxyhydroxides within the biofilm (Chan et al., 2004) and account for high Fe concentrations within the organic fraction of the sediments.

Organic acids within EPS deprotonate at variable pH, which may enhance metal adsorption and Fe-oxide formation within the organic fraction. In circum-neutral pH systems, including neutral-chloride hydrothermal systems, trace metals (As, Sb, Au, Ag, Cu, Zn) bind to Fe-oxides forming within microbial biofilms (Landrum et al., 2009; Simmons and Brown, 2007; Tan, 2011); however metal adsorption to Fe-oxides/-oxyhydroxides is pH dependent and relatively minor below minerals' zpc (5-8; Cornell and Schwertmann, 2003; Roberts, 2004; Tan, 2011; McKenzie et al., 2001). In PDA II, Cu preferentially adsorbs to microbial cells and Fe-oxides within mineralized biofilms (Figure 6).

In PDA I and II As preferentially partitions into the organic fraction. Arsenic speciation influences it's cycling in hydrothermal systems and this speciation is influenced by pH, microbial metabolisms, and biofilms (Handley et al., 2013). In microcosm experiments at circum-neutral pH and T=20-40^{o}C, iron oxidation and sulfate reduction metabolisms were shown to facilitate As adsorption to ferrihydrite (Handley et al., 2013). Arsenic has been shown to bind Fe-oxides in the hydrothermal discharge at El Tatio's thermal field (Landrum et al., 2009). In PDA I and II, the dominant species of As is expected to be arsenate, as $H_2AsO_4^-$, based on modelling by Lafferty and Loeppert (2005). Arsenate adsorption to Fe-oxides should be greatest between pH 3.5-5.5, which is within 1 pH unit of PDA I and II's solution pH (pH 2.6-2.8).

In PDA I and II Ag is bound within the organic matter (Table 2; Figure 5). Silver adsorption to Fe-oxides/-oxyhydroxides is pH dependent and relatively minor below pH 7, however, below pH 4 Ag adsorption may increase as a result of bridging by thiosulfate ions sorbed to ferrihydrite (Cornell and Schwertmann, 2003). Thiosulfate was not detected in PDA I and II waters, however, sulfate concentration (14-38 mM) may have obscured the presence of thiosulfate. Moreover, S is primarily present in the oxide and organic fractions of PDA I-1, making it unlikely that thiosulfate bridges account for Ag in all Las Pailas springs.

Depending on the composition of the EPS, trace metals binding to organic matter may outcompete Fe-oxides (Scheinost et al., 2001), resulting in direct metal binding to microbial cell surfaces and EPS. In low T (8-15^{o}C), acidic (pH 3.1) environments, microorganisms bind metals to organic acids within the biofilm that deprotonate at variable pH (Ferris et al., 1989; Drever, 1997). Fulvic acids have higher affinities for Cu and Pb than ferrihydrite at low pH ($\leq$5; Scheinost et al., 2001) and humic acids concentrations in excess of 50 mg L^{-1} reduce the net surface charge of Fe-oxides negatively influencing metal adsorption to the Fe-oxide surface (Baalousha, 2009). Organic acids may bind to and effectively passivate the Fe-oxide surface, making them inaccessible to trace metals like Ag (Cornell and Schwertmann, 2003). EPS passivation of Fe-oxides and the development of localized higher pH microenvironments likely facilitate direct binding of trace metals to EPS and microbial cell surfaces, as observed in Figure 7 and may account for the concentration of Ni, Cu, and Ag in PDA I and II. More likely than not, a combination of direct adsorption to microbial cells, EPS, and Fe-oxides bound within the EPS account for the preferentially partitioning of these metals in the organic fraction of PDA I and II sediments.

Biofilms are designed to protect microbial cells from changes in environmental conditions (Decho, 2000). EPS, while potentially influencing Fe-oxide ability to sorb metals, may also protect oxide surfaces. Trace metals, like Cu, bound to Fe-oxides (Figure 6) entrained within biofilm may remain largely inaccessible to acid attack until the organic matter associated with them is combusted (Dong et al., 2000).

Trace Metal Toxicity

In PDA I and II, acidic pH waters solubilize potentially toxic trace metals including Ni and Cu (Doelman and Haanstra, 1984). Because microorganisms acquire nutrients through osmosis, the removal of toxic trace metals from solution is necessary to protect microbial populations. In hydrothermal systems where high temperatures, UV radiation, high metal concentrations and fluctuating geochemical conditions can create cellular distress, EPS provides a semi-permeable protective membrane for microbial communities (Ferris et al., 1989; Phoenix et al., 2001; Sutherland, 2001; Teitzel and Parsek, 2003; Hunter and

Beveridge, 2005; Phoenix and Konhauser, 2008; Beech and Sunner, 2004; Madigan et al., 2009). Trace metal partitioning into the organic fraction may reflect microbial detoxification processes.

In order to better determine the role and function of microbially induced metal sequestration in the Las Pailas hydrothermal pools, we compared the As, Ni, Cu, Zn, Au, and Ag concentrations in the springs (Table 3-5) to published toxic concentrations for microbial populations. These concentrations required to induce toxicity were adjusted to the estimated population size in Pailas de Agua I (10^6 cells, Phillips-Lander et al., 2014) in order to compare the total concentrations of metals measured in the spring to expected metals requirements. Neither Zn nor Au preferentially partition into the organic fraction within Las Pailas spring sediments and notably no toxic concentration is established for either metal. However, Zn, Cu, and Ni may act synergistically to enhance Ni and Cu toxicity (Babich and Stotzky, 1983a; Babich and Stotzky, 1983).

Nickel concentrations (2.4- 7.4 mg kg^{-1}) in PDA I and II overlap with toxic concentrations for a similar sized microbial population (5-50 mg kg^{-1}; Table 3; Laskin et al., 1983; Babich and Stotzky, 1982a; Babich and Stotzky, 1982b; Babich and Stotzky, 1982c; Babich and Stotzky, 1983). Copper concentrations in PDA I exceed microbial nutrition requirements by several orders of magnitude ($1.3x10^{-7}$ mg kg^{-1}; Konhauser et al., 2002). Microbial toxicity may be induced at low Cu concentrations ($5.0x10^{-2}$-0.5 mg kg^{-1}; Table 3); however, toxicity is dependent on Cu's accessibility. Copper adsorption to Fe-oxides has been shown in circum-neutral pH systems to reduce Cu toxicity (Babich and Stotzky, 1983a; Babich and Stotzky, 1983). Therefore, adsorption to Fe-oxides and microbial cell surfaces within mineralized biofilms may reduce Cu toxicity in acid-sulfate systems (Figure 6 and 7). While Ni is not observed directly bound to Fe-oxides, it's presence within the organic fraction suggests biofilm binds and sequesters Ni to overcome microbial toxicity.

While some metals, like As are toxic to microorganisms in very low concentrations (5 μg L^{-1}; Diorio et al., 1995; Páez-Espino et al., 2009; Bachate et al., 2009; Mukhopadhyay and Rosen, 2002), Ag toxicity is

Table 6: Nutritional and Toxicity Concentrations			
Metal	**Las Pailas (mg/kg)**	**Toxicity * (mg/kg)/10^6 cells**	**Toxic Concentration Reference**
As	0.15-16	0.05 µg/l 58 mg/kg in As -resistant bacteria	Diorio et al (1995) Bachate et al. (2009)
Ni	3-9	5-50	Babich and Stotzky (1982; 1983); Laskin et al. (2003)
Au	1.7-2.3		none established
Ag	4-13	>0.0002	Silver (2003); Xiu et al. (2012)
Cu	4-56	0.05-0.5	Babich and Stotzky (1983)
Zn	3-12		none established

*Las Pailas values represent the range of values presented for PDAI 1-4 and PDAII 1-2.
**values tabulated from published data and mathematically adjusted to the estimated population size for PDAI.

strongly dependent on speciation. Silver exhaled in rising hot spring waters rapidly oxidizes as the solutions degas (Drummond and Ohmoto, 1985). These oxidative processes have been shown experimentally to result in the formation of Ag^+ and $AgClOH^-$ as dominant Ag species below temperatures of 100°C and between pH 3.7 to 12 (Stefánsson and Seward, 2003). The net of these processes result is an increase in Ag toxicity. Silver (Ag^+) toxicity may be induced between $<2.0x10^{-4}$ mg kg^{-1} to 25% biomass dry weight (Table 3; Silver, 2003; Panáček et al., 2006; Xiu et al., 2012). Both As and Au concentrations in PDA I and II exceed toxic concentrations for these metals (Table 3) and these metals are bound and sequestered within the biofilms present in the springs. While Ni, Cu, As, and Ag in Las Pailas exceed toxic concentrations for the microbial population in the springs, sequestration of these metals in the sediment reduces the concentration of these metals in solution to below toxic concentrations. This inhibits microbial toxicity by limiting diffusion of these metals into microbial cells. Microorganisms use biofilm's protective effects to limit toxicity induced created by acid pH conditions.

Microorganisms as Near-Surface Indicators of Epithermal Ore Formation

In circum-neutral hydrothermal systems, trace metal enrichment has been linked with shallow epithermal ore formation. Epithermal Au- Ag deposits have been observed in Ladolam, Papua New Guinea and in the Taupo Volcanic Zone, New Zealand (Simmons and Brown, 2006; 2007). Siliceous sinters,

precipitated from these low-sulfidation metal-rich waters are enriched in Ag, Au, and Cu and are associated with microorganisms and microbial biofilms (Simmons and Brown, 2006; 2007). Hydrothermal fluids in Yellowstone have also shown anomalously high Cu (16 mmol L^{-1}) and As (13 mmol L^{-1}) concentrations (Walker et al., 2005) indicating potential ore formation at depth. Arsenic and Sb enrichments occur also in the El Tatio hydrothermal field in Chile (Landrum et al., 2009).

While As enrichment is common in hydrothermal systems, the total As concentrations (11-16 mg kg^{-1}) in PDA I and II are lower than other studied hydrothermal systems. For example, As concentrations in El Tatio's hydrothermal field in Chile range from 260-21,000 mg kg^{-1} (Landrum et al., 2009) and sediments from the Taupo Volcanic Zone, NZ have As concentrations that range from 0-1,600 mg kg^{-1} (McKenzie et al., 2001). Nevertheless, As concentrations in PDA I and II exceed average crustal abundances (2.1 mg kg^{-1}) in all samples except PDA I-1 (As= 0.2 mg kg^{-1}). Nickel (2.4- 7.4 mg kg^{-1}) and copper (3.7- 56 mg kg^{-1}) concentrations in PDA I and II sediments are depleted relative to average crustal abundances (90 mg kg^{-1} and 68 mg kg^{-1} respectively. However, Cu concentrations within the MacArthur River H-Y-C range from 2-80 mg kg^{-1} (Large et al., 2000) and are similar to PDA I and II.

Hot spring Ag concentrations are commonly enriched relative to average crustal abundances (0.08 mg kg^{-1}). Silver concentrations in Taupo Volcanic Zone range from 2.0 μg kg^{-1} to 2.4 mg kg^{-1} (Simmons and Brown, 2007) and are considered to represent an actively forming shallow epithermal ore deposit. Silver concentrations observed in the Las Pailas sediments (3.8-12 mg kg^{-1}) exceed those present in the Taupo Volcanic Zone. Pailas de Agua I and II gold concentrations (1.4-2.3 mg kg^{-1}) also exceed Taupo's Au concentrations (<0.1-23 μg kg^{-1}; Simmons and Brown, 2007). Where detectable within Las Pailas' sediments, Au exceeds the cutoff grade (0.00001 wt. %) for determining an economic deposit, indicating the formation of shallow high-sulfidation epithermal systems.

Both acid-sulfate and neutral-chloride hydrothermal systems are the surficial expression of water-rock interactions occurring at depth. When Simmons and Brown (2006) sampled deep magmatic geothermal brines, they found these waters were enriched in Au (<0.1-16 μg kg^{-1}) and Ag (<1-6 μg kg^{-1}). They

calculated that at these concentrations, an epithermal ore deposit could form within ~55 Ky. Therefore, both acid-sulfate and neutral-chloride spring systems represent surficial expressions of epithermal Au-Ag deposits forming at depth. Microbial processes, including the binding of trace metals to biofilms and biofilm associated Fe-oxides, capture trace metals from solution and likely serve as shallow indicators of ore formation at depth.

Conclusions and Implications

Hydrothermal systems associated with actively forming epithermal deposits are differentiated by geochemistry and mineralogy into low- and high-sulfidation systems. Despite these differentiations, microbial processes are responsible for trace metal sequestration in both end members once solutions cool below ~121^{o}C (Kashefi et al., 2007). In circum-neutral pH, low-sulfidation systems, microbial metabolic processes influence the redox chemistry and facilitate the binding of trace metals to Fe-oxides and siliceous sinters associated with microbial biofilms (Simmons and Brown, 2007; Landrum et al., 2009). In high-sulfidation (acid-sulfate) systems like Las Pailas microbial EPS influences the distribution of trace metals by: 1) regulation of the internal pH of the biofilm to drive the precipitation of nano- to micro-scale Fe-oxides/-oxyhydroxides, which in turn adsorb trace metals and 2) direct binding of trace metals to microbial cell surfaces and EPS. Organic acids may passivate some Fe-oxide surfaces, which enhances adsorption of trace metals to organic acids within the EPS. Microorganisms sequester trace metals within their biofilms as a detoxification process.

The magnitude of trace metal enrichment in acid-sulfate systems falls within the low end of enrichments reported for neutral-chloride hydrothermal systems for Cu and Zn, however, Au and Ag in Las Pailas sediments are enriched relative to neutral chloride systems. Therefore, microbial processes not only play a ubiquitous role in concentrating trace metals in shallow hydrothermal systems, but they may also provide indicators of the actively forming epithermal deposits from which their fluids are sourced. The preservation of microbial biosignatures in ancient ore deposits like MacArthur River HYC and Huinquintipa and Mina Sur porphyry copper deposits suggests microbial processes have influenced

shallow ore deposition throughout geologic time, as long as the conditions for life are met. While main epithermal ore bodies form at T>121^{o}C, the data from ancient and modern high- and low- sulfidation systems strongly suggest that metal enriched halos surrounding the higher temperature core of epithermal ore deposits may result from microbially enhanced sequestration of Au, Ag, and possibly Cu to overcome metal toxicity.

Author Contributions

Field Work: Charity Phillips-Lander, Jennifer Roberts, Walter Hernandez, and Marielos Mora participated in the field sampling that underpins this work.

Lab work: Laboratory analyses, including characterization of the mineralogy by X-ray diffraction, trace metal distributions by sequential extraction, and transmission electron microscopy were performed by Charity Phillips-Lander.

Writing: The paper was written by Charity Phillips-Lander with the assistance of Jennifer Roberts.

Revisions: Paper revisions were contributed by Charity Phillips-Lander, Jennifer Roberts, David Fowle, and Marielos Mora.

Funding

This work would not be possible without the financial support of the University of Kansas-University of Costa Rica Research Collaboration Fund (awarded to Jennifer Roberts and Marielos Mora), as well as the support of the Costa Rica National Parks Service, which provided access to the site. Microscopy, laboratory, and fieldwork support were provided by a University of Kansas Dissertation Fellowship, a Geological Society of America Student Research Grant, an Ernest Angino Geochemistry Scholarship and an ExxonMobil Student Research Grant (awarded to Charity Phillips-Lander).

Acknowledgments

We thank Masato Ueshima, Karla Leslie, and Gwen Macpherson for their laboratory support. We thank Victor Day of the X-ray Crystallography Laboratory and Heather Shinogle of the KU Microscopy and Analytical Imaging Laboratory for their technical assistance with the XRD and TEM respectively.

References

Arribas A. (1995) Characteristics of high-sulfidation epithermal deposits, and their relation to magmatic fluid. In: J. F. Thompson (ed), Magmas, Fluids, and Ore Deposits, *Association of Canada Short Course Series* **23**, 419-454.

Baalousha M. (2009) Aggregation and disaggregation of iron oxide nanoparticles: Influence of particle concentration, pH and natural organic matter. *Science of The Total Environment* **407**, 2093-2101.

Babich H. and Stotzky G. (1982a) Nickel toxicity to fungi: Influence of environmental factors. *Ecotoxicology and Environmental Safety* **6**, 577.

Babich H. and Stotzky G. (1982b) Nickel toxicity to microbes: effect of pH and implications for acid rain. *Environmental Research* **29**, 335-350.

Babich H. and Stotzky G. (1982c) Toxicity of nickel to microorganisms in soil: Influence of some physiochemical characteristics. *Environmental Pollution Series A, Ecological and Biological* **29**, 303-315.

Babich H. and Stotzky G. (1983) Synergism between nickel and copper in their toxicity to microbes: mediation by pH. *Ecotoxicology and Environmental Safety* **7**, 576-587.

Bachate S. P., Cavalca L. and Andreoni V. (2009) Arsenic-resistant bacteria isolated from agricultural soils of Bangladesh and characterization of arsenate-reducing strains. *Journal of Applied Microbiology* **107**, 145-156.

Beech I. B. and Sunner J. (2004) Biocorrosion: towards understanding interactions between biofilms and metals. *Current Opinion in Biotechnology* **15**, 181-186.

Brocks J. J., Love G. D., Summons R. E., Knoll A. H., Logan G. A. and Bowden S. A. (2005) Biomarker evidence for green and purple sulphur bacteria in a stratified Palaeoproterozoic sea. *Nature* **437**, 866-870.

Chan C. S., Stasio G. D., Welch S. A., Girasole M., Frazer B. H., Nesterova M. V., Fakra S., and Banfield J. F. (2004) Microbial polysaccharides template assembly of nanocrystal fibers. *Science* **303**, 1656-1658.

Cornell R. M. and Schwertmann U. (2003) The iron oxides: Structure, properties, reactions, occurrences, and uses. Wiley and Sons, Hoboken, 664 p.

Crist, R. H., Oberholser, K., McGarrity, J., Crist, D. R., Johnson, J. K., and Brittsan, J. M. (1992) Interaction of metals and protons with algae. 3. Marine algae, with emphasis on lead and aluminum. *Environmental Science and Technology* **26**, 496-502.

Decho A. 2000. Microbial biofilms in intertidal systems: an overview. *Continental Shelf Research* **20**: 1257-1273. doi:10.1016/S0278-4343(00)00022-4

Dexter-Dyer B., Kretzschmar M., and Krumbein W. E. (1984). Possible microbial pathways in the formation of Precambrian ore deposits. *Journal of the Geological Society of London* **141**, 251-262.

Diorio C., Cai J., Marmor J. and Shinder R. (1995) An Escherichia coli chromosomal ars operon homolog is functional in arsenic detoxification and is conserved in gram-negative bacteria. *Journal of Bacteriology* **177**, 2050-2056.

Doelman P. and Haanstra L. (1984) Short- and long-term effects of cadmium, chromium, copper, nickel, lead, and zinc on soil microbial respiration in relation to abiotic factors. *Plant and Soil* **79**, 317-327.

Dold, B. (2003) Speciation of the most soluble phases in a sequential extraction procedure adapted for geochemical studies of copper sulfide mine waste. *Journal of Geochemical Exploration* **80**, 55-68.

Donahoe-Christiansen, J., D'Imperio, S., Jackson, C. R., Inskeep, W. P., and McDermott, T. R. (2004) Arsenite-Oxidizing Hydrogenobaculum Strain Isolated from an Acid-Sulfate-Chloride Geothermal Spring in Yellowstone National Park. *Applied and Environmental Microbiology* **70**, 1865-1868. doi: 10.1128/AEM.70.3.1865-1868.2004Drever J. (1997) *The geochemistry of natural waters: Surface and groundwater environments.* Prentice Hall, Upper Saddle River.

Dong, D., Nelson, Y. M., Lion, L. W., Shuler, M. L., and Ghiorse, W. C. (2000) Adsorption of Pb and Cd onto metal oxides and organic material in natural surface coatings as determined by selective extractions:

new evidence for the importance of Mn and Fe oxides. *Water Research* **34**, 427-436. doi: 10.1016/S0043-1354(99)00185-2

Drever, J. I. (1997) The Geochemistry of Natural Waters. Pearson Education Canada, Ontario.

Drummond, S. E. and Ohmoto, H. (1985) Chemical evolution and mineral deposition in boiling hydrothermal systems. *Economic Geology* **80**, 126-147.

Egal M., Casiot C., Morin G., Parmentier M., Bruneel O., Lebrun S. and Elbaz-Poulichet F. (2009) Kinetic control on the formation of tooeleite, schwertmannite and jarosite by Acidithiobacillus ferrooxidans strains in an As(III)-rich acid mine water. *Chemical Geology* **265**, 432-441.

Ferris F. G., Schultze S., Witten T. C., Fyfe W. S. and Beveridge T. C. (1989) Metal interactions with microbial biofilms in acidic and neutral pH environments. *Applied and Environmental Microbiology* **55**, 1249-1257.

Finsinger K., Scholz I. and Serrano A. (2008) Characterization of true-branching cyanobacteria from geothermal sites and hot springs of Costa Rica. *Environmental Microbiology* **10**, 460-473.

Gehring A., Schosseler P. and Weidler P. (1999) Mineral formation and redox-sensitive trace elements in a near-surface hydrothermal alteration system. *Geochimica et Cosmochimica* **63**, 2061-2069.

Giggenbach W. and Soto R. (1992) Isotopic and chemical composition of water and steam discharges from volcanic-magmatic-hydrothermal systems of the Guanacaste Geothermal Province, Costa Rica. *Applied Geochemistry* **7**, 309-332.

Gleyzes C., Tellier S. and Astruc M. (2002) Fractionation studies of trace elements in contaminated soils and sediments: a review of sequential extraction procedures. *TrAC Trends in Analytical Chemistry* **21**, 451-467.

Handley K. M., McBeth J. M., Charnock J. M., Vaughan D. J., Wincott P. L., Polya D. A. and Lloyd J. R. (2013) Effect of iron redox transformations on arsenic solid-phase associations in an arsenic-rich, ferruginous hydrothermal sediment. *Geochimica et Cosmochimica Acta* **102**, 124-142.

Harris D. and Lottermoser B. (2003) Ephemeral acid mine drainage at the Montalbion silver mine, north Queensland. *Australian Journal of Earth Sciences* **50**, 797-809.

He, L. M., and Tebo, B M. (1998) Surface charge properties of and Cu(II) adsorption by spores of the marine Bacillus sp. strain SG-1. *Applied and Environmental Microbiology* **64**, 1123-1129.

Heald P., Foley N. K. and Hayba D. L. (1987) Comparative anatomy of volcanic-hosted epithermal deposits; acid-sulfate and adularia-sericite types. *Economic Geology* **82**, 1-26.

Hernandez, W. (2012) Caracterización de dos comunidades microbianas de ambientes extremos ácidos del Parque Nacional Volcán Rincón de la Vieja, Guanacaste, Costa Rica (Master's Thesis). Universidad de Costa Rica, San Jose, Costa Rica.

Hunter R. C. and Beveridge T. J. (2005) Application of a pH-Sensitive Fluoroprobe (C-SNARF-4) for pH Microenvironment Analysis in Pseudomonas aeruginosa Biofilms. *Applied and Environmental Microbiology* **71**, 2501-2510. doi:10.1128/AEM.71.5.2501-2510.2005.

Inskeep, W. P., Macur, R. E., Harrison, G., Bostick, B. C., and Ferndorf, S. (2004) Biomineralization of As(V)-hydrous ferric oxyhydroxide in microbial mats of an acid-sulfate-chloride geothermal spring, Yellowstone National Park. *Geochimica et Cosmochimica Acta* **68**, 3141-3155. doi: 10.1016/j.gca.2003.09.020

Kabata-Pendias, A. (2004). Soil–plant transfer of trace elements—an environmental issue. Geoderma, 122(2), 143-149.

Kashefi K., Shelobolina E. S., Elliott W. C. and Lovley D. R. (2007) Growth of Thermophilic and Hyperthermophilic Fe(III)-Reducing Microorganisms on a Ferruginous Smectite as the Sole Electron Acceptor. *Applied and Environmental Microbiology* **74**, 251-258.

Kempter K., Benner S. and Williams S. (1996) Rincón de la Vieja volcano, Guanacaste province, Costa Rica: geology of the southwestern flank and hazards implications. *Journal of Volcanology and Geothermal Research* **71**, 109-127.

Konhauser K., Hamade T., Raiswell R. and Morris R. (2002) Could bacteria have formed the Precambrian banded iron formations? *Geology* **30**, 1079-1086.

Konhauser, K. (2006) Introduction to Geomicrobiology. John Wiley and Sons, Hoboken. 440 p.

Lafferty B. J. and Loeppert R. H. (2005) Methyl Arsenic Adsorption and Desorption Behavior on Iron Oxides, *Environmental Science and Technology* **39**, 2120-2127.

Large, R. R., Bull, S. W., and McGoldrick, P. J. (2000) Lithogeochemical halos and geochemical vectors to stratiform sediment hosted Zn–Pb–Ag deposits Part 2. HYC deposit, McArthur River, Northern Territory. *Journal of Geochemical Exploration* **68**, 105-126.

Landrum J. T., Bennett P. C., Engel A. S., Alsina M. A., Pastén P. A. and Milliken K. (2009) Partitioning geochemistry of arsenic and antimony, El Tatio Geyser Field, Chile. *Applied Geochemistry* **24**, 664-676.

Laskin A., Bennett J. and Gadd G. eds. (2003) *Advances in Applied Microbiology*. A. Laskin, J. Bennett, and G. Gadd eds. Academic Press, Waltham.

Leblanc M., Achard B., Othman D. and Luck J. (1996) Accumulation of arsenic from acidic mine waters by ferruginous bacterial accretions (stromatolites). *Applied Geochemistry* **11**, 541-554.

Lengke M. and Southam G. (2006) Bioaccumulation of gold by sulfate-reducing bacteria cultured in the presensence of gold(I)-thiosulfate complex. *Geochimica et Cosmochimica Acta* **70**, 3646-3661.

Liermann L. J., Barnes A. S., Kalinowski B. E., Zhou X., and Brantley S. L. (2000) Microenvironments of pH in biofilms grown on dissolving silicate surfaces. *Chemical Geology* **171**: 1-16. doi:10.1016/S0009-2541(00)00202-3

Leslie K., van Geffen P. W. G., Macfarlane B., Oates C. J., Kyser T. K., and Fowle D. A. (2013) Biogeochemical indicators of buried mineralization under cover, Talbot VMS Cu-Zn prospect, Manitoba. *Applied Geochemistry* **37**, 190-202.

Madigan M. T., Martinko J. M., Dunlap P. V. and Clark D. P. (2009) *Brock Biology of Microorganisms*. 12nd ed., Benjamin Cummings, San Francisco.

McBride, M. B., and Blasiak, J. J. (1979) Zinc and Copper Solubility as a Function of pH in an Acid Soil. *Soil Science Society of America Journal* **43**, 866-870. doi:10.2136/sssaj1979.03615995004300050009x

McKenzie E., Brown K., Cady S. and Campbell K. (2001) Trace metal chemistry and silicification of microorganisms in geothermal sinter, Taupo Volcanic Zone, New Zealand. *Geothermics* **30**, 483-502.

Mukhopadhyay R. and Rosen B. (2002) Microbial arsenic: from geocycles to genes and enzymes. *FEMS microbiology* **26**, 311-325.

Nelson M., Kyser K., Clark A. and Oates C. (2007) Carbon Isotope Evidence for Microbial Involvement in Exotic Copper Silicate Mineralization, Huinquintipa and Mina Sur, Northern Chile. **102**, 1311-1320.

Páez-Espino D., Tamames J., Lorenzo V. and Cánovas D. (2009) Microbial responses to environmental arsenic. *BioMetals* **22**, 117-130.

Panáček A., Kvítek L., Prucek R., Kolář M., Večeřová R., Pizúrová N., Sharma V. K., Nevěčná T. and Zbořil R. (2006) Silver Colloid Nanoparticles: Synthesis, Characterization, and Their Antibacterial Activity. *The Journal of Physical Chemistry B* **110**, 16248-16253.

Peltier E., Dahl A. L. and Gaillard J. (2005) Metal Speciation in Anoxic Sediments: When Sulfides Can Be Construed as Oxides. *Environmental Science & Technology* **39**, 311-316.

Phillips-Lander C. M., Fowle D. A., Taunton A., Hernandez W., Mora M., Moore D., Shinogle H., and Roberts J. A. (2014) Silicate dissolution in Las Pailas Thermal Field: Implications for microbial weathering in acidic volcanic hydrothermal spring systems. *Geomicrobiology Journal* **31**, 23-41.

Phoenix R. V. and Konhauser K. O. (2008) Benefits of bacterial biomineralization. *Geobiology* **6**, 303-308.

Phoenix V., Konhauser K., Adams D. and Bottrell S. (2001) Role of biomineralization as an ultraviolet shield: Implications for Archean life. *Geology* **29,** 823-826.

Rainbow A., Kyser T. K. and Clark A. H. (2006) Isotopic evidence for microbial activity during supergene oxidation of a high-sulfidation epithermal Au-Ag deposit. *Geology* **34**, 269.

Roberts, J. A. (2004) Inhibition and enhancement of microbial surface colonization: the role of silicate composition. *Chemical Geology* **212**, 313-327.

Scheinost A. C., Abend S., Pandya K. I. and Sparks D. L. (2001) Kinetic Controls on Cu and Pb Sorption by Ferrihydrite. *Environmental Science & Technology* **35**, 1090-1096.

Semenez M., Viera M., Curutchet G. and Donati E. (2002) The role of *Acidithiobacillus caldus* in the bioleaching of metal sulfides. *Latin American Applied Research* **32**, 303-306.

Semrau J. D., DiSpirito A. A., and Yoon S. (2010) Methanotrophs and Copper. *FEMS Microbiology Reviews* **34**, 496-531.

Sigel A., Sigel H. and Sigel R. K. eds. (2007) *Nickel and its surprising impact in nature*. A. Sigel, H. Sigel, and R. K. Sigel eds. Wiley, Somerset.

Silver S. (2003) Bacterial silver resistance: molecular biology and uses and misuses of silver compounds. *FEMS microbiology reviews* **27**, 341-353.

Simmons S. F. and Brown K. L. (2006) Gold in Magmatic Hydrothermal Solutions and the Rapid Formation of a Giant Ore Deposit. *Science* **314**, 288-291.

Simmons, S. F. and Brown, K. L. (2007) The flux of gold and related metals through a volcanic arc, Taupo Volcanic Zone, New Zealand. *Geology* **35**, 1099.

Sittenfeld A., Mora M., Ortega J. M., Albertazzi F., Cordero A., Roncel M., Sánchez E., Vargas M., Fernández M., Weckesser J. and Serrano A. (2006) Characterization of a photosynthetic Euglena strain isolated from an acidic hot mud pool of a volcanic area of Costa Rica. *FEMS Microbiology Ecology* **42**, 151-161.

Stefánsson A. and Seward T. M. (2003) Experimental determination of the stability and stoichiometry of sulphide complexes of silver(I) in hydrothermal solutions to 400°C. *Geochimica et Cosmochimica Acta* **67**, 1395-1413.

Sutherland I. (2001) Biofilm exopolysaccharides: a strong and sticky framework. *Microbiology* **147**, 3-9.

Tan K. H. (2011) *Principles of Soil Chemistry*. 4 ed., CRC Press, Boca Raton.

Teitzel G. M. and Parsek M. R. (2003) Heavy Metal Resistance of Biofilm and Planktonic Pseudomonas aeruginosa. *Applied and Environmental Microbiology* **69**, 2313-2320.

Tessier A., Campbell P. and Bisson M. (1979) Sequential extraction procedure for the speciation of particulate trace metals. *Analytical Chemistry* **51**, 844-851.

Torres E. and Auleda M. (2013) A sequential extraction procedure for sediments affected by acid mine drainage. *Journal of Geochemical Exploration* **128**, 35-41.

Torres E., Ayora C., Canovas C. R., García-Robledo E., Galván L. and Sarmiento A. M. (2013) Metal cycling during sediment early diagenesis in a water reservoir affected by acid mine drainage. *Science of The Total Environment* **461-462**, 416-429.

Walker J., Spear J. and Pace N. (2005) Geobiology of a microbial endolithic community in the Yellowstone geothermal environment. *Nature* **434**, 1011-1014.

White N. and Hedenquist J. (1995) Epithermal gold deposits: styles, characteristics and exploration. *SEG newsletter* **23**, 9-13.

White N. and Poizat V. (1995) Epithermal deposits, diverse styles, diverse origins? *Australian Institute of Mining and Metallurgy, Series 9*, 623-628.

Xiu Z., Zhang Q., Puppala H. L., Colvin V. L. and Alvarez P. J. (2012) Negligible Particle-Specific Antibacterial Activity of Silver Nanoparticles. *Nano Letters* **12**, 4271-4275.

Yee, N. and Fein, J. (2001) Cd adsorption to bacterial surfaces: a universal adsorption edge? *Geochimica et Cosmochimica Acta* **65**, 2037-2042.

Supplementary Table

Suppl. Table 1: Sequential Extraction Protocol

Fraction	Reagent	Reagent Volume (ml)	T(^{o}C)	Reaction Time	Continuous Agitation
Exchangeable	Ammonia Acetate (buffered to pH 8.2)	1.00	25	15 min	Yes
		0.75	25	15 min	Yes
	DI	1.00	25	30 sec	Yes
Carbonate/ Sulfate	4% Acetic Acid	0.15	25	1 hr	No
			25	10 min	Yes
			25	15 min	Centrifuge
	DI	1.00	25	1 hr	No
			25	15 min	Centrifuge
Oxide	0.04 M NH_2OH ·HCl in 25% v/v Acetic Acid	1.00	96+3	6 hr	Yes
			25	1hr	No
			25	15 min	Centrifuge
		1.00	96+3	6 hr	Yes
			25	1hr	No
			25	15 min	Centrifuge
		1.00	25	30 sec	Yes
			25	1 hr	No
			25	15 min	Centrifuge
		1.00	25	30 sec	Yes
			25	1 hr	No
			25	15 min	Centrifuge
	DI	1.00	25	30 sec	Yes
			25	15 min	Centrifuge
Organic	0.02 M HNO_3 and 30% v/v H_2O_2 adjusted to pH 2	0.80	85+2	2 hr	Yes
			25	1 hr	No
		0.50	85+2	3 hr	Yes
	3.2 M Ammonia Acetate in 20% v/v HNO_3	1.50	25	1 hr	No
			25	30 min	Centrifuge
	DI	2.00	25	1 hr	Centrifuge
Residual	DI	2.00	105	1-4 hr	No
	~7N HNO_3	6.00	85-95	24 hr	No
	HF	2.00			
			25	2-4 hr	No
	~7N HNO_3	6.00	80	12 hr	No
			25	2-4 hr	No
	DI	10.00	80	1 hr	No
	ICP-OES Internal Standard	2.00			No
	DI				No
	DI	dilute to1500x mass			No

Chapter 4. Early smectite nucleation in acid-sulfate systems: Implications for clay formation on Mars

To be submitted as a separate article:
Phillips-Lander C. M., Roberts, J. A., Zhao, L., Dong, H. and Fowle, D. A., Early smectite nucleation in acid-sulfate systems: Implications for clay formation on Mars *(to be submitted to Earth and Planetary Science Letters)*

Abstract

Models of clay mineral formation on Mars suggest clays form through hydrothermal processes in shallow, neutral-alkaline reservoirs, because models indicate nontronite is only stable at pH>4. Mixed-layer clays, including nontronite, are abundant in acid-sulfate hydrothermal systems on Earth, which contradicts these models. Here we examine the nature of clay mineral formation in acid-sulfate systems, by varying temperature, ligand concentration, and proxies for microbial surfaces that serve as nucleation sites in a model hydrothermal solution based on the dry-season aqueous geochemistry of Las Pailas hot springs (pH 2.6, T=80^{o}C, [SO_4^{2-}]=38 mM, [Fe^{2+}]=22-38 mM, [Al^{3+}]=0.1-15 mM, [F^{-}]=0-0.1 mM, and [Ca^{2+}]= 0-0.1 mM), Costa Rica, which are known for their clay rich hot springs, mud pots, and fumaroles. X-ray diffraction analysis of precipitates shows authigenic mixed-layer smectites, nontronite, illite, kaolinite/halloysite, and Fe-oxides form within 7 days under all experimental parameters.

Replicates of experiments at 25^{o}C indicate Al-complexation by fluoride, a ligand with high affinity for Al, enhances authigenic clay formation. Geochemical modeling of aqueous data from experiments indicate the activity of the fluoride ion in solution expands the stability field of nontronite to pH 2, and therefore, fluoride mediates the formation of authigenic clay minerals through Al-complexation.

Surrogates for microbial surfaces, which are covered by carboxyl functional groups, were also added to one half of experimental solutions. While their presence exhibited little influence on authigenic clay formation in 80^{o}C experiments, their presence exerted a weak effect on nontronite formation in 25^{o}C experiments. Microbial influence, therefore, is likely limited in low pH systems because carboxyl groups are largely protonated below pH 4.5.

These data are particularly important for our understanding of Mars' evolution because they indicate nontronite and kaolinite form under a broad diversity of geochemical conditions, and are therefore not specifically indicative of neutral-alkaline pH environments. Moreover, Al activity plays an important role in authigenic clay formation and Al activity is directly related to the anion composition of the fluid.

Introduction

Orbital and rover observations of the Martian surface have confirmed the presence of phyllosilicate minerals, principally Fe/Mg-smectites, with montmorillonite and kaolinite overlying these clays (Bishop et al., 2008). The presence of clay minerals indicates liquid water was present at or near the Martian surface and involved in the chemical weathering of basaltic crust during the Noachian (4.1-3.7 Ga; Ehlmann and Edwards, 2014). The nature of clay mineral formation on Mars, however, has been a topic of debate due to significant geochemical unknowns, including the amount of liquid water present, the temperature, pH, and geochemical composition of these fluids, and the composition of the atmosphere, all of which influence the interpretation of the Martian geochemistry during the Noachian (Madden et al., 2004; Ehlmann et al., 2008; Ehlmann et al., 2011; Fairen et al., 2011). Geomorphological features appear to indicate the presence of fluvial and lacustrine environments; however the geochemical nature of the solutions remains unresolved. For example, Yellowknife Bay (Gale Crater) has been interpreted as originating in a fluvial/lacustrine environment based on the presence of bedding and cross-stratification of sandstones, and erosional scouring contacts at the base of beds, and the presence of mudstones observed in images obtained from the Curiosity Rover (Grotzinger, 2014).

One interpretation of Mars' mineralogy to infer geochemistry is that Fe/Mg-smectites may have formed from anoxic, alkaline, hydrothermal groundwater circulation, while the majority of the Martian surface remained cold and arid (Ehlmann et al 2011; Fairen et al., 2011). Brown et al. (2010), however, argued that shallow hydrothermal alteration of the Martian surface could drive the formation of Mg-rich clay minerals in the present in the clay-rich Nili Fossae region. Chevrier et al. (2007) modeled stability relationships between Fe-oxides and nontronite ($Na_{0.3}Fe_2(Si,Al)_4O_{10}(OH)_2$•n(H2O)) based on a theoretical solution derived from weathered basalt. Based on this model, Chevrier et al. (2007) suggested

hydrothermal weathering on Mars was driven by weakly acidic-alkaline hydrothermal alteration, because nontronite was only stable above pH 4 in the mixed Fe-oxide-nontronite system.

Authigenic clay formation on Earth

Under most Earth surface conditions, clay minerals are expected to form as the result of incongruent dissolution of feldspar (Drever, 1997). Conversion of feldspar to clay minerals depends on acid leaching of cations into solution. The net addition of metals to solution may then aid homogenous authigenic clay nucleation (La Inglesia et al., 1976), making it difficult to differentiate clays formed from proton-promoted dissolution at the surface and those formed from solution supersaturation. Furthermore, organic matter, such as microbial cell surfaces may bind metals and lower the energy required to form critical nuclei required for clay mineral formation (Konhauser and Urrutia, 1999). Microbial surfaces and organic acids, whose functional groups chelate metals and provide a template for mineral formation, have been implicated in authigenic clay formation in a variety of Earth's environments including lakes, rivers, and oceans (Alt and Mata, 2000; Konhauser and Urrutia, 1999; Tazaki, 1997; Fortin et al., 1988; Ueshima and Tazaki, 2001; Loucaides et al., 2010). Additionally, microorganisms encrusted in clay minerals, particularly nontronite, have been observed in a number of seafloor hydrothermal systems and off-axis diffuse vents below 100^{o}C (Alt, 1988; Juniper and Fouquet, 1988; Hekinian et al., 1993; Köhler et al., 1994; Bogdanov et al., 1997; Fortin et. al., 1998; Masuda, 2005; Dekov et al., 2007; Kyle and Schroder, 2007).

Dekov et al. (2007) suggested that the same process that occurs in low temperature systems, i.e. precipitation of iron oxides and silica onto microbial cells surfaces, results in microbial encrustation by clay minerals in hydrothermal systems. The generalized model for clay biomineralization by microorganisms in low temperature systems includes cation sorption on the cell surface as the first step. Adsorption of Fe to the cell surface creates excess positive charge that attracts and facilitates the binding of silica polymers, as has been shown during silicification (Konhauser and Urrutia, 1999; Lalonde et al., 2007). This process is the similar for the initiation of clay formation in circum-neutral pH systems

(Konhauser and Urrutia, 1999). Konhauser and Urrutia (1999) summarized the basic characteristics of clays produced in association with microorganisms as amorphous to poorly ordered, < 1 μm though many are <0.1 μm typically dominated by iron, aluminum and silicon with some potassium.

However, Dekov et al. (2008) indicated not all hydrothermal clays were microbially associated. In high temperature systems (150->250^{o}C) outside the known range for microbial life, authigenic clay formation is governed by the behavior of Al in solution (Dekov et al., 2008). Aluminum activity in solution is governed by pH, temperature, and Al-complexation, which increases Al solubility (Plankey et al., 1986; Stumm and Morgan, 1996; Dekov et al., 2008). The role of pH in clay formation has been primarily modeled by Chevrier et al. (2007) for theoretical geochemical models of Mars and most laboratory studies have focused on clay formation in circum-neutral pH systems. However, economic geologists have noted the association between acid-sulfate solutions and clay minerals in hydrothermal systems on Earth (White and Poizat, 1995; White and Hedenquist, 1995). Authigenic clay formation was shown to occur in laboratory experiments conducted at T>60^{o}C (Tosca et al., 2008). Despite this, authigenic smectites, nontronite, and montmorillonite have been produced from across a wide variety of temperature conditions (<3-80^{o}C) circum-neutral pH solutions under reducing conditions (Harder, 1972; 1976). Aluminum complexation has been studied in high and low temperature systems, however, low temperature systems have focused primarily on organic ligands and high temperature systems have focused on the influence of fluoride, where F- is an abundant ligand in solution (Thomas et al., 1977).

Organic acids, which can occur in many sedimentary environments but are most concentrated in soil environments, influence Al activity by forming Al-organic complexes which react to form clay minerals. Laboratory studies have shown that kaolinite has been experimentally produced from solution at pH 2-9 when organic acids, including oxalate and fulvic acids, were added (Linares and Huerta, 1971; Hem and Lind, 1974; Fiore et al. 2011). Fulvic acids have also facilitated the production of mixed-layer smectites at circum-neutral pH (Linares and Huertas, 1971; La Inglesia et al., 1976). While organic acids accelerate authigenic clay formation in some systems, organic acids may also shield mineral surfaces from chemical

attack by reducing diffusion of released cations away from the mineral surface (Banfield et al., 1999). Therefore, organic matter may either accelerate or limit the degree of chemical weathering and authigenic clay formation in a given location.

Examination of hydrothermal clays indicates fluoride often substitutes for hydroxyl groups in the mineral structure (Chipera and Bish, 2002; Labouriau et al., 1995). Experimental studies have synthesized montmorillonite from high temperature (220^{o}C), circum-neutral pH (pH 5-8.5), fluoride (0.5M fluoride) solutions within 36-288 h (1.5-12 d; Reinholdt et al., 2001; Reinholdt et al., 2005). Decarreau et al. (1987) showed fluoride positively influenced the thermal stability of experimentally produced mixed-layer smectites at temperatures 75-150^{o}C, however, this study indicated the formation of these clays was not dependent upon Al-complexation by F-. Caullet et al. (2005) showed fluoride can form structures that act as a template for early alumino-silicate formation in high temperature experimental systems. Therefore it is unclear what role fluoride plays in clay authigenesis.

Clay mineral formation in hydrothermal systems

Clay mineral formation has been observed in a variety of hydrothermal systems and both inorganic and organic processes have been implicated in authigenic clay nucleation, including microbially-induced clay nucleation, and Al-complexation. The association of microbial cell surfaces and clays does not necessarily implicate them in clay authigenesis, as pre-formed clay minerals may sorb onto microbial surfaces and the role of fluoride in clay formation is inconclusive because it has only been studied in high temperature systems. It remains unclear what factors specifically control authigenic clay formation, particularly in acid-sulfate hydrothermal systems where clay minerals, including mixed-layer smectites, nontronite, and kaolinite/halloysite, are expected to be abundant (Marcucci et al., 2013; White and Poizat, 1995; White and Hedenquist, 1995; Phillips-Lander et al., 2014). As we seek to understand the geochemical evolution of exoplanets, including Mars, it becomes increasingly important to understand what the presence of clay minerals indicates for past environmental conditions and define the geochemical factors that specifically influence authigenic clay formation. To do this, we require a

comprehensive research lexicon that defines the underlying geochemical controls on clay mineral formation across the pH spectrum.

Here, we examine the influence of an inorganic ligand, microbial surfaces, and temperature on authigenic clay formation. In order to determine the main influences on clay formation, we developed a model hydrothermal solution, based on acidic (pH 2.6-4), sulfate (SO_4^{2-}= 38 mM) waters collected from the Pailas de Agua I hot (T=80-89^{o}C) spring, whose mineralogy includes mixed-layered smectite, nontronite, kaolinite, ferrihydrite, goethite, jarosite and quartz (Phillips-Lander et al., 2014; Phillips-Lander unpublished data). These solutions contain high Fe (4.0-7.0 mM), Al (15 mM), and Si (8.2 mM) concentrations. Concentrations of other cations are relatively low (Ca=0.7 mM, Na=0.4 mM, Mg=0.7 mM) and anion concentrations, other than sulfate, show similar trends (F^-= 0.1 mM, Cl=0.05; Phillips-Lander et al., 2014). These data will then be used to determine the controls on authigenic clay formation in acid-sulfate systems specifically, and in conjunction with other geochemical data to determine the role of these processes more broadly in clay formation.

Methods

Experimental Design

Using the data derived from the field sampling of PDA I, an acid (pH 2.6-4) -sulfate (SO_4^{2-}= 38 mM), hot (T=80-89^{o}C) spring, the geochemistry of the system was modeled using PhreeqC, a geochemical modeling software (Parkhurst and Appello, 2008). PDA I spring solutions contain high concentrations of Fe (4.0-7.0 mM), Al (15 mM), and Si (8.2 mM). Concentrations of other cations are relatively low (Ca=0.7 mM, Na=0.4 mM, Mg=0.7 mM) and anion concentrations, other than sulfate, show similar trends (F^-= 0.1 mM, Cl=0.05; Phillips-Lander et al., 2014). The solution chemistry of PDA I was used to create our experimental solutions (Table 1). Specifically, this solution was used to test the influences of temperature, an inorganic ligand (F-), and microbial surfaces on clay mineral formation in acid-sulfate systems. The solution pH was adjusted using hydrochloric acid to a starting pH of 2.6. A water bath was heated to 25 or 80^{o}C, depending on experimental conditions, to which 1L reactor vessels containing model hydrothermal solutions were added. Solutions were constantly mixed using magnetic stir bars.

Silicon was added as hydrous sodium metasilicate ($Na_2SiO_3 \cdot 5H_2O$). Aluminum was added as aluminum hydroxide ($AlOH_3$). In order to determine the influence of sulfate on clay mineral formation, different iron salts were added to the experiments. For sulfate experiments, iron and sulfate were added as iron sulfate heptahydrate ($FeSO_4 \cdot 7H_2O$).

Table 1: Solution chemistry is based on Pailas de Agua I, Rincon de la Vieja. Full solution chemistry for this spring can be viewed in Phillips-Lander et al. (2014). All values are in mM.

Table 1: Initial Solution Chemistry

Parameter	Concentration
Temperature (^oC)	25 and 80
pH	2.6
SO_4	38
Fe	38
Al	15
Si	8.2
Cl	0.054
Ca	0.69
Na	16
F	0,0.055

To model the influence of inorganic ligands on clay formation, fluoride, as calcium fluoride, was added to half of the reactor vessels in concentrations of 0.1 mM (Table 1). To one half of the reactor vessels in each experiment, 1 μm diameter polycarbonate microspheres with carboxyl functional groups were added at a concentration of 10^6 spheres$\cdot$ ml^{-1}, which is the approximate concentration of cells in Pailas de Agua I (Phillips-Lander et al., 2014) to model the effect of microbial surfaces on clay mineral nucleation without the influence of metabolism.

Data Collection

Reactor vessels were sampled (pH, T, solution, and precipitate) at 24 h intervals for the 14 day experiment. In order to correct pH for temperature effects, a sample of pH calibration solution was measured at 80^{o}C and used to calculate the deviance of measured pH using the following equation, (pH_1-pH_2)*(T_1-T_2)$^{-1}$=pH correction factor. This correction factor was then applied to the measured pH of experimental samples. Water samples were filtered using 0.45 μm polycarbonate filters, and samples for cation analysis were acidified with 2% high purity nitric acid to pH 2. All samples were kept at 4°C after

collection. Major cations were analyzed using inductively coupled plasma optical emission spectroscopy on a Perkin Elmer ICP-OES Optima 5300 DV. Mineral precipitates were collected and freeze-dried in the laboratory and then powdered and analyzed using a Bruker SMART APEX II X-ray Diffractometer (XRD) with a copper charge coupled detector (CCD). Samples from days 7 and 15 of the experiment were freeze-dried and split for further analyses. One split was reacted with glycol vapor in a sealed container at 60^{o}C for 24 h. Glycolated clay samples were then examined using XRD to determine basal spacing and clay mineral type. A second split from 80^{o}C was suspended in deionized water and mounted on lacey carbon grids using grid on drop mounting technique. These samples were analyzed using a JOEL JEM-2100 TEM/STEM High Resolution Transmission Electron Microscope in order to determine the relationship between reaction products and microspheres (microbial proxies).

Results

High Temperature (80^{o}C) Experiments

Over the course of the experiment, temperature remained constant once the solution reached experimental temperature (80^{o}C), while pH varied up to one pH unit (Table 2A). pH initially increased from 2.6 to 3-3.5 within 24h and remained constant after 24h, regardless of the presence or absence of fluoride or microbial proxies (Table 2A). In the first 24 h, Al concentrations in solution increased ~5% in solutions to which F- was added and 20-40% to solutions without F-.

Influence of Fluoride

Although the general trend in Al concentration is similar to pH, fluoride directly influenced the concentration of Al in solution. In fact, fluoride influences major cation chemistry in all 80^{o}C experimental trials. In experiments where F- is present, Al concentrations (Al=6.0-6.5 mM) are approximately six-fold greater than in experiments where F- is absent (Al=1.2-1.3 mM; Table 3A). Fe concentrations are nearly double in experiments containing F- (Fe=1.7x10^{+1} mM) than those in which F- was absent (Fe=7.2-7.3 mM; Table 3A). Silicic acid concentrations, in contrast, increase by only 15% in the presence of F^{-} ($Si_{\text{with fluoride}}$=7.9-8.0 mM v. $Si_{\text{without fluoride}}$=7.0-7.2 mM; Table 3A).

Table 2A: Temperature and pH of 80°C fluoride experiments. MS=Microbial Surrogates

Table 2A: Temperature and pH of fluoride experiments (80°C)					
[F-]		0.11 mM		0 mM	
Day	T (oC)	-MS pH	+MS pH	-MS pH	+MS pH
0	25	2.6	2.6	2.6	2.6
1	80	3.5	3.5	3.3	3.4
2	80	3.2	3.3	3.2	3.2
3	80	3.7	3.6	3.5	3.6
4	80	3.6	3.6	3.5	3.4
5	80	3.4	3.2	1.8	3.1
6	80	3.4	3.2	1.8	3.1
7	80	3.4	3.4	3.2	3.1
11	80	4.9	2.9	2.8	2.8
15	80	2.9	3.0	2.9	3.1

Influence of Microbial Surrogates

The presence of microbial surrogates in 80°C experiments exerts a small effect on the aqueous geochemistry in solution. When fluoride is present in solution, the presence of microbial surrogates in solution reduces the total concentration of Al by ~1% ($Al_{with\ surrogates}$=6.0 mM, $Al_{without\ surrogates}$=6.5 mM; Table 3A). In contrast, the concentration of Fe and Si are approximately the same between experiments with fluoride regardless of whether or not microbial surrogates were added to solution ($Fe=1.7x10^{+1}$ mM; Si=7.9-8.0 mM; Table 3A).

When fluoride is not present in solution, microbial surrogates *increase* the aqueous concentration of aluminum in solution by 1% ($Al_{with\ surrogates}$=1.3 mM, $Al_{without\ surrogates}$=1.2 mM; Table 3A). This is the opposite effect observed when fluoride is present in solution. The presence of microbial surrogates also slightly decreases Fe (~1%; $Fe_{with\ surrogates}$=7.2 mM, $Fe_{without\ surrogates}$=7.3 mM) and Si (~4%; $Si_{with\ surrogates}$=6.9 mM, $Si_{without\ surrogates}$=7.2 mM) concentration (Table 3A).

Authigenic Mineral Formation

Amorphous precipitates form in all 80°C experimental trials within the first 24 hours of the experiment. After 7 days, samples display broadly similar mineralogy between all experimental trials, including amorphous silica, jarosite, illite and mixed-layer smectite (Figure 1A). The presence of fluoride in

solution does not appear to influence the clay mineralogy; however it does influence the formation Fe-oxides/Fe-oxyhydroxylsulfates (Figure 1A). When fluoride is present, goethite is the dominant oxide phase (black lines; Figure 1A), however, when fluoride is absent, both goethite and schwertmannite form (grey lines; Figure 1A). Microbial surrogates did not exert influence on the mineralogy, however when microbial surrogates are present kaolinite peaks are obvious in unglycolated samples (solid lines) indicating a more crystalline character for these clay minerals (Figure 1A).

Table 3A: 80°C Aqueous Data

Day	0.1 mM					
	-Microbial Surrogates			+Microbial Surrogates		
	Al	Fe	Si	Al	Fe	Si
0	2.4E-02	2.6E+01	7.4E+00	3.6E-02	2.5E+01	8.0E+00
1	6.4E-01	2.8E+01	7.3E+00	7.5E-01	2.6E+01	7.9E+00
2	1.4E+00	2.7E+01	7.9E+00	1.4E+00	2.7E+01	8.3E+00
3	1.9E+00	2.6E+01	7.9E+00	1.8E+00	2.6E+01	8.3E+00
4	2.4E+00	2.5E+01	7.9E+00	2.3E+00	2.5E+01	8.4E+00
5	2.3E+00	2.0E+01	6.5E+00	2.7E+00	2.4E+01	8.3E+00
6	2.9E+00	2.2E+01	7.3E+00	2.5E+00	2.0E+01	7.0E+00
7	3.6E+00	2.2E+01	8.0E+00	3.3E+00	2.1E+01	8.2E+00
11	5.5E+00	1.9E+01	7.9E+00	5.1E+00	1.8E+01	8.1E+00
15	6.5E+00	1.7E+01	7.9E+00	6.0E+00	1.7E+01	8.0E+00
Day	0 mM					
	-Microbial Surrogates			+Microbial Surrogates		
	Al	Fe	Si	Al	Fe	Si
0	8.4E-03	7.9E+00	7.0E+00	2.0E-02	8.0E+00	7.2E+00
1	4.0E-02	7.9E+00	7.0E+00	4.7E-02	7.9E+00	6.8E+00
2	8.5E-02	7.9E+00	7.0E+00	9.0E-02	7.8E+00	6.8E+00
3	1.4E-01	7.8E+00	7.0E+00	1.5E-01	7.8E+00	6.8E+00
4	2.0E-01	7.8E+00	7.0E+00	2.2E-01	7.7E+00	6.8E+00
5	2.7E-01	7.6E+00	6.6E+00	2.7E-01	7.6E+00	6.3E+00
6	3.2E-01	7.7E+00	7.0E+00	3.5E-01	7.6E+00	6.8E+00
7	4.1E-01	7.6E+00	6.9E+00	4.2E-01	7.5E+00	6.4E+00
11	8.2E-01	7.3E+00	6.9E+00	9.1E-01	7.3E+00	6.8E+00
15	1.2E+00	7.3E+00	7.2E+00	1.3E+00	7.2E+00	6.9E+00

*Error is +/-0.1 mM for all samples

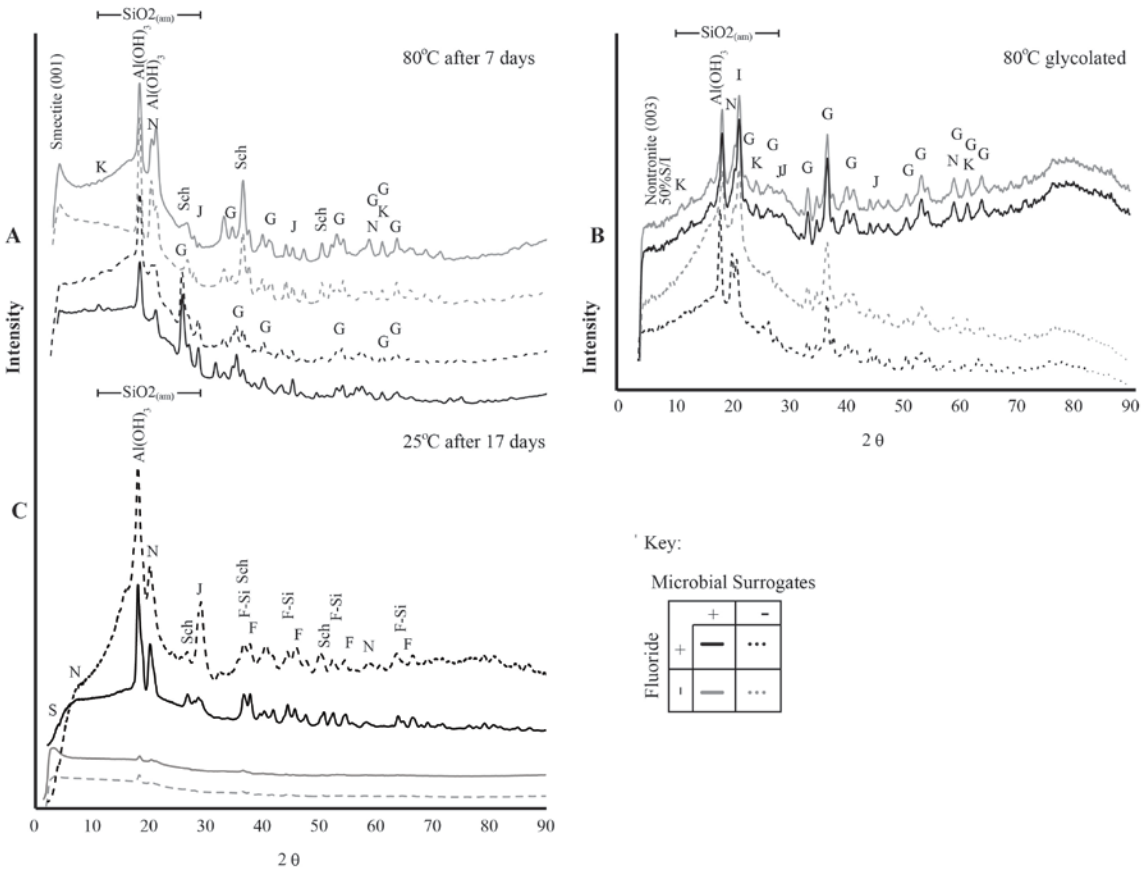

Figure 1: (A) XRD spectra of freeze-dried precipitates collected from experiments conducted at 80°C. Samples from experiments without fluoride precipitate schwertmannite in addition to the smectite, and goethite present in all experimental precipitates. Kaolinite forms only in experiments to which microbial surrogates were added. (B) XRD spectra of ethylene glycol treated precipitates from experiments conducted at 80°C. Samples with microbial surrogates are identical to each other and indicate a 50% mixture of smectite/illite. Samples without microbial surrogates tend to be less crystalline. (C) Experiments at 25°C show the influence of fluoride on mineralogy and degree of crystallinity. The addition of fluoride results in nontronite and Fe-oxide formation, while microbial surrogates have no effect on oxide formation.

Precipitates from 80°C experiments were glycolated in order to determine the type of clay minerals formed. Mixed-layer smectites are composed of a ~50% illite/nontronite mixture (Figure 1B). The presence of kaolinite was confirmed after glycolation (solid lines; Figure 1B) for samples containing microbial surrogates. Samples from experimental trials without microbial surrogates do not have detectable kaolinite peaks (dashed lines; Figure 1B). The presence of amorphous silica is more pronounced in experimental trials that contain neither fluoride, nor microbial surrogates (Figure 1B).

Transmission Electron Microscopy

Solid phase material from 80°C experiments was analyzed using TEM in order to determine the size, distribution and ordering of clay minerals in the precipitated phase. Mixed-layer smectite (1.45 nm/layer) was observed in 80°C samples collected from experimental trials containing fluoride and microbial surrogates (Figure 2A). Sample thickness makes clay mineral observations difficult; however, Fe-oxides are abundant only in samples with fluoride but without microbial surrogates (Figure 2B).

Low Temperature (25°C) Experiments

Experimental trials at 25°C displayed approximately constant pH and temperature over the course of the 21 day experiment (pH 2.3-2.6; Table 2B). Fluoride was added to half of the experimental trials ([F-]= 0.1 mM; Table 3B). Initial amorphous precipitates were detected after 7 days in experiments containing microbial surrogates and 11 days in samples without microbial surrogates. After 17 days, precipitates were more crystalline when F- was present in solution.

Table 2B: Temperature and pH of 80°C fluoride experiments. MS=Microbial Surrogates

Table 2B: Temperature and pH of fluoride experiments (25°C)

[F-]		0.055 mM		0 mM	
Day	T (°C)	-MS pH	+MS pH	-MS pH	+MS pH
0	25	2.7	2.7	2.6	2.7
3	25	2.8	2.8	2.9	3.0
7	25	2.8	2.8	2.9	3.0
10	25	2.6	2.6	2.8	2.9
14	25	2.7	2.7	2.7	2.8
17	25	2.7	2.7	2.6	2.8
21	25	2.6	2.6	2.6	2.7

Influence of Fluoride

The addition of fluoride to solution exerts significant influence on the Al solution concentration. In trials where microbial surrogates are absent, the addition of fluoride increases the Al concentration by an order of magnitude ($Al_{with\ fluoride}=4.6x10^{-2}$ mM v. $Al_{without\ fluoride}=3.3x10^{-3}$ mM; Table 3B). When microbial

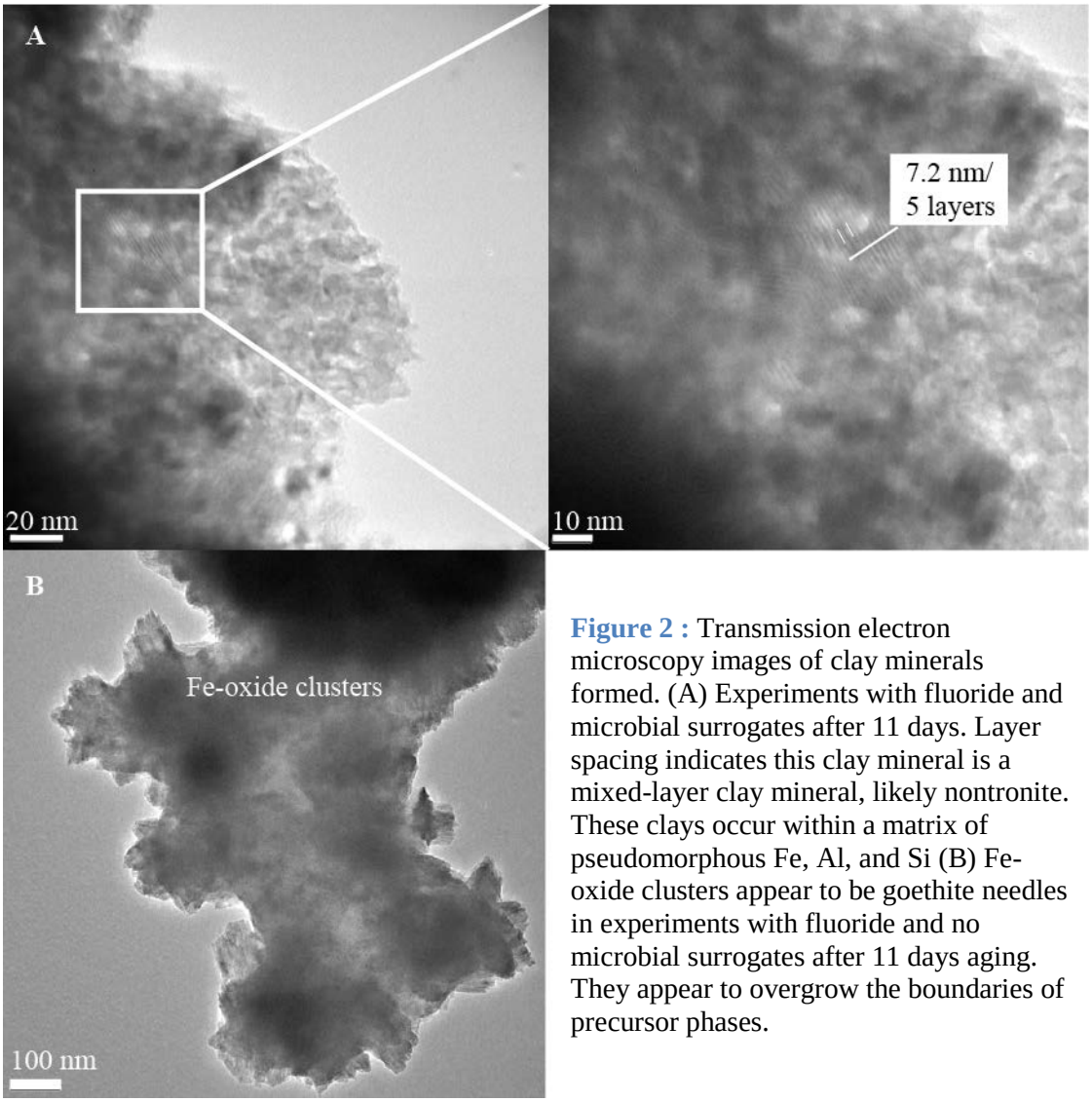

Figure 2 : Transmission electron microscopy images of clay minerals formed. (A) Experiments with fluoride and microbial surrogates after 11 days. Layer spacing indicates this clay mineral is a mixed-layer clay mineral, likely nontronite. These clays occur within a matrix of pseudomorphous Fe, Al, and Si (B) Fe-oxide clusters appear to be goethite needles in experiments with fluoride and no microbial surrogates after 11 days aging. They appear to overgrow the boundaries of precursor phases.

surrogates are present, the same general trend is observed ($Al_{\text{with fluoride}}=1.9x10^{-2}$ mM v. $Al_{\text{without fluoride}}=2.5x10^{-3}$ mM; Table 3B). In contrast, the Fe concentration in solution displays a five-fold decrease when fluoride is present in solution ($Fe_{\text{with fluoride}}=5.1\text{-}6.4$ mM v. $Fe_{\text{without fluoride}}=25\text{-}26$ mM; Table 3B). Silicic acid concentrations follow the same trend as Fe, with a ten-fold decrease in solutions containing fluoride ($Si_{\text{with fluoride}}=0.5\text{-}0.6$ mM v. $Si_{\text{without fluoride}}=5.7\text{-}6.0$ mM; Table 3B).

Influence of Microbial Surrogates

The presence of microbial surrogates in 25°C experiments exerts a small effect on the behavior of Fe and Si in solution. When fluoride is not present in solution, microbial surrogates do not significantly influence the aqueous Al concentration ($Al_{\text{with surrogates}}=2.5x10^{-3}$ mM, $Al_{\text{without surrogates}}=3.3x10^{-3}$ mM; Table 3B). However, in experiments to which fluoride has been added, the presence of microbial surrogates in solution reduces the total concentration of Al by half ($Al_{\text{with surrogates}}=1.9x10^{-2}$ mM, $Al_{\text{without surrogates}}=4.6x10^{-2}$ mM; Table 3B).

Table 3B: 25°C Aqueous Data

	0.1 mM					
Day	-Microbial Surogates			+Microbial Surogates		
	Al	Fe	Si	Al	Fe	Si
0	4.1E-02	6.2E+00	5.2E-01	1.8E-02	6.0E+00	4.3E-01
4	2.8E-02	6.2E+00	5.1E-01	2.4E-02	6.4E+00	4.7E-01
7	3.8E-02	7.0E+00	5.9E-01	3.4E-02	6.8E+00	4.9E-01
11	3.7E-02	6.4E+00	5.3E-01	4.1E-02	6.6E+00	4.7E-01
14	3.8E-02	6.1E+00	5.0E-01	3.4E-02	5.3E+00	3.6E-01
17	5.4E-01	6.7E+00	5.5E-01	4.1E-02	6.3E+00	4.3E-01
21	4.6E-02	6.4E+00	5.2E-01	1.9E-02	5.0E+00	6.6E-01
	0 mM					
Day	-Microbial Surogates			+Microbial Surogates		
	Al	Fe	Si	Al	Fe	Si
0	2.1E-03	3.6E+01	8.7E+00	1.6E-03	3.1E+01	7.9E+00
4	9.5E-04	3.0E+01	7.1E+00	bdl	2.4E+01	5.6E+00
7	2.7E-03	3.3E+01	6.8E+00	2.4E-03	2.8E+01	6.0E+00
11	4.0E-05	2.6E+01	6.1E+00	2.0E-03	2.6E+01	5.5E+00
14	1.0E-03	2.6E+01	6.1E+00	8.8E-04	2.4E+01	5.6E+00
17	1.4E-03	2.7E+01	6.2E+00	3.2E-03	2.6E+01	5.8E+00
21	3.3E-03	2.6E+01	6.0E+00	2.5E-03	2.5E+01	5.7E+00

*Maximum error: +/-0.1 mM for all samples

Authigenic Mineral Formation

The presence of fluoride in solution influences the precipitates mineralogy and degree of crystallinity in 25°C experiments. When fluoride is present in solution, precipitates' mineralogy is similar regardless of the presence/absence of microbial surrogates (Figure 1C). Fluoride facilitates the formation of mixed-layer smectites, nontronite, jarosite, goethite, $Al(OH)_3$, and amorphous silica. When fluoride is absent samples are mostly amorphous, with small peaks for $Al(OH)_3$ and smectite (Figure 1C).

Discussion

This study investigates the rapid formation of authigenic clay minerals in acidic (pH 2.6-3) oxidizing systems at 80°C and 25°C. Initial solution geochemistry was based on the fluids in Pailas de Agua I, an acid-sulfate spring within the Las Pailas hydrothermal vent field, Costa Rica, which is characterized by mixed layer smectites, nontronite, and kaolinite/halloysite clay mineralogy, and a diverse microbial population (Table 1; Phillips-Lander et al., 2014). The data from this study at 80°C approximately replicates the mineralogy present in Pailas de Agua I. One of the most intriguing findings of these experiments is that nontronite synthesis detected in acid-sulfate springs may occur under oxidizing conditions, which contrasts with previous work by Harder (1978) who indicated reducing conditions are necessary for nontronite formation. These data additionally demonstrate microbial surfaces influence the degree of crystallinity in early precipitates in experiments at 80°C over geologically instantaneous timescales (t=7 days). Moreover, both fluoride and microbial surrogates influence clay mineral nucleation in 25°C systems by reducing the activation energy required to form critical nuclei, although fluoride plays a greater role in authigenic clay nucleation.

Influence of Temperature and pH

While T and pH influence the dissolved Al concentration, in most natural waters (pH =5-8), Al is primarily found in the solid phase (Hitch et al., 2008). Elevated aqueous aluminum concentrations typically occur in acidic pH (<4) solutions (Plankey et al., 1986; Von Damm et al., 1985 a; however pH is not the dominant factor influencing the aqueous Al concentration in our experiments. Between 80°C and 25°C experimental trials, there is ~0.3 pH unit difference (Table 2A, B), and yet aqueous Al concentrations in 25°C systems were 2-3 orders of magnitude less than in 80°C experiments. The higher Al concentration in 80°C experiments serves to increase effective collisions between Al and Si ions in solution, resulting in increased reaction rates and authigenic clay mineral formation (Stumm and Morgan, 1996; Figure 1).

Increased Al solubility at higher T may partially explain why Tosca et al. (2008) observed that nontronite does not precipitate from circum-neutral pH solutions at T≤60°C. Temperature impact on Al activity may

explain why acid mine drainage is dominated by Fe-oxides and Fe- and Al-hydroxysulfates (McCarty et al., 1998; Bingham and Nordstrom, 2000) in Earth systems and why previous geochemical models place the lower pH limit for nontronite formation at pH≤4 (Chevrier et al., 2007). Despite these observations, our data indicates lower pH systems may form clay minerals in the presence of a complexing ligand or microbial surfaces.

Influence of Ligands

Ligands complex metal ions, including Fe and Al, and form coordination complexes which increase the total dissolved metal concentrations in solution. This process allows metals to exist in solution at higher concentrations than would otherwise be present (Drever, 1997).

Organic Ligand Effects

In many natural waters, organic acids effectively complex Al, facilitating the formation of Al-Si gels, which subsequently ripen to clay minerals (Fiore et al., 2011; Linares and Huerta., 1971). However, the type and concentration of organic acid present in solution influences the mineral formation (Huang and Violante, 1986; Blake and Walter, 1999; Gallup, 1998). Fulvic and humic acids, which are common in soils, have been implicated in authigenic clay formation across a wide pH range (pH 2-9; Linares and Huerta, 1971). Ueshima and Tazaki (2001) experimentally showed that polysaccharides in circum-neutral pH systems facilitate the formation of nontronite.

The influence of shorter-chain organic acids including oxalate, EDTA, and citric acid on clay formation is pH dependent. For example, in circum-neutral pH systems, oxalate forms strong complexes with Al (β_1= 7.26, β_2=13, β_3=16.3; Ding et al. 2003) and appears to facilitates kaolinite and mixed-layer smectite formation (Ding et al., 2003; Blake and Walter, 1999); however the degree of crystallinity of these clays are governed by temperature. In contrast, Gallup found clay mineral formation was retarded in the presence of oxalate, Na-EDTA, and citric acid below pH 5. Oxalic acid may only weakly complex Al at acid pH because the pKa_2=4.27; therefore the organic ligand is at least partially protonated at low pH.

In acid-sulfate hydrothermal systems, the presence of 0-0.1 mM oxalate does not appear to effectively complex Al in solution (Suppl. Table 1B). Oxalate may preferentially bind with iron in our model hydrothermal solution (β_1=7.58, β_2=13.81, β_3=18.60; Dellien, 1977). Primarily Fe-oxides including ferrihydrite and goethite were produced from these 80^{o}C experiments. Carboxyl functional groups present on microbial surrogate surfaces appear to facilitate the formation of goethite needles (Suppl. Figure 2). It is possible longer-chain organic acids may have a greater effect on Al-Si gel formation because these acids have more potential binding sites that deprotonate at variable pH and chelate metals; however, modeling the interaction between Al and organic acids is difficult due to the broad pH range over which binding sites deprotonate (Vance et al., 1996). Additional research is required to more fully establish the influences of organic acids and microbial biofilms in acidic pH hydrothermal systems.

Inorganic Ligand Effects

Inorganic ligands, including F- and SO_4^{2-}, also complex Al, increasing the total aqueous concentration. Fluoride strongly complexes Al in acidic (pH 3-5) systems (Plankey et al., 1986; β_1=7.0, β_2=12.7, β_3=16.8, β_4=19.4, β_5=20.6, β_6=20.6) outcompeting sulfate for binding sites (β_5=3.5, β_2=5.6; Nordstrom and May, 1986). PhreeqC model results indicate that Al in our model hydrothermal solutions is present primarily as $AlSO_4^+$, $Al(SO_4)_2^-$, and AlF^{2+} complexes. Sulfate may complex more Al because of its high concentration (38 mM) in solution. Despite this, the addition of fluoride to solution increased the Al concentration approximately six–fold from 1.2 mM to 6.5 mM in 80^{o}C experiments (Table 3A). Al complexation may not, however, strongly influence nontronite formation in 80^{o}C experiments, because total Al in solution is relatively high compared to other natural waters where clays are known to form (Table 3A; Schlesinger, 1997).

The importance of Al complexation by F^- is demonstrated in 25^{o}C experiments, where Al concentrations increased by approximately an order of magnitude when F- was present. Al concentrations, in the presence of F-, are approximately an order of magnitude greater than standard mean river water (Table 3B; Schlesinger, 1997), indicating F- plays an important role in Al solubility at low temperatures.

Fluoride can form structures that act as a template for early alumino-silicate formation (Caullet et al., 2005); therefore, net results of Al complexation by F^- in our experiments are (1) increased degree of crystallinity of precipitates and (2) changes in the mineralogy, specifically the formation of nontronite, schwertmannite, jarosite, and 6-line ferrihydrite vs. pseudomorphous phases (Figure 1C).

Experiments performed at 25^{o}C indicate that in low temperature solutions Al-complexation is critical to clay mineral formation and F- is commonly abundant hydrothermal solutions in similar concentrations to those measured in our hot springs (Thomas et al., 1977; Phillips-Lander et al., 2014). However, F- abundances in seawater are also similar to our model hydrothermal solution, indicating that F- may play a role in the Al-activity in seawater and in clay formation as Dekov et al. (2008) proposed. In contrast, fluvial and lacustrine systems F- concentrations are strongly governed by the geochemistry of the watershed's country rock. Therefore, F may not represent the primary ligand responsible for Al-complexation in all systems and sulfate, phosphate and other inorganic ligands may also aid in Al-Si gel sol formation and authigenic clay precipitation. Al complexation by phosphate in natural lake systems is dependent on a variety of factors including the Si concentration and organic matter (de Vicente et al., 2008). Si outcompetes phosphate for Al in solutions where the phosphate concentration is low, and organic matter often adsorbs phosphate from solution (de Vicente et al., 2008). The role of sulfate in Al-complexation in natural systems has been poorly studied and will be the subject of future research. The role of inorganic ligands in Al complexation is of great importance when considering authigenic clay formation in the absence of life as organic matter plays a significant role in clay formation in the most low temperature Earth systems (Konhauser and Urrutia, 1999).

The Influence of Microbial Surfaces

Microbial cell surfaces have been shown to influence clay mineral formation in a variety of Earth's environments, including lakes, rivers and hydrothermal systems (Alt and Mata, 2000; Konhauser and Urrutia, 1999; Tazaki, 1997; Fortin et al., 1998; Ueshima and Tazaki, 2001; Loucaides et al., 2010). Polystyrene microspheres coated in carboxyl groups have been used to approximate microbial cell

surfaces in experimental systems to model the role of microbes in mineral precipitation without the influence of metabolism (Roberts et al., 2013). In this study, microbial surrogates were used to examine how microbial surfaces and organic matter influence clay mineral authigenesis in half of the experimental trials. The overall degree of crystallinity is greater when microbial surrogates are present in 80^{o}C experiments (Figure 1B). Microbial cell surfaces adsorb metals (in this case Fe or Al), which lowers the interfacial energy required for critical nuclei formation (Konhauser, 2006). In our 25^{o}C experimental solutions, samples with microbial surrogates record early (t- 7-17 days) $Al(OH)_3$ and smectite nucleation, though these phases are poorly crystalline (Figure 1C). It should be noted that when fluoride is also present, 25^{o}C precipitates are mineralogically similar to those from the 80^{o}C experiments, indicating that fluoride plays a more important role in clay formation in low pH systems.

At low pH (1-4.5), carboxyl groups associated with microbial surrogate surfaces carry an net neutral to slightly positive surface charge (Yee and Fein 2001; He and Tebo, 1998; Crist et al. 1992); therefore total cation adsorption should be relatively low and the microbial impact on clay formation in acidic pH systems should be minimal. In order for positively charged carboxyl groups on the microbial surrogate surfaces to bond with positively charged ions and complexes, electrostatic repulsion must be overcome. The relatively high ionic strength of the solution (I=0.47; Phillips-Lander et al., 2014), in this case, would aid electric double layer compression, resulting in more effective collisions than might be otherwise expected (Wightman and Fein, 2005).

XRD analysis of 25^{o}C precipitates shows ferrihydrite precipitates and then sorbs Si from solution in experiments (Figure 1C). Silicic acid rapidly adsorbs to ferrihydrite across broad temperature (25-91^{o}C) and pH (3-12.5) ranges, resulting in the progressive transformation of ferrihydrite to goethite with time ($t \leq$ 1 week; Vempati and Loeppert, 1989; Phillips-Lander, unpublished data). Si adsorption to ferrihydrite present in 25^{o}C experiments likely leads to the formation of goethite in 80^{o}C experiments. Progressive binding of Al to Si onto goethite's surface has been shown to result in authigenic nontronite precipitation in other low temperature systems on Earth (Konhauser and Urrutia, 1999). However, the transformation

of goethite to mixed-layer smectites, including nontronite, is dependent on the availability of Al in solution. While microbial surfaces may stabilize early authigenic precipitates and lower the activation energy required for critical nuclei to form, the increased Al solubility associated with complexation appears to be a key parameter in clay formation in our 25°C experiments.

Clay Authigenesis in Acidic Systems

Solution chemistry was modeled in PhreeqC (Parkhurst and Appello, 2008) for 80°C experiments at t=0 and 7 days to determine the stability field of nontronite under the experimental conditions operating at these time slices. All experimental solutions are at or near equilibrium at the time of sampling and XRD analysis (7 days for 80°C; 17 days for 25°C). All models of experimental data resulted in nontronite and kaolinite precipitation. Total molar ratios were the same between experimental trials at the same temperature, therefore for simplicity, Table 4A presents the PhreeqC model for 80°C experiments and Table 4B for 25°C experiments regardless of conditions. PhreeqC effectively models the nontronite and goethite precipitation from solution; however, it does not predict the formation of kaolinite and schwertmannite from 80°C solutions (Table 4A). In contrast, PhreeqC indicates Fe-oxides, nontronite, and amorphous silica are present at saturation in both samples with and without fluoride (Table 4B). Despite this, our experimental results indicate the early onset of clay formation from solutions only when microbial surrogates and fluoride are present and complex Al in solution.

While the model may be limited, comparison of our 80°C experimental Pourbaix diagram with data from Chevrier et al.'s (2007) low temperature diagram for hypothetical Martian surface waters (Figure 3) denotes a broadening of the nontronite stability field in higher ionic strength solutions. Higher ionic strength solutions, such as used in this study ($I_{\text{this study}}$=0.4; I_{Chevrier}= $1x10^{-3}$), increases the effective collisions, aiding critical nuclei growth. Additional examination of the Pourbaix diagrams indicates Al activity in solution influences nontronite's stability field (Figure 3). In our experiments, the addition of fluoride increases the concentration, and therefore activity of the Al ion in solution.

Table 4: PhreeqC models were generated using the Lawrence Livermore National Laboratories database (llnl.dat)

Table 4A: PhreeqC model of solution chemistry (80°C)				
Mineral	SI (t=0)	Moles produced	SI (t=7)	Moles produced
Nontronite	0.0	$2.1x\ 10^{-3}$	0.0	$2.6x\ 10^{-3}$
Kaolinite	-4.9	Not predicted to form	-5.9	Not predicted to form
Goethite	0.0	$1.8x\ 10^{-2}$	-0.0	$1.8x\ 10^{-2}$
Schwertmannite/GreenRust	-17	Not predicted to form	-15	Not predicted to form

Table 4B: PhreeqC model of solution chemistry (25°C)				
Mineral	SI (t=0)	Moles produced	SI (t=7)	Moles produced
Nontronite	-0.00	$2.1x\ 10^{-3}$	-0.00	$1.5x\ 10^{-3}$
Kaolinite	-11.03	Not predicted to form	-42.64	Not predicted to form
Goethite	0.00	$1.4x10^{-3}$	0.00	$1.3x\ 10^{-2}$
Schwertmannite/GreenRust	-17	Not predicted to form	-17	Not predicted to form

Factors that Control Authigenic Clay Formation

Clay minerals are nearly ubiquitous in Earth's environments and form in a variety of pH and redox environments. Temperature plays a key role in clay mineral formation, with reaction kinetics dominating solutions at high temperatures ($T \leq 60^{o}C$; Tosca et al., 2008). Mixed-layer clays, nontronite, and kaolinite form in 80°C experiments. Despite this, clay minerals have been show to form in a variety of low temperature environments. Microbial surfaces act as a nucleation sites for Fe-oxide precipitation, however this process is most effective in circum-neutral pH systems where Fe-adsorption to cellular surfaces is most significant (Yee and Fein, 2001).

Authigenic nontronite formed in our experiments at lower pH than previously documented (pH 2.6-3). Previous research indicates clay mineralogy is strongly dependent on the total Al concentration in solution (Dekov et al., 2008) and the presence of microorganisms (Dekov et al., 2008; Konhauser and Urrutia, 1999). Our 25°C experiments indicate nontronite precipitation at low pH is related to Al activity in solution. In the absence of fluoride, Al activity decreases by an order of magnitude relative to when fluoride is present in solution. Our modeling has shown Al-complexation by F- positively influences

nontronite stability at low pH; however, fluoride is not a common ion in solution. Therefore, it is possible that the tendency of acid-mine drainage (AMD) systems to form Fe-oxides instead of clay minerals (Peretyazhko et al., 2009; Knorr and Blodau, 2007; Kumpulainen et al., 2007) may be related to the anionic chemistry of AMD solutions. In circum-neutral pH systems, Al solubility is expected to be low; however, Al-complexation by organic acids has already been shown to increase Al activity in solution and aid authigenic clay formation. Based on these associations, we may infer that Al-complexation is a key to authigenic clay formation across a broad diversity of geochemical systems.

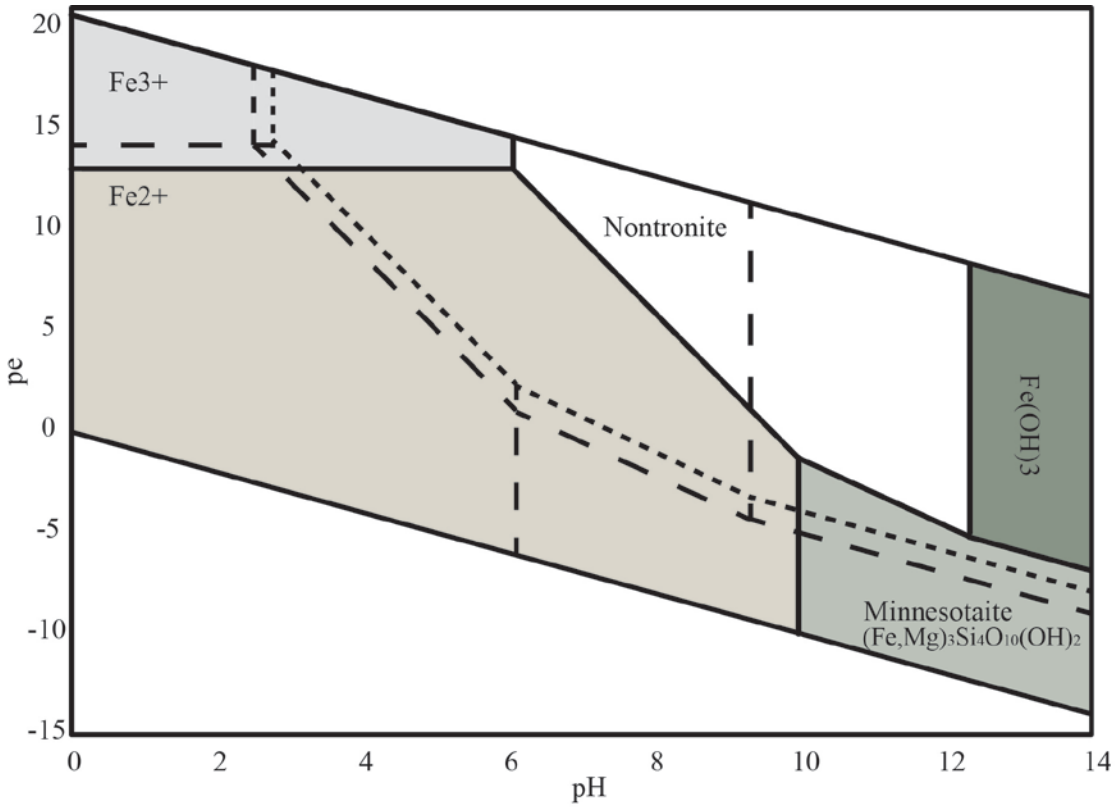

Figure 3: Stability field of nontronite, based on solution chemisty data from t=7 days. Nontronite is predicted to be stable above pH 2 for 80°C experiments (large dashed line). The small dashed line represents the stability field based on data from 25°C experiments, which contracts at lower temperature. Both dashed lines overlap on the y-axis. These data are plotted against Chevrier et al. (2007) model of nontronite stability for Mars (colored boxes). Aluminum activity in solution influences the stability of nontronite in solution. Holding all other data except Al constant, a plot of nontronite stability with lower Al concentration decreases the low pH bounaryof Al stability by 1 pH unit (smaller dashed line). Decreasing temperature contracts the stability field as well (not shown).

Implications for Mars

While most researchers postulate that clay mineral formation on Mars during the Noachian occurred in hydrothermal waters (Ehlmann et al., 2011; Ehlmann et al., 2008; Fairen et al., 2011; Brown et al., 2010), the exact temperature and pH of these solutions remains unknown. In Earth systems, clay minerals represent only a minor component of the mineralogy in circum-neutral hydrothermal systems (White and Poizat, 1995; White and Hedenquist, 1995); however mixed-layer smectites, nontronite, and kaolinite are a dominant mineralogical characteristic in acid-sulfate systems. Our experimental results, therefore, support Marcucci et al.'s (2013) observation that acid-sulfate hydrothermal systems produce similar mineralogy to the Martian surface. While our research expands the range of geochemical conditions which may have been present on Mars, it should also be noted that our data set the lower limit for nontronite formation in acidic pH systems is ~pH 2. Therefore, extremely acidic environments are likely not appropriate analogs for Mars.

Geomorphological evidence of the past existence of fluvial and lacustrine deposits on Mars' surface, suggests the potential for a well-developed hydrologic system during the Noachian (Ehlmann and Edwards, 2014), which may represent a broad diversity of potential geochemical environments. The current state of knowledge sheds no light on whether life evolved on Mars. In the absence of life, Al-complexation by inorganic ligands, as demonstrated in this study therefore, would play a key role in clay mineral formation. Additional research is required to determine the anionic chemistry required to foment authigenic clay formation on Mars in the absence of life. At the same time, if a record of life is found in the Martian rock record, we propose this life played an important role in the Noachian evolution of Mars' surface by facilitating authigenic clay mineral formation, as has been shown on Earth.

Acknowledgements

This work would not be possible without the financial support of a University of Kansas Dissertation Fellowship, a Geological Society of America Student Research Grant, an ExxonMobil Student Research Grant, an AWG Chevron Research Scholarship, and an AWG Sean S. Thompson Service Research Scholarship (awarded to Charity M. Phillips-Lander). We thank Masato Ueshima and Karla Leslie for

their laboratory support. We thank Victor Day of the X-ray Crystallography Laboratory for his technical assistance with the XRD.

Disclosure Statement

No competing financial interests exist.

Author Contributions

Lab work: Experimental design was undertaken by Charity Phillips-Lander with assistance from David Fowle. Laboratory analyses, including characterization of the mineralogy by X-ray diffraction, and aqueous geochemistry were performed by Charity Phillips-Lander. Transimission electron microscoy was performed by Charity Phillips-Lander and Linduo Zhao.

Writing: The paper was written by Charity Phillips-Lander with the assistance of Jennifer Roberts.

Revisions: Paper revisions were contributed by Charity Phillips-Lander, Jennifer Roberts, Hailiang Dong, and David Fowle.

References

Alt, J., and Mata, P (2000). On the role of microbes in the alteration of submarine basaltic glass: a TEM study. Earth and Planetary Science Letters 181, 301-313.

Alt, J. (1988). Hydrothermal oxide and nontronite deposits on the seamounts of the Eastern Pacific. Marine Geology 81, 227-239.

Banfield, J., Barker, W., Welch, S., and Taunton, A. (1999). Biological impact on mineral dissolution: application of the lichen model to understanding mineral weathering in the rhizosphere. Proceedings of the National Academies of Science of the United States of America 96, 3404-341.

Bingham, J. M. and Nordstrom, D. K. (2000). Iron and aluminum hydroxysulfates from acid-sulfate waters. Reviews in Mineralogy and Geochemistry 40, 351-403 DOI: 10.2138/rmg.2000.40.7.

Bishop, J. L., Dobrea, E. Z. N., McKeown, N. K., Parente, M., Ehlmann, B. L., Michalski, J. R., Milliken, R. E., Poulet, F., Swayze, G. A., Mustard, J. F., Murchie, S. L., and Bibring, J. (2008). Phyllosilicate

Diversity and Past Aqueous Activity Revealed at Mawrth Vallis, Mars. Science, 321(5890), 830-833. doi:10.1126/science.1159699

Blake, R. E., and Walter, L. M. (1999). Kinetics of feldspar and quartz dissolution at 70–80 C and near-neutral pH: effects of organic acids and NaCl. Geochimica et Cosmochimica Acta, 63(13), 2043-2059.

Bogdanov, Y. A., Lisitzin, A. P., Binns, R. A., Gorshkov, A. I., Gurvich, E. G., Dritz, V. A., and Kuptsov, V. M. (1997). Low-temperature hydrothermal deposits of Franklin seamount, Woodlark basin, Papua New Guinea. Marine geology, 142(1), 99-117.

Brown, A. J., Hook, S. J., Baldridge, A. M., Crowley, J. K., Bridges, N. T., Thomson, B. J., Marione, G. M., de Souza Filho, C. R., Bishop, J. L. (2010). Hydrothermal formation of Clay-Carbonate alteration assemblages in the Nili Fossae region of Mars. Earth and Planetary Science Letters, 297, 174-182.

Caullet, P., Paillaud, J. L., Simon-Masseron, A., Soulard, M., & Patarin, J. (2005). The fluoride route: a strategy to crystalline porous materials. Comptes Rendus Chimie, 8(3), 245-266.

Chevrier, V., Poulet, F., and Bibring, J (2007). Early geochemical environment of Mars as determined from thermodynamics of phyllosilicates. Nature, 448(7149), 60-63. doi:10.1038/nature05961

Chipera S. J. and Bish, D. L. (2002). Thermal evolution of fluorine from smectite and kaolinite. Clay and Clay Minerals, 50, 38-46.

Crist, R H, Oberholser, K, McGarrity, J, Crist, D R, Johnson, J K, and Brittsan, J M. (1992). Interaction of metals and protons with algae. 3. Marine algae, with emphasis on lead and aluminum. Environmental Science and Technology, 26, 496-502.

Decarreau, A., Bonnin, D., Badaut-Trauth, D., Couty, R., and Kaiser, P. (1987). Synthesis and crystallogenesis of ferric smectite by evolution of Si-Fe coprecipitates in oxidizing conditions. Clay Minerals, 22(2), 207-223.

Dellien, I. (1977). Thermodynamic Properties of Iron Oxalates and Malonates in Perchlorate Medium. Acta Chemica Scandinavica A, 31, 473-479.

Dekov, V., Cuadros, J., Shanks, W., and Koski, R. (2008). Deposition of talc — kerolite–smectite — smectite at seafloor hydrothermal vent fields: Evidence from mineralogical, geochemical and oxygen isotope studies. Chemical Geology, 247(1-2), 171-194. doi:10.1016/j.chemgeo.2007.10.022

Dekov, V., Kamenov, G., Stummeyer, J., Thiry, M., Savelli, C., Shanks, W., Fortin, D., Kuzmann, E., and Vertes, A. (2007). Hydrothermal nontronite formation at Eolo Seamount (Aeolian volcanic arc, Tyrrhenian Sea). Chemical Geology, 245(1-2), 103-119. doi:10.1016/j.chemgeo.2007.08.006

de Vicente, I., Jensen, H. S., & Andersen, F. Ø. (2008). Factors affecting phosphate adsorption to aluminum in lake water: Implications for lake restoration. Science of the total environment, 389(1), 29-36.

Ding, Z., Zhang, M., andHan, J. (2003). Synthesis of magnesium aluminate powders utilizing the solubility relationships in the Mg-Al-Oxalic Acid-H_2O system.Bulgarian Journal of Physics 30, 152-157.

Drever, J. I. (1997). The geochemistry of natural waters: Surface and groundwater environments (3rd edition). Prentice Hall, Upper Saddle River. 436 p.

Ehlmann, B. L. and Edwards, C. S. (2014). Mineralogy of the Martian surface. Annual Reviews of Earth and Planetary Science, 42, 291-315. DOI: 10.1146/annurev-earth-060313-055024

Ehlmann, B. L., Mustard, J. F., Murchie, S. L., Bibring, J., Meunier, A., Fraeman, A. A., and Langevin, Y (2011). Subsurface water and clay mineral formation during the early history of Mars. Nature, 479, 53-60. doi:10.1038/nature10582

Ehlmann, B. L., Mustard, J. F., Fassett, C. I., Schon, S. C., Head III, J. W., des Marais, D. J., Grant, J. A., and Murchie, S. L. (2008). Clay minerals in delta deposits and organic preservation potential on Mars. Nature Geoscience, 1(6), 355-358. doi:10.1038/ngeo207

Fairén, A. G., Davila, A. F., Gago-Duport, L., Haqq-Misra, J. D., Gil, C., McKay, C. P., and Kasting, J. F (2011). Cold glacial oceans would have inhibited phyllosilicate sedimentation on early Mars. Nature Geoscience, 4, 667-670. doi:10.1038/ngeo1243

Fiore, S., Dumontet, S., Huertas, F. J., and Pasquale, V (2011). Bacteria-induced crystallization of kaolinite. Applied Clay Science, 53(4), 566-571. doi:10.1016/j.clay.2011.05.005

Fortin, D., Ferris, G., and Scott, S. D. (1998). Formation of Fe-silicates and Fe-oxides on bacterial surfaces in samples collected near hydrothermal vents on the Southern Explorer Ridge in the northeast Pacific Ocean. American Mineralogist, 83, 1399-1408.

Gallup, D. L. (1998). Aluminum silicate scale formation and inhibition (2): scale solubilities and laboratory and field inhibition tests. Geothermics, 26(4), 483-499.

Grotzinger, J. P., Sumner, D. Y., Kah, L. C., Stack, K., Gupta, S., Edgar, L., Lewis, K., Schieber, J., Mangold, N., Milliken, R., Conrad, P. G., DesMarais, D., Farmer, J., Siebach, K., Calef III, F., Hurowitz, J., McLennan, S. M., Ming, D., Vaniman, D., Crisp, J., Vasavada, A., Edgett, K. S., Malin, M., Blake, D., Gellert, R., Mahaffy, P., Wiens, R. C., Maurice, S., Grant, J. A., Wilson, S., Anderson, R. C., Beegle, L., Arvidson, R., Hallet, B., Sletten, R. S., Rice, M., Bell III, J., Griffes, J., Ehlmann, B., Anderson, R. B., Bristow, T. F., Dietrich, W. E., Dromart, G., Eigenbrode, J., Fraeman, A., Hardgrove, C., Herkenhoff, K., Jandura, L., Kocurek, G., Lee, S., Leshin, L. A. , Leveille, R., Limonadi, D., Maki, J., McCloskey, S., Meyer, M., Minitti, M., Newsom, H., Oehler, D., Okon, A., Palucis, M., Parker, T., Rowland, S., Schmidt, M., Squyers, S., Steele, A., Stolper, E., Summons, R., Treiman, A., Williams, R., Yingst, A., and the MSL Science Team (2014). A habitable fluvio-lacustrine environment at Yellowknife Bay, Gale crater, Mars. Science, 343(6169), 1242777.

Harder, H. (1978). Synthesis of iron layer silicate minerals under natural conditions. Clays Clay Minerals, 26(1), 65-72.

Harder, H. (1976). Nontronite synthesis at low temperatures. Chemical Geology, 18(3), 169-180.

Harder, H. (1972). The role of magnesium in the formation of smectite minerals. Chemical Geology, 10(1), 31-39.

He, L M, and Tebo, B M. (1998) .Surface charge properties of and Cu(II) adsorption by spores of the marine Bacillus sp. strain SG-1. Applied and Environmental Microbiology, 64, 1123-1129.

Hekinian, R., Hoffert, M., Larque, P., Cheminee, J. L., Stoffers, P., and Bideau, D. (1993). Hydrothermal Fe and Si oxyhydroxide deposits from South Pacific intraplate volcanoes and East Pacific Rise axial and off-axial regions. Economic Geology, 88(8), 2099-2121.

Hem, J. D., and Lind, C. J. (1974). Kaolinite synthesis at 25^{o}C. Science, 184, 1171-1173.

Hitch, B. F., Mesmer, R. E., Baes, C. F., Jr., and Sweeton, F. H (1980). The solubility of gibbsite (α - $Al(OH)_3$) in 1 MOLAL NaCl as a function of pH and temperature ORNL-5623, 1-37.

Huang, P. M., and Violante, A. (1986). Influence of organic acids on crystallization and surface properties of precipitation products of aluminum. Interactions of soil minerals with natural organics and microbes, 17, 159-221.

Juniper, S. K. and Fouquet, Y. (1988) Filamentous iron-silica deposits from modern and ancient hydrothermal sites. Canadian Mineralogist, 26, 859-869.

Knorr, K. H., & Blodau, C. (2007). Controls on schwertmannite transformation rates and products. Applied Geochemistry, 22(9), 2006-2015.

Köhler, B., Singer, A., and Stoffers, P. (1994). Biogenic nontronite from marine white smoker chimneys. Clays and Clay Minerals, 42(6), 689-701.

Konhauser, K. O. (2006). Introduction to Geomicrobiology. Wiley-Blackwell, Hoboken, 440 p.

Konhauser, K., and Urrutia, M. (1999). Bacterial clay authigenesis: a common biogeochemical process. Chemical Geology,161, 399-413.

Kumpulainen, S., Carlson, L., & Räisänen, M. L. (2007). Seasonal variations of ochreous precipitates in mine effluents in Finland. Applied Geochemistry, 22(4), 760-777.

Kyle, J. E., and Schroeder, P. A. (2007). Role of smectite in siliceous-sinter formation and microbial-texture preservation: Octopus Spring, Yellowstone National Park, Wyoming, USA. Clays and Clay Minerals, 55, 189-199.

Labouriau, A., Kim, Y., Chipera, S., Bish, D. A., and Earl, W. L. (1995). A ^{19}F nuclear magnetic resonance study of natural clays. Clay and Clay Minerals, 43, 697-704.

La Iglesia, A., Martin-Vivaldi, J., and Aguayo, F (1976). Kaolinite crystallization at room temperature by homogeneous precipitation. III. Hydrolysis of feldspars. Clays And Clay Minerals, 24, 36-42.

Lalonde, S. V., Amskold, L., McDermott, T. R., Inskeep, W. P., and Konhauser, K. O. (2007). Chemical reactivity of microbe and mineral surfaces in hydrous ferric oxide depositing hydrothermal springs. Geobiology, 5, 219-234. DOI: 10.1111/j.1472-4669.2007.00113.x

Linares, J., and Huertas, F (1971). Kaolinite: synthesis at room temperature. Science, 171, 896-897.

Loucaides, S., Michalopoulos, P., Presti, M., Koning, E., Behrends, T., and van Cappellen, P (2010). Seawater-mediated interactions between diatomaceous silica and terrigenous sediments: Results from long-term incubation experiments. Chemical Geology, 270(1-4), 68-79. doi:10.1016/j.chemgeo.2009.11.006

Madden, M. E., Bodnar, R. J., and Rimstidt, J. D. (2004). Jarosite as an indicator of water-limited chemical weathering on Mars. Nature, 431(7010), 821-823.

Marcucci, E., Hynek, B. M., Kierein-Young, K. S., and Rogers, K. L. (2013). Visible-near-infrared reflectance spectroscopy of volcanic acid-sulfate alteration in Nicaragua: Analogs for early Mars. Journal of Geophysical Research: Planets, 118, 1-21. doi:10.1002/jgre.20159

Masuda, H. 1995. Iron-rich smectite formation in the hydrothermal sediment of the Iheya Basin, Okinawa Trough. In: Sakai, H. and Nozaki, Y. editors. Biogeochemical Processes and Ocean Flux in the Western Pacific. Terra Scientific Publishing Company, p. 509-521.

McCarty, D. K., Moore, J. N., and Marcus, W. A. (1998). Mineralogy and trace element association in an acid mine drainage iron oxide precipitate; comparison of selective extractions. Applied Geochemistry, 13, 165-176. DOI: 10.1016/S0883-2927(97)00067-X.

Nordstrom, D., and May, H (1989). Aqueous equilibrium data for mononuclear aluminum species. In G. Sposito, The Environmental Chemistry of Aluminum (2nd ed., pp. 39-80). CRC Press, Boca Raton, Florida.

Parkhurst, D., and Appello, C (2008). PHREEQC (Version 2) A Computer Program for Speciation, Batch-Reaction, One-Dimensional Transport, and Inverse Geochemical Calculations. United States Geological Survey.

Peretyazhko, T., Zachara, J. M., Boily, J. F., Xia, Y., Gassman, P. L., Arey, B. W., & Burgos, W. D. (2009). Mineralogical transformations controlling acid mine drainage chemistry. Chemical Geology, 262(3), 169-178.

Phillips-Lander, C. M., Fowle, D. A., Taunton, A., Hernandez, W., Mora, M., Moore, D., Shinogle, H., and Roberts, J. A. (2014). Silicate Dissolution in Las Pailas Thermal Field: Implications for Microbial Weathering in Acidic Volcanic Hydrothermal Spring Systems. Geomicrobiology Journal, 31, 23-41. DOI:10.1080/01490451.2013.802395

Plankey, B. J., Patterson, H. H., and Cronan, C. S. (1986). Kinetics of aluminum fluoride complexation in acidic waters. Environmental Science and Technology, 20(2), 160-165.

Reinholdt, M., Miehé-Brendlé, J., Delmotte, L., Le Dred, R., & Tuilier, M. H. (2005). Synthesis and characterization of montmorillonite-type phyllosilicates in a fluoride medium. Clay Minerals, 40(2), 177-190.

Reinholdt, M., Miehé-Brendlé, J., Delmotte, L., Tuilier, M. H., le Dred, R., Cortès, R., & Flank, A. M. (2001). Fluorine route synthesis of montmorillonites containing Mg or Zn and characterization by XRD,

thermal analysis, MAS NMR, and EXAFS spectroscopy. European Journal of Inorganic Chemistry 2001, 2831-2841.

Roberts, J. A., Kenward, P. A., Fowle, D. A., Goldstein, R. H., Gonzalez, L. A., & Moore, D. S (2013). Surface chemistry allows for abiotic precipitation of dolomite at low temperature. Proceedings of the National Academy of Sciences of the United States of America, 110(36), 14540-14545. doi:10.1073/pnas.1305403110

Schlesinger, W (1997). Biogeochemistry: An Analysis of Global Change (2nd ed., p. 588). Academic Press, San Diego, CA.

Stumm, W., and Morgan, J. J (1996). Aquatic Chemistry: Chemical Equilibria and Rates in Natural Waters (3rd ed., p. 1022). Wiley-Interscience.

Tazaki, K. (1997). Biomineralization of layer silicates and hydrated Fe/Mn oxides in microbial mats; an electron microscopical study. Clays and Clay Minerals, 45(2), 203-212.

Thomas Jr., J., Glass, H. D., White, W. A., and Trandel, R. M. (1977). Fluoride content of clay minerals and argillaceous Earth materials. Clay and Clay Minerals, 25, 278-284.

Tosca, N. J., Milliken, R. J. and Michael, F. M. (2008). Smectite formation on early Mars: Experimental constraints, in *Workshop on Martian Phyllosilicates: Recorders of Aqueous Processes?*, Abstract 7030.

Trefry, J. H., Trocine, R. P., Klinkhammer, G. P., and Rona, P. A. (1985). Iron and copper enrichment of suspended particles in dispersed hydrothermal plumes along the mid-Atlantic Ridge. Geophysical Research Letters, 12(8), 506-509.

Ueshima, M., and Tazaki, K (2001). Possible role of microbial polysaccharides in nontronite formation. Clays and Clay Minerals, 49, 292-299.

Von Damm, K. L., Edmond, J. M., Grant, B., Measures, C. I., Walden, B., and Weiss, R. F. (1985a). Chemistry of submarine hydrothermal solutions at 21 N, East Pacific Rise. Geochimica et Cosmochimica Acta, 49(11), 2197-2220.

Vance, G. Stevenson, F. J. and Sikora, F. J. (1996). Environmental chemistry of almninum-organic complexes. In 'The Environmental Chemistry of Aluminum.' Sposito,G. (ed.) 2nd edition. pp. 169-220, (CRC Press, Boca Raton, Florida.)

Vempati, R., and Loeppert, R (1989). Influence of structural and adsorbed Si on the transformation of synthetic ferrihydrite. Clays and Clay Minerals, 37, 273-279.

Welch, S. A., and Ullman, W. J. (1993). The effect of organic acids on plagioclase dissolution rates and stoichiometry. Geochimica et Cosmochimica Acta, 57(12), 2725-2736.

White, N., and Hedenquist, J. (1995). Epithermal gold deposits: styles, characteristics and exploration. SEG Newsletter, 23, 9-13.

White, N., and Poizat, V. (1995). Epithermal deposits: diverse styles, diverse origins. Pancrim95.

Wightman, P., and Fein, J. (2005). Iron adsorption by Bacillus subtilis bacterial cell walls. Chemical Geology, 216(3-4), 177-189. doi:10.1016/j.chemgeo.2004.11.008

Yee, N and Fein, J. (2001). Cd adsorption to bacterial surfaces: a universal adsorption edge? Geochimica et Cosmochimica Acta, 65, 2037-2042.

Supplementary Information

Suppl Table 1: Aqueous chemistry of experimental solutions at 80^{o}C in the presence of Ca-oxalate

Table 1: Temperature and pH of oxalate experiments			
[Oxalate]		0.11 mM	
Day	T (oC)	-MS pH	+MS pH
0	25	2.5	2.5
1	83	3.3	3.3
2	79	3.2	3.2
3	80	3.0	3.1
4	80	3.3	3.0
5	80	3.0	2.8
6	80	2.8	2.7
11	80	2.8	2.7
15	80	1.7	1.8

Table 2: 80°C Aqueous Data Oxalate Experiments						
	0.1 mM					
Day	-Microbial Surrogates			+Microbial Surrogates		
	Al	Fe	Si	Al	Fe	Si
0						
1	4.9E-2	2.0E+1	6.8E+0	8.6E-2	2.0E+1	6.7E+0
2	7.6E-2	2.0E+1	6.9E+0	1.1E-1	2.0E+1	7.3E+0
3	1.1E-1	2.1E+1	7.4E+0	2.1E-1	2.0E+1	7.3E+0
4	1.5E-1	1.9E+1	7.0E+0	2.4E-1	2.0E+1	7.7E+0
5	2.1E-1	1.8E+1	7.4E+0	4.1E-1	2.0E+1	7.8E+0
6	2.8E-1	1.8E+1	7.3E+0	5.2E-1	2.0E+1	7.8E+0
7						
11	8.3E-1	1.7E+1	7.7E+0	1.2E+0	1.82E+1	8.2E+0
15	1.4E+0	1.5E+1	7.8E+0	1.8E+0	1.68E+1	7.9E+0
	0 mM					
Day	-Microbial Surrogates			+Microbial Surrogates		
	Al	Fe	Si	Al	Fe	Si
0						
1	7.2E-2	2.0E+1	6.9E+0	8.6E-2	2.0E+1	6.7E+0
2	1.4E-1	2.1E+1	7.2E+0	1.1E-1	2.0E+1	7.3E+0
3	1.5E-1	1.8E+1	6.5E+0	2.1E-1	2.0E+1	7.3E+0
4	3.8E-1	2.0E+1	7.4E+0	2.4E-1	2.0E+1	7.7E+0
5	3.3E-1	2.0E+1	7.9E+0	4.1E-1	2.0E+1	7.8E+0
6	4.0E-1	1.8E+1	7.4E+0	5.2E-1	2.0E+1	7.8E+0
7						
11	9.4E-1	1.8E+1	7.9E+0	1.2E+0	1.8E+1	8.2E+0
15	1.4E+0	1.6E+1	7.8E+0	1.8E+0	1.7E+1	7.9E+0

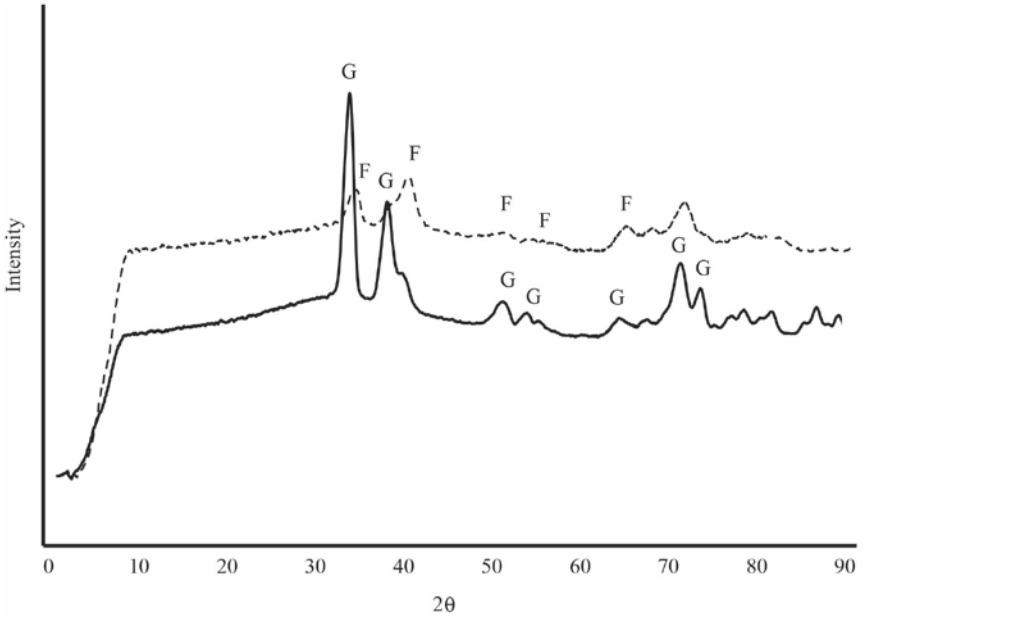

Suppl. Figure 3: XRD spectra of 80°C experiments to which Ca-Oxalate was added, shows primarily Fe-oxide/-oxyhydroxide formation. When microbial surrogates are present, precipitated ferrihydrite converts to goethite. The presence of oxalate (0.1 mM) in solution may inhibit clay mineral formation because the pKa2 oxalic acid=4.27 which is outside our experimental pH range and therefore, it may not effectively complex Al in solution.

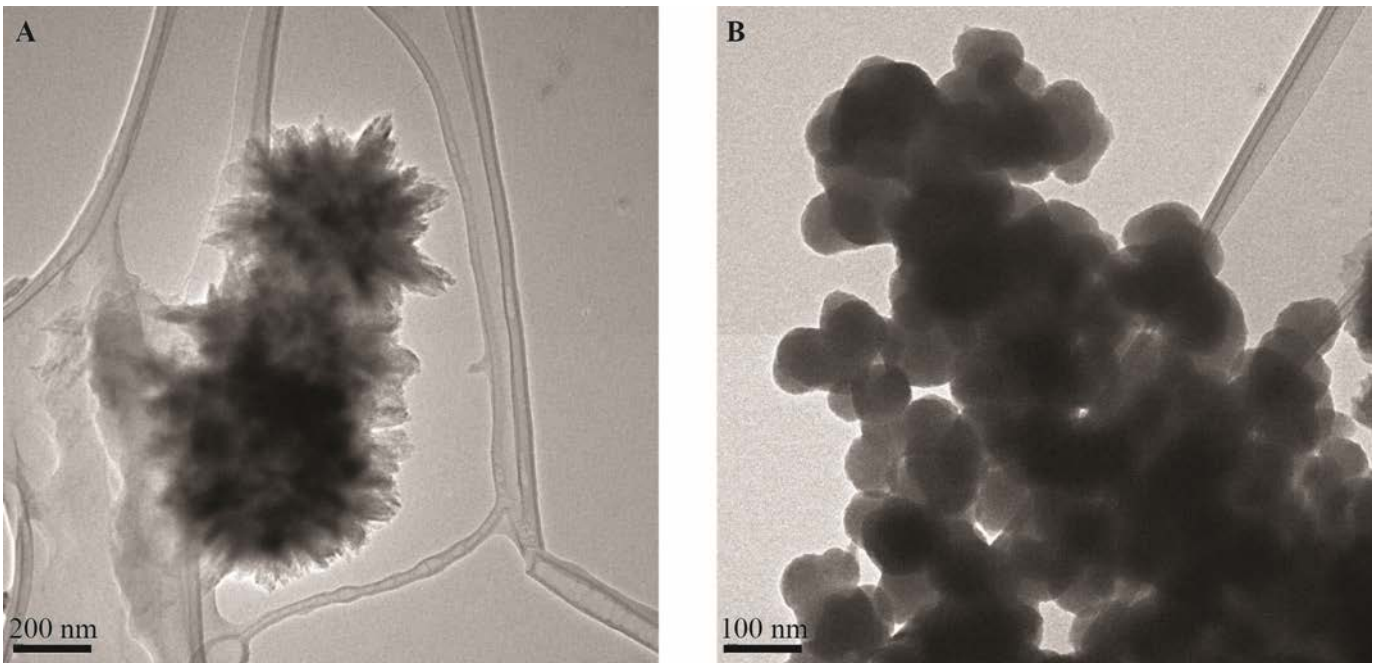

Suppl. Figure 4: Low magnification TEM images of 80°C experiments to which Ca-Oxalate and microbial surrogates were added shows the formation of (A) goethite and (B) amorphous silica spherules.

Chapter 5. Conclusions and Implications

Previous research has focused on circum-neutral pH hydrothermal systems in order to guide our understanding of microbial processes on early Earth because the geochemistry of these systems facilitates exceptional preservation of microbial structures (Kandianis et al., 2008; Phoenix and Konhauser, 2008). These previous studies have indicated that microorganisms have played a role in the alteration of Earth's environments, since the evolution of microbial life on Earth (t>3.0 Ga; Wacey, 2012) and have helped develop the parameters by which we look for life on other planets.

Microbially enhanced dissolution and element cycling

Because acid-sulfate systems have been largely ignored, this study may essentially be considered a reconnaissance study of the influences of microbial and chemical weathering processes in acid-sulfate systems. My results from field colonization experiments indicate microorganisms do more than simply live in these extreme environments, they also modify them by similar means to what has been observed in neutral-chloride hydrothermal systems. In these systems, microbially-induced dissolution of phosphate-doped anorthoclase is enhanced by an order of magnitude relative to abiotic rates. Similar trends were not detected for amphibole and pyroxene, indicating dissolution is dependent on nutrient limitation within the community. In sum, these results demonstrate that quantifying microbially-induced dissolution has important ramifications for major and trace element cycling in acid-sulfate systems.

Rates calculated for anorthoclase weathering represent initial dissolution rates (t=24 h; 2 mo) and no long-term studies were performed. While initial microbial colonization of the surface, including biofilm production that covers mineral surfaces, enhances short-term weathering and dissolution rates, this does not mean long-term weathering will be enhanced in microbial systems (e.g. Welch et al., 1999). Long-term weathering and mineral dissolution rates are governed by geochemical controls including: pH, mineralogy, and the types of organic functional groups present. The combination of these processes may either enhance or retard long-term dissolution and major and trace element mobilization in hydrothermal systems (Banfield et al., 1999). For example, in a year-long study by Templeton et al (2009), basalt

dissolution in neutral-chloride hydrothermal waters at the Loihi seamount was minimal. No such complimentary research has been done in acid-sulfate hydrothermal systems. Therefore, it remains unclear what long-term impact microorganisms have on mineral dissolution in acid-sulfate springs.

Phosphate-limitation in microbial communities

Microorganisms in Las Pailas enhance mineral dissolution to overcome phosphate limitation, in much the same way as microorganisms mine minerals to overcome nutrient limitation in low temperature systems (Roberts, 2004). Analysis of element partitioning in Las Pailas further indicates that while dissolved phosphate is low (bdl-0.03 mM; Chapter 2), abundant phosphate is present in Las Pailas sediments, with the highest concentrations (bdl-120 mg kg^{-1}) observed to weakly adsorbed in the exchangeable fraction (Appendix A). These results suggest a holistic approach is required to define nutrient limitation within microbial communities, as P may be present within the sediment where it may be "mined" by microorganisms. Understanding the total available P-concentration has important ramifications for interpreting microbial endemism, which has been linked to P-limitation (Souza et al., 2008). Microbial community shifts in response to P-limitations may simply measure community shifts toward microorganisms that are better adapted to acquire mineral-bound phosphate. If so, it is possible that there are specific genes that govern which microorganisms are best adapted to low phosphate conditions or to solubilizing phosphate bound within the sediment. Alternatively, additional research may indicate the development of microbial endemism is related to something other than the apparent P-limitations measured. Understanding what constitutes P-limitation in microbial communities is particularly important within astrobiological contexts. As we search for life on other planets, we must first understand the requirements for life on Earth. Failure to fully capture the resources available to microbial communities may potentially mislead our interpretations regarding the "habitability of other worlds."

Microbial trace element cycling and ore formation

Because apatite present in apatite-bearing anorthoclase occurred in association with Fe-oxide inclusions, the acquisition of P/Fe from these minerals by microorganisms could have important ramifications for the liberation of other metals into solution, as many trace metals typically adsorb to Fe-oxides, including Fe,

Cu, Ni, among others. These metals, in low concentrations, may be micronutrients for microorganisms and therefore have established nutritional requirements (Chapter 3, Table 4). However, as the research in Chapter 3 demonstrates, Las Pailas spring sediments contain toxic concentrations of these metals. Therefore, any microbially-induced dissolution of the sediments to obtain phosphate may also liberate toxic metals into solution. In examining Las Pailas sequential extraction data, we found that microorganisms sequester these toxic trace metals within the organic fraction of the sediments through adsorption of the metals to cellular surfaces, Fe-oxides within the biofilm, and possibly to the biofilm itself. I postulate that this occurred as a result of internal regulation of biofilm pH, however, we were unable to directly establish this based on the bulk samples we examined. In order to test the establishment of pH microenvironments within the biofilms present, which could positively influence adsorption of trace metals to Fe-oxides and cellular surfaces, we would need to use pH microelectrodes to record internal *in situ* biofilm pH. We could also more systematically examine the structure of the biofilm by doing biofilm extractions to identify the organic compounds present and their ability to chelate metals to determine how much and what type of trace metals may actually be bound to organic acids within these biofilms.

Even without this knowledge, I showed that microorganisms form shallow epithermal Au-Ag deposits. Though their limited extent makes them relatively uneconomic, microbially-induced ore formation at the surface is linked to deeper hydrothermal circulation and may act as an indicator of active epithermal ore deposition at depth. Because microbially-induced ore formation appears to occur in hydrothermal systems regardless of pH, I hypothesize trace metal sequestration and associated ore formation may be a common biogeochemical process which would be observed in the rock record. Some Cenozoic epithermal ore deposits display variations in carbon isotopes that may be indicative of microbial processes and the association between biomarkers and ore deposition in the MacArthur River H-Y-C sedex deposit also suggest microorganisms play an intimate role in ore formation. Together these studies suggest that microorganisms may be involved in low temperature ($<121^{o}C$, Kashefi and Lovely, 2001) ore formation,

regardless of ore deposit type. In order to establish whether microorganisms are intimately related to shallow ore deposition throughout geologic time, a systematic survey of low temperature ore deposits for indicators of microbial processes would be required. More broadly, these findings suggest that microbial processes may be distinguishable in the rock record even when exceptional preservation of microbial morphologies is absent.

Clay mineral formation is abiotic

Not all weathering processes occurring in Las Pailas springs system are microbially-influenced. While microorganisms aid in silicification and the formation of Fe-oxides in neutral-chloride hydrothermal systems (Phoenix and Konhauser, 2003; Lalonde et al., 2005; Yee et al., 2003; Konhauser et al., 2004), bulk mineral formation in acid-sulfate hydrothermal systems appears to be governed by abiotic processes. PhreeqC modeling of the hydrothermal solution in PDA I indicates nontronite and kaolinite should form authigenically within the spring and experimental work conducted supports these models. Clay minerals, including mixed-layer smectites, nontronite, and kaolinite, form in our model hydrothermal solutions within 7 days, which is geologically instantaneous. In these high (80^{o}C) temperature conditions, clay minerals form regardless of the presence or absence of microorganisms. In low temperature (25^{o}C) experiments, microorganisms aid in initial critical nuclei formation, however, even low concentrations of fluoride (0.1 mM) increase the degree of crystallinity in low temperature experiments, resulting in detectable nontronite peaks within 17 days. These results are particularly important because they suggest that while the presence of clay minerals in sediment may indicate the liquid water was present in the past, these clays may have formed under a variety of geochemical conditions. Therefore we cannot extrapolate from mineralogy to past environmental conditions without additional supporting evidence. In the case of Mars, additional atmospheric and sediment geochemical data, and understanding of modern weathering on the surface will be required in order to determine the environmental conditions which produced nontronite and kaolinite during the Noachian.

Hot spring clay formation is dependent on sulfate

Clay minerals rapidly form from acid-sulfate solutions in almost all cases and previous descriptions of epithermal ore bodies note the development of dominant clay mineralogy as an indicator of high-sulfidation type deposits (White and Poizat, 1995; White and Hedenquist, 1995). Low-sulfidation deposits, in contrast, have been linked to silicification (White and Poizat, 1995; White and Hedenquist, 1995). This raised the question of whether the presence of the sulfate ion in solution is a controlling factor in clay formation. While sulfate is not the strongest complexing ligand in solution, sulfate complexed more Al and Fe than F- because of its concentration in solution (Appendix B). To determine whether sulfate plays a role in clay mineral precipitation, I repeated these experiments with chloride substituted for sulfate in solution. These data are presented in Appendix B.

Chloride, like fluoride, is a halogen group element and should behave similarly in solution. In addition chloride is more common in natural waters (19,000 mg kg^{-1} mean seawater; 5.8 mg kg^{-1}mean river water) than fluoride (1.3 mg kg^{-1} mean seawater; 0.10 mg kg^{-1} mean river water; Schlesinger, 1997). XRD results indicate after 7 days, clay minerals form abiotically, regardless of the presence or absence of additional fluoride in solution (Appendix B, Figures 1-4). Moreover, clays produced in acid-chloride waters are more crystalline than their acid-sulfate counterparts. These data suggest chloride, like fluoride, may facilitate the organization of early proto-clays. Evidence of this process in natural systems would be based on (1) evolution of chloride from the clay structure (Chipera and Bish., 2002), (2) NMR analyses of chloride within the clay mineral (Labouriau et al., 1995).

Initial visual comparison of samples collected from low temperature (25^{o}C) chloride and sulfate experiments appears to indicate that while acid-sulfate precipitates are less crystalline, they are more abundant. I allowed low temperature chloride and sulfate experiments to run for ~2 years to evaluate the long-term crystallization of clay minerals from these solutions and to determine whether the total weight of clays produced from solution are equivalent. These samples are presently being dried in order to weigh them and examine them with XRD for mineralogical changes.

I anticipate the total amount of clays produced from the acid-sulfate solutions will be greater than those produced from acid-chloride solutions. While clays form in neutral-chloride solutions, the mineralogy is dominated by siliceous sinters. Kyle and Schroeder (2007) showed that precipitation of smectites in neutral-chloride hot springs precedes the onset of sinter formation. They argued sinter formation occurred as a result of alteration of feldspar to clay, which should raise pH and increase the silica concentration in solution. My results, however, indicate that interactions between the anions in solution and aluminum may influence the formation of clay minerals. If this is true, then neutral-chloride and acid-sulfate spring mineralogy reflect not the total water flux through springs (Ehlmann et al., 2011), nor strictly the influence of microorganisms (Konhauser and Urrutia, 1999). Instead the types of anions in solution may how much clay precipitates.

A better understanding of the geochemical factors influencing abiotic authigenic clay formation may be the most important result gleaned from this dissertation, simply because so little is known about clay formation, despite its broad treatment in the literature. The presence of abundant clays on Mars has raised interesting questions about the nature and evolution of the Martian surface and Mars' hydrologic cycle. The mineralogical and geomorphological diversity present on the Martian surface indicates that both acidic and circum-neutral pH waters were present in some context, though the total water content and composition on Mars remains unclear. Ehlmann and Edwards (2014) indicated the next great frontier in Mars research is a solid understanding of the potential anions present in waters on Mars. Currently, the sulfate concentration in Martian soils (1-1.7 wt.% ; 980-1,700 mM; Smith et al., 2014) is several orders of magnitude greater than the total sulfate in our springs (38 mM) and the ocean (84 mM; Schlesinger, 1997). If sulfate is intimately related to clay formation, then the voluminous clays present on Mars' surface may be related to the activity of the sulfate ion when liquid water was present on Mars. The current MAVEN mission may shed light on the evolution of Mars' atmosphere and therefore its hydrologic cycle. This treatment of clay mineral formation, may therefore, provide important clues to understanding the evolution of Mars brines.

Conclusion

Taken together, the data presented in this dissertation provide a broad geochemical overview of acid-sulfate hydrothermal systems and the contributions of chemical and microbial aluminosilicate mineral weathering in these systems. These data indicate exceptional preservation is not the only indication of microbial processes and that trace metal cycling may be used as an indicator of microbial processes throughout geologic time, regardless of system pH. Moreover, microorganisms may play a key role in low temperature ore formation throughout geologic time.

While microbial processes are important in acid-sulfate hydrothermal systems, clay mineral formation is driven by abiotic processes and may be linked to the activity of the sulfate ion in solution. Fluoride, which is often incorporated into clay minerals, aids in rapid nucleation of clay minerals and increases their degree of crystallinity. Chloride may play a similar role to fluoride, however, even when present in solution, it may result in less clay formation than sulfate. Therefore, abiotic clay formation may be dependent on the anion chemistry in solution and these data have important ramifications for our understanding of clay mineral formation on Mars.

References

Banfield, J. F., Barker, W. W., Welch, S. A. and Taunton, A. (1999). Biological impact on mineral dissolution: Application of the lichen model to understanding mineral weathering in the rhizosphere. Proceedings of the National Academy of Sciences for the United States of America 96, 3404-3411. DOI: 10.1073/pnas.96.7.3404

Chipera S. J. and Bish, D. L. (2002). Thermal evolution of fluorine from smectite and kaolinite. Clay and Clay Minerals 50, 38-46.

Ehlmann, B. and Edwards, C. (2014). The mineralogy of Mars: A view from orbital infrared spectroscopy. Goldschmidt Abstracts 2014.

Ehlmann, B. L., Mustard, J. F., Murchie, S. L., Bibring, J., Meunier, A., Fraeman, A. A., and Langevin, Y (2011). Subsurface water and clay mineral formation during the early history of Mars. Nature, 479, 53-60. doi:10.1038/nature10582

Kandianis, M. T., Fouke, B., Johnson, R. W., Veysey II, J., and Inskeep, W. P (2008). Microbial biomass: A catalyst for $CaCO_3$ precipitation in advection-dominated transport regimes. GSA Bulletin 120, 442-450.

Kashefi, K, and Lovley, D R. 2003. Extending the upper temperature limit for life. Science 301, 934. doi:10.1126/science.1086823

Konhauser, K., Jones, B., Phoenix, V., & Ferris, G (2004). The microbial role in hot spring silicification. AMBIO: A Journal Of The Human Environment 33, 552-558. DOI: 10.1579/0044-7447-33.8.552

Konhauser, K., and Urrutia, M (1999). Bacterial clay authigenesis: a common biogeochemical process. Chemical Geology.

Kyle, J. E., and Schroeder, P. A. (2007). Role of smectite in siliceous-sinter formation and microbial-texture preservation: Octopus Spring, Yellowstone National Park, Wyoming, USA. Clays and clay minerals, 55(2), 189-199.

Labouriau, A., Kim, Y., Chipera, S., Bish, D. A., and Earl, W. L. (1995). A ^{19}F nuclear magnetic resonance study of natural clays. Clay and Clay Minerals 43, 697-704.

Lalonde, S., Konhauser, K., Reysenbach, S. and Ferris, F. G. (2005). The experimental silicification of Aquificales and their role in hot spring sinter formation. Geobiology, 3, 41-52.

Phoenix, V. and Konhauser, K (2003). Experimental study of iron and silica immobilization by bacteria in mixed Fe-Si systems: implications for microbial silicification in hot springs. Canadian Journal Of Earth Science 40, 1669-1678. DOI: 10.1139/E03-044

Phoenix, V. R. and Konhauser, K. O. (2008) Benefits of bacteria biomineralization. Geobiology 6, 303-308. DOI: 10.1111/j.1472-4669.2008.00147.x

Roberts, J. A. R. and Bennett, P. (2004) . Mineral stimulation of subsurface microorganisms: release of limiting nutrients from silicates. Chemical Geology 203, 91-108.

Schlesinger, W (1997). Biogeochemistry: An Analysis of Global Change (2nd ed.). Academic Press, San Diego, CA, 558 p.

Smith, M. L., Claire, M. W., Catling, D. C., and Zhanle, K. J. (2014) The formation of sulfate, nitrate and perchlorate salts in the Martian atmosphere. Icarus, 231, 51-64.

Souza, V., Eguiarte, Siefert, J., and Elser, J (2008). Microbial endemism: does phosphorus limitation enhance speciation Nature Reviews Microbiology 6, 559-564.

Templeton, A., Knowles, E., Eldridge, D., Arey, B., Dohnalkova, A. C., Webb, S. M., Bailey, B. E., Tebo, B. M., and Staudigel, H. (2009). A seafloor microbial biome hosted within incipient ferromanganese crusts. Nature Geoscience 2, 872-876. DOI:10.1038/NGEO696

Wacey, D. (2012) Earliest evidence for life on Earth: an Australian perspective. Australian Journal of Earth Sciences 59, 153-166. DOI:10.1080/08120099.2011.592989

Welch, S, Barker, W W, and Banfield, J F. 1999. Microbial extracellular polysaccharides and plagioclase dissolution. Geochimica et Cosmochimica Acta 63: 1405-1419. doi:10.1016/S0016-7037(99)00031-9

White, N., and Hedenquist, J. (1995). Epithermal gold deposits: styles, characteristics and exploration. SEG Newsletter 23, 9-13.

White, N., and Poizat, V. (1995). Epithermal deposits: diverse styles, diverse origins. Pancrim95.

Yee, N., Phoenix, V. R., Konhauser, K. O., Benning, L. G., and Ferris, F. G (2003). The effect of cyanobacteria on silica precipitation at neutral pH: implications for bacterial silicification in geothermal hot springs. Chemical Geology, 199(1-2), 83-90. doi:10.1016/S0009-2541(03)00120-7

Appendix A: Elemental Distribution in Las Pailas Hot Spring Sediments

Major Element Distribution in Las Pailas Sediments

	Major Elements (weight percent by fraction)							
Exchangeable	**Al_2O_3**	**CaO**	**Fe_2O_3**	**K_2O**	**MgO**	**MnO**	**Na_2O**	**SiO_2**
Standard	1.1E+00	1.1E+01	6.5E-01	bdl	7.5E-01	1.0E-01	bdl	bdl
Yellowstone Paint Pots	1.4E-04	1.2E-03	3.2E-05	4.3E+01	bdl	bdl	bdl	bdl
Laguna Fumarolica	1.5E-04	3.9E-04	3.4E-03	5.2E+01	bdl	bdl	2.4E-03	bdl
Poza de Hongo	2.8E-03	bdl	1.6E-03	saturated	9.4E-03	bdl	4.4E-03	bdl
Pailas de Agua II								
RVCR4-09	1.6E-02	1.1E-03	1.4E-02	bdl	bdl	bdl	3.3E-03	bdl
RVCR8-09	2.3E+00	2.9E-01	2.3E+01	4.1E+01	2.5E-02	bdl	7.0E-01	bdl
RVCR12-09	2.1E+00	6.6E-02	2.0E+00	bdl	5.6E-02	1.1E-03	1.4E+00	5.3E-02
RVCR13-09	2.8E-02	2.5E-02	1.8E-02	saturated	1.1E-03	bdl	8.4E-03	bdl
RVCR14-09	2.0E-03	3.0E-04	1.4E-03	7.3E+01	bdl	bdl	2.0E-03	bdl
RVCR65-09	1.0E+01	3.0E-01	6.1E+00	3.2E-01	5.3E-01	1.7E-02	6.0E-01	bdl
Pailas de Agua I								
RVCR1-09	1.5E-05	bdl	bdl	1.1E+02	bdl	bdl	2.1E-03	bdl
RVCR9-09	2.6E+00	2.7E-02	2.3E+00	bdl	8.0E-02	3.1E-03	bdl	3.3E-02
RVCR17g-09	1.6E+01	1.1E+00	1.2E+01	7.2E-02	6.5E-01	3.7E-02	5.0E-02	1.0E-01
RVCR17r-09	2.9E-01	4.9E-02	9.4E-01	bdl	3.6E-02	2.2E-03	1.1E-01	1.1E-01
RVCR17b-09	1.1E-01	2.5E-02	1.7E+00	bdl	4.7E-02	1.9E-03	1.3E+00	2.6E-02
Pailas de Barro								
RVCR6-09	4.4E-03	bdl	1.1E-04	saturated	3.3E-03	bdl	2.9E-03	bdl
RVCR7-09	9.4E-02	2.1E-01	bdl	bdl	5.0E-02	2.1E-04	1.3E+00	2.0E-02
RVCR23-09	1.4E-03	9.2E-03	4.7E-05	8.0E+01	bdl	bdl	2.3E-03	bdl
Hornillas	bdl	bdl	bdl	6.4E+01	bdl	bdl	bdl	bdl

*bdl=below detection limits

Major Elements (weight percent by fraction)

Carbonate	Al_2O_3	CaO	Fe_2O_3	K_2O	MgO	MnO	Na_2O	SiO_2
Standard	3.3E-01	1.1E-01	6.2E-02	bdl	bdl	bdl	1.0E-02	bdl
Yellowstone Paint Pots	1.5E-02	bdl	1.7E-03	bdl	bdl	bdl	bdl	bdl
Laguna Fumarolica	2.1E-02	8.4E-03	2.2E-01	bdl	bdl	bdl	1.4E-03	2.9E+00
Poza de Hongo	2.2E-01	4.0E-02	1.5E-01	bdl	bdl	bdl	bdl	bdl
Pailas de Agua II								
RVCR4-09	bdl	bdl	bdl	bdl	bdl	bdl	bdl	bdl
RVCR8-09	3.9E-01	3.0E-03	1.4E+00	bdl	bdl	bdl	bdl	bdl
RVCR12-09	3.4E-01	5.7E-03	1.5E-01	bdl	bdl	1.8E-04	bdl	bdl
RVCR13-09	5.1E-01	3.4E-02	3.6E-01	bdl	bdl	bdl	1.3E-02	bdl
RVCR14-09	5.3E-01	8.8E-03	3.3E-01	bdl	bdl	bdl	bdl	bdl
RVCR65-09	1.2E+00	1.8E-02	3.8E-01	5.9E-03	3.1E-03	3.3E-04	9.9E-01	bdl
Pailas de Agua I								
RVCR1-09	2.3E-02	3.2E-03	bdl	bdl	bdl	bdl	3.1E-02	bdl
RVCR9-09	3.3E-01	1.9E-03	3.6E-01	bdl	bdl	3.2E-04	1.4E-02	bdl
RVCR17g-09	1.3E+00	2.6E-02	4.1E-01	bdl	4.2E-03	5.6E-04	2.4E-02	3.5E-02
RVCR17r-09	2.9E-01	4.9E-02	9.4E-01	bdl	3.6E-02	2.2E-03	1.1E-01	1.1E-01
RVCR17b-09	1.8E-01	1.2E-02	3.4E-01	bdl	bdl	2.9E-04	1.4E-02	bdl
Pailas de Barro								
RVCR6-09	2.5E-01	1.2E-02	3.2E-02	bdl	bdl	bdl	bdl	bdl
RVCR7-09	6.6E-02	2.3E-02	2.6E-02	bdl	2.1E-03	2.6E-04	1.3E-02	bdl
RVCR23-09	1.1E+01	5.1E-03	1.5E-02	bdl	bdl	bdl	8.5E-03	bdl
Hornillas	7.6E-02	3.6E-03	4.2E-02	bdl	bdl	bdl	4.9E-03	2.0E+00

*bdl=below detection limits

Major Elements (weight percent by fraction)

Oxide	Al_2O_3	CaO	Fe_2O_3	K_2O	MgO	MnO	Na_2O	SiO_2
Standard	1.9E+00	8.3E-01	2.6E+00	bdl	4.0E-01	bdl	1.7E-01	bdl
Yellowstone Paint Pots	4.9E-01	6.3E-02	3.5E-01	bdl	bdl	bdl	6.1E-02	bdl
Laguna Fumarolica	Bdl	bdl	1.9E+01	bdl	bdl	bdl	bdl	bdl
Poza de Hongo	3.6E+00	3.9E-01	2.2E+00	bdl	1.6E-01	bdl	1.1E-01	bdl
Pailas de Agua II								
RVCR4-09	5.6E-01	2.8E-02	1.2E+01	bdl	bdl	bdl	8.1E-02	bdl
RVCR8-09	1.7E-01	4.7E-02	3.9E+00	bdl	bdl	bdl	1.3E-01	bdl
RVCR12-09	2.6E+00	bdl	2.9E+01	6.5E-01	bdl	1.7E-02	6.7E-02	2.8E-01
RVCR13-09	6.8E-01	6.0E-02	4.0E+00	bdl	bdl	bdl	7.3E-02	bdl
RVCR14-09	1.1E+00	6.0E-02	1.3E+01	3.3E-01	bdl	bdl	2.8E-01	bdl
RVCR65-09	2.2E-01	7.7E-03	2.0E-01	6.2E-04	7.1E-03	3.8E-04	1.9E-01	5.1E-02
Pailas de Agua I								
RVCR1-09	1.2E+00	1.9E-02	2.3E+00	bdl	bdl	bdl	6.8E-02	6.9E-01
RVCR9-09	5.3E-01	bdl	1.3E+00	4.6E-02	4.1E-03	8.4E-04	bdl	3.9E-02
RVCR17g-09	2.0E+00	2.0E-02	1.2E+00	1.5E-02	1.3E-02	2.0E-03	1.6E-01	4.8E-02
RVCR17r-09	1.8E+00	bdl	6.8E+00	3.4E-02	8.9E-03	4.9E-03	bdl	5.3E-02
RVCR17b-09	5.7E-01	2.3E-02	4.0E+00	8.5E-03	2.6E-03	2.3E-03	bdl	3.4E-02
Pailas de Barro								
RVCR6-09	Bdl	bdl	bdl	bdl	bdl	bdl	bdl	bdl
RVCR7-09	4.1E+00	2.9E-01	1.6E+01	1.8E-03	1.3E-01	3.0E-02	8.9E+00	4.1E+00
RVCR23-09	9.4E-01	7.4E-02	5.0E+00	bdl	bdl	bdl	9.2E-02	bdl
Hornillas	1.0E+00	6.2E-02	4.3E+00	bdl	bdl	bdl	2.0E-01	bdl

*bdl=below detection limits

	Major Elements (weight percent by fraction)							
Organic Fraction	**Al_2O_3**	**CaO**	**Fe_2O_3**	**K_2O**	**MgO**	**MnO**	**Na_2O**	**SiO_2**
Standard	1.5E-03	2.3E-03	2.7E-04	bdl	bdl	bdl	1.1E-03	3.0E-02
Yellowstone Paint Pots	Bdl	bdl	bdl	bdl	bdl	bdl	bdl	bdl
Laguna Fumarolica	1.6E-04	6.5E-04	bdl	bdl	bdl	bdl	4.1E-04	9.9E-02
Poza de Hongo	Bdl	bdl	bdl	bdl	bdl	bdl	bdl	7.1E-04
Pailas de Agua II								
RVCR4-09	4.9E-04	4.1E-04	7.6E-04	bdl	bdl	bdl	2.7E-04	5.5E-02
RVCR8-09	1.2E-04	6.9E-04	bdl	bdl	bdl	bdl	3.4E-04	9.4E-03
RVCR12-09	1.6E-01	9.1E-03	7.8E-02	bdl	1.1E-03	bdl	bdl	2.9E-01
RVCR13-09	2.3E-04	bdl	9.6E-04	bdl	bdl	bdl	7.4E-05	1.9E-02
RVCR14-09	4.2E-04	3.8E-04	bdl	bdl	bdl	bdl	3.7E-04	2.9E-02
RVCR65-09	Bdl	bdl	1.2E-02	bdl	bdl	bdl	bdl	bdl
Pailas de Agua I								
RVCR1-09	8.1E-04	1.7E-04	bdl	bdl	bdl	bdl	4.9E-04	1.5E-02
RVCR9-09	1.4E-01	2.6E-02	3.1E+01	bdl	bdl	2.1E-02	bdl	2.7E-01
RVCR17g-09	4.1E-01	7.1E-02	9.9E-01	bdl	5.8E-03	bdl	bdl	7.5E-01
RVCR17r-09	4.5E-01	9.2E-02	1.9E+00	bdl	4.1E-03	3.0E-04	bdl	3.0E-01
RVCR17b-09	1.1E-01	7.7E-02	1.8E+00	bdl	1.6E-03	3.0E-04	bdl	2.7E-01
Pailas de Barro								
RVCR6-09	3.3E-04	2.2E-04	bdl	bdl	bdl	bdl	bdl	8.5E-03
RVCR7-09	5.5E-01	1.2E-01	2.4E-01	7.9E-03	5.6E-03	3.1E-04	1.7E-02	5.0E-01
RVCR23-09	1.0E-01	2.0E-02	9.3E-02	6.4E-02	8.8E-04	bdl	1.0E-01	2.4E+00
Hornillas	1.7E-03	9.4E-04	bdl	bdl	bdl	bdl	2.4E-04	1.0E-01

*bdl=below detection limits

Major Elements (weight percent by fraction)

Residual	Al_2O_3	CaO	Fe_2O_3	K_2O	MgO	MnO	Na_2O	SiO_2
Standard	sample lost							
Yellowstone Paint Pots	1.3E-01	5.9E+00	bdl	1.3E-03	2.2E-04	2.1E-05	1.5E-03	1.9E-04
Laguna Fumarolica	6.5E-03	2.6E+00	7.9E-02	7.6E-04	1.4E-05	4.2E-05	1.5E-04	3.1E-04
Poza de Hongo	2.2E-01	6.8E+01	1.9E-02	3.3E-03	6.5E-03	1.2E-04	2.7E-03	7.3E-04
Pailas de Agua II								
RVCR4-09	4.1E-02	9.8E+00	8.6E-02	3.5E-03	3.3E-04	6.5E-05	1.8E-03	2.3E-04
RVCR8-09	sample lost							
RVCR12-09	1.3E-01	2.5E+01	1.1E-01	7.6E-03	5.9E-04	7.2E-05	2.6E-03	1.0E-03
RVCR13-09	8.7E-02	2.4E+01	3.9E-02	1.1E-02	9.2E-04	4.9E-05	4.4E-03	bdl
RVCR14-09	9.9E-02	2.3E+01	2.7E-02	5.5E-03	5.3E-04	3.0E-05	2.2E-03	5.9E-04
RVCR65-09	2.3E-04	6.5E+00	1.4E-05	3.0E-05	1.7E-05	bdl	6.2E-04	bdl
Pailas de Agua I								
RVCR1-09	6.2E-02	2.8E+01	2.4E-03	8.8E-03	3.3E-04	1.5E-05	3.5E-03	2.1E-04
RVCR9-09	5.7E-02	4.3E+01	3.8E-02	8.5E-03	1.0E-03	7.8E-05	4.3E-03	bdl
RVCR17g-09	2.0E-01	3.2E+01	5.5E-03	6.2E-03	1.7E-03	4.0E-05	3.3E-03	8.8E-04
RVCR17r-09	2.0E-01	2.5E+01	8.2E-02	1.3E-02	1.0E-03	1.1E-04	7.1E-03	9.8E-04
RVCR17b-09	1.5E-02	6.4E-01	2.7E-03	5.3E-04	1.3E-04	bdl	2.8E-04	bdl
Pailas de Barro								
RVCR6-09	2.6E-01	3.4E+01	7.2E-03	4.0E-03	6.5E-04	2.1E-05	2.5E-03	1.2E-04
RVCR7-09	8.5E-02	4.9E+00	bdl	2.4E-03	3.1E-04	bdl	1.6E-03	3.6E-04
RVCR23-09	2.7E-01	2.7E+01	5.7E-03	4.2E-03	7.0E-04	2.0E-05	2.6E-03	9.8E-04
Hornillas	9.2E-02	3.1E+00	3.8E-03	6.9E-04	2.9E-04	1.0E-05	5.2E-04	2.4E-04

*bdl=below detection limits

Exchangeable Fraction Distribution in Las Pailas Sediments

	Trace Metals							
Exchangeable	**Ag**	**As**	**Au**	**Ba**	**Be**	**Cd**	**Co**	**Cr**
Standard	1.4E+00	3.4E-01	bdl	bdl	7.0E-02	1.7E+00	7.3E-01	1.7E-01
Yellowstone Paint Pots	Bdl	bdl	bdl	6.4E-03	bdl	bdl	bdl	4.5E-02
Laguna Fumarolica	4.4E-02	bdl	bdl	2.2E-02	bdl	1.8E-03	bdl	2.4E-02
Poza de Hongo	Bdl	bdl	bdl	4.4E-01	bdl	1.7E-03	bdl	2.3E-02
Pailas de Agua II								
RVCR4-09	Bdl	bdl	bdl	1.2E-02	bdl	2.7E-03	3.6E-03	5.1E-02
RVCR8-09	Bdl	bdl	bdl	2.1E-01	4.5E-03	3.1E-02	1.9E-02	2.1E-01
RVCR12-09	Bdl	bdl	bdl	bdl	4.2E-03	bdl	5.7E-03	bdl
RVCR13-09	Bdl	bdl	bdl	1.0E-01	7.0E-05	1.1E-03	7.6E-03	4.5E-02
RVCR14-09	Bdl	bdl	bdl	bdl	bdl	bdl	1.0E-03	1.9E-02
RVCR65-09	Bdl	bdl	bdl	bdl	1.4E-03	bdl	1.6E-02	4.3E-02
Pailas de Agua I								
RVCR1-09	Bdl	bdl	bdl	5.9E-04	bdl	5.0E-04	bdl	2.1E-02
RVCR9-09	Bdl	bdl	bdl	bdl	7.9E-04	bdl	7.4E-02	6.0E-04
RVCR17g-09	Bdl	bdl	bdl	bdl	8.2E-03	1.1E-02	8.3E-02	9.3E-02
RVCR17r-09	Bdl	bdl	bdl	bdl	bdl	bdl	1.5E-02	bdl
RVCR17b-09	Bdl	bdl	bdl	bdl	1.9E-03	bdl	4.4E-02	bdl
Pailas de Barro								
RVCR6-09	Bdl	bdl	bdl	bdl	bdl	1.6E-03	1.3E-02	2.8E-02
RVCR7-09	Bdl	bdl	bdl	bdl	7.3E-04	bdl	1.5E-03	bdl
RVCR23-09	Bdl	bdl	bdl	6.8E-03	bdl	1.9E-03	bdl	2.0E-02
Hornillas	Bdl	3.2E-03	bdl	bdl	bdl	bdl	bdl	bdl

values reported in mg/l
*bdl=below detection limits

	Trace Metals							
Exchangeable	**Cu**	**Li**	**Mo**	**Ni**	**P**	**Pb**	**S**	**Sb**
Standard	Bdl	bdl	bdl	9.8E-01	1.9E+01	3.9E-02	bdl	bdl
Yellowstone Paint Pots	Bdl	bdl	bdl	bdl	1.8E+01	bdl	5.9E+00	bdl
Laguna Fumarolica	Bdl	bdl	bdl	bdl	2.0E+01	bdl	5.2E+01	bdl
Poza de Hongo	Bdl	bdl	bdl	bdl	2.6E+01	bdl	5.3E+00	bdl
Pailas de Agua II								
RVCR4-09	Bdl	bdl	bdl	bdl	3.3E+01	bdl	1.0E+02	bdl
RVCR8-09	Bdl	bdl	bdl	bdl	2.3E+01	bdl	2.3E+02	bdl
RVCR12-09	3.5E-02	bdl	bdl	bdl	1.2E+02	bdl	1.1E+02	bdl
RVCR13-09	Bdl	bdl	bdl	bdl	2.7E+01	bdl	1.2E+02	bdl
RVCR14-09	Bdl	bdl	bdl	bdl	1.9E+01	bdl	5.2E+01	bdl
RVCR65-09	6.9E-03	4.2E+00	bdl	2.6E-03	9.5E+01	bdl	3.7E+02	bdl
Pailas de Agua I								
RVCR1-09	Bdl	bdl	bdl	bdl	2.0E+01	bdl	1.3E+01	bdl
RVCR9-09	9.4E-02	2.5E-02	bdl	2.7E-02	1.0E+02	bdl	7.7E+01	bdl
RVCR17g-09	1.7E-01	bdl	bdl	3.8E-02	9.8E+01	bdl	5.6E+02	5.4E-03
RVCR17r-09	Bdl	4.4E+00	bdl	2.3E-03	8.9E+01	bdl	bdl	bdl
RVCR17b-09	3.7E-02	9.5E-03	bdl	3.6E-03	1.2E+02	bdl	3.9E+01	bdl
Pailas de Barro								
RVCR6-09	Bdl	bdl	bdl	bdl	2.6E+01	bdl	7.1E+01	bdl
RVCR7-09	4.4E-02	2.4E-02	bdl	bdl	1.2E+02	bdl	8.6E+00	bdl
RVCR23-09	Bdl	bdl	bdl	bdl	1.8E+01	bdl	5.2E+00	bdl
Hornillas	Bdl	bdl	bdl	bdl	bdl	bdl	bdl	bdl

values reported in mg/l
*bdl=below detection limits

	Trace Metals					
Exchangeable	**Se**	**Sr**	**Ti**	**Tl**	**V**	**Zn**
Standard	bdl	5.8E-01	bdl	bdl	bdl	1.6E+00
Yellowstone Paint Pots	bdl	bdl	bdl	bdl	bdl	bdl
Laguna Fumarolica	bdl	bdl	bdl	bdl	bdl	bdl
Poza de Hongo	bdl	2.2E-01	bdl	bdl	bdl	8.5E-01
Pailas de Agua II						
RVCR4-09	bdl	bdl	bdl	bdl	bdl	9.1E-02
RVCR8-09	bdl	bdl	6.4E-01	bdl	bdl	bdl
RVCR12-09	bdl	1.9E-01	1.8E-02	bdl	7.5E-02	bdl
RVCR13-09	bdl	2.0E-02	bdl	bdl	bdl	9.2E-02
RVCR14-09	bdl	bdl	bdl	bdl	bdl	bdl
RVCR65-09	bdl	6.3E+00	1.4E-01	bdl	1.5E-01	bdl
Pailas de Agua I						
RVCR1-09	bdl	bdl	bdl	bdl	bdl	bdl
RVCR9-09	1.5E-02	1.3E-01	3.0E-02	bdl	4.2E-02	2.6E-02
RVCR17g-09	bdl	1.5E+00	8.3E-02	bdl	4.6E-01	8.4E-02
RVCR17r-09	3.6E-04	1.0E-01	4.4E-02	bdl	bdl	bdl
RVCR17b-09	bdl	7.5E-02	1.6E-02	bdl	2.8E-02	3.6E-02
Pailas de Barro						
RVCR6-09	bdl	bdl	bdl	bdl	bdl	5.8E-01
RVCR7-09	2.7E-02	6.4E-02	1.2E-02	bdl	bdl	1.6E-02
RVCR23-09	bdl	bdl	bdl	bdl	bdl	bdl
Hornillas	bdl	bdl	bdl	bdl	bdl	bdl

values reported in mg/l
*bdl=below detection limits

Carbonate Fraction Distribution in Las Pailas Sediments

	Trace Metals							
Carbonate	**Ag**	**As**	**Au**	**Ba**	**B**	**Be**	**Cd**	**Co**
Standard	2.6E-01	8.2E-01	bdl	6.8E-01	bdl	3.7E-01	1.7E-01	2.4E-01
Yellowstone Paint Pots	Bdl	bdl	bdl	2.0E-03	bdl	6.1E-04	5.7E-04	bdl
Laguna Fumarolica	Bdl	bdl	bdl	1.1E-02	bdl	8.9E-04	2.2E-03	7.6E-03
Poza de Hongo	Bdl	bdl	bdl	4.0E-02	bdl	1.2E-03	1.6E-03	4.2E-03
Pailas de Agua II								
RVCR4-09	Bdl	1.7E-03	bdl	bdl	bdl	bdl	bdl	bdl
RVCR8-09	Bdl	bdl	bdl	8.4E-02	bdl	7.3E-04	3.8E-03	9.6E-04
RVCR12-09	1.0E-03	1.0E-02	1.0E-03	1.0E-04	bdl	3.4E-04	2.1E-04	1.0E-03
RVCR13-09	1.4E-03	2.0E-03	bdl	6.5E-02	bdl	7.9E-04	1.1E-03	1.2E-03
RVCR14-09	Bdl	bdl	bdl	9.6E-03	1.5E-01	1.1E-03	1.2E-03	1.3E-03
RVCR65-09	1.0E-03	1.0E-02	1.0E-03	1.0E-04	bdl	1.0E-04	1.0E-04	1.0E-03
Pailas de Agua I								
RVCR1-09	Bdl	3.0E-03	0.0E+00	2.1E-03	bdl	8.3E-04	5.9E-04	bdl
RVCR9-09	1.0E-03	1.0E-02	1.0E-03	1.0E-04	bdl	1.0E-04	1.0E-04	1.0E-03
RVCR17g-09	1.0E-03	1.0E-02	1.0E-03	1.0E-04	bdl	1.0E-04	1.0E-04	1.0E-03
RVCR17r-09	1.0E-03	1.0E-02	1.0E-03	1.0E-04	bdl	1.0E-04	1.0E-04	1.0E-03
RVCR17b-09	1.0E-03	1.0E-02	1.0E-03	1.0E-04	bdl	1.0E-04	1.0E-04	1.0E-03
Pailas de Barro								
RVCR6-09	bdl	1.1E-03	0.0E+00	1.5E-03	bdl	9.7E-04	5.2E-04	1.1E-02
RVCR7-09	bdl	bdl	bdl	bdl	bdl	bdl	bdl	bdl
RVCR23-09	1.2E-01	bdl	bdl	3.7E-03	bdl	8.1E-04	1.4E-03	bdl
Hornillas	bdl	bdl	bdl	2.3E-02	bdl	6.5E-04	1.8E-03	bdl

values reported in mg/l
*bdl=below detection limits

	Trace Metals							
Carbonate	**Cr**	**Cu**	**Li**	**Mo**	**Ni**	**P**	**Pb**	**S**
Standard	4.8E-01	bdl	bdl	bdl	8.2E-02	2.7E-01	7.2E-02	bdl
Yellowstone Paint Pots	6.7E-03	bdl	bdl	bdl	bdl	bdl	bdl	bdl
Laguna Fumarolica	2.3E-02	bdl	bdl	bdl	bdl	6.5E-01	bdl	bdl
Poza de Hongo	1.8E-02	bdl	bdl	bdl	bdl	bdl	bdl	bdl
Pailas de Agua II								
RVCR4-09	bdl	bdl	bdl	bdl	bdl	bdl	bdl	bdl
RVCR8-09	4.0E-02	bdl	bdl	bdl	bdl	2.4E-01	bdl	bdl
RVCR12-09	1.0E-03	1.0E-03	1.0E-04	1.0E-03	1.0E-03	1.0E-02	1.0E-02	2.2E-01
RVCR13-09	2.7E-02	bdl	bdl	bdl	bdl	8.3E-01	bdl	bdl
RVCR14-09	1.7E-02	bdl	bdl	bdl	bdl	bdl	bdl	1.4E-01
RVCR65-09	1.0E-03	1.0E-03	1.0E-04	1.8E-03	1.0E-03	1.5E+01	1.0E-02	1.5E+01
Pailas de Agua I								
RVCR1-09	9.2E-03	bdl	bdl	Bdl	bdl	bdl	bdl	bdl
RVCR9-09	1.0E-03	1.0E-03	1.0E-04	1.0E-03	1.0E-03	1.0E-02	1.0E-02	1.0E+00
RVCR17g-09	1.0E-03	1.0E-03	1.0E-04	1.0E-03	1.0E-03	1.0E-02	1.0E-02	1.5E-01
RVCR17r-09	1.0E-03	1.0E-03	1.0E-04	1.0E-03	1.0E-03	1.0E-02	1.0E-02	1.0E-02
RVCR17b-09	1.0E-03	1.6E-02	1.0E-04	2.4E-03	1.0E-03	1.0E-02	1.0E-02	1.2E+01
Pailas de Barro								
RVCR6-09	7.8E-03	bdl	bdl	bdl	bdl	bdl	bdl	bdl
RVCR7-09	bdl	bdl	bdl	4.3E-04	bdl	bdl	bdl	1.6E-01
RVCR23-09	2.1E-02	bdl	bdl	bdl	bdl	3.1E+00	bdl	bdl
Hornillas	1.9E-02	bdl	bdl	bdl	bdl	1.7E+00	bdl	bdl

values reported in mg/l
*bdl=below detection limits

	Trace Metals						
Carbonate	**Sb**	**Se**	**Sr**	**Ti**	**Tl**	**V**	**Zn**
Standard	2.1E-01	bdl	bdl	bdl	bdl	bdl	5.5E-01
Yellowstone Paint Pots	bdl	bdl	bdl	bdl	bdl	bdl	bdl
Laguna Fumarolica	bdl	bdl	bdl	bdl	bdl	bdl	bdl
Poza de Hongo	bdl	bdl	bdl	bdl	bdl	bdl	bdl
Pailas de Agua II							
RVCR4-09	bdl	bdl	bdl	bdl	bdl	bdl	bdl
RVCR8-09	bdl	bdl	bdl	bdl	bdl	bdl	bdl
RVCR12-09	1.0E-02	1.3E-02	1.0E-04	8.8E-04	1.0E-02	4.6E-03	1.0E-03
RVCR13-09	bdl	bdl	bdl	bdl	bdl	bdl	bdl
RVCR14-09	bdl	bdl	bdl	4.4E-03	bdl	3.3E-03	bdl
RVCR65-09	1.0E-02	1.7E-02	4.9E-03	7.5E-03	1.0E-02	6.6E-03	1.0E-03
Pailas de Agua I							
RVCR1-09	bdl	bdl	bdl	bdl	bdl	bdl	bdl
RVCR9-09	1.0E-02	1.0E-02	1.0E-04	4.8E-03	1.0E-02	1.0E-03	1.0E-03
RVCR17g-09	1.0E-02	1.3E-02	2.9E-02	9.5E-03	1.0E-02	4.8E-03	1.0E-03
RVCR17r-09	1.0E-02	1.0E-02	1.0E-04	1.0E-03	1.0E-02	1.0E-03	1.0E-03
RVCR17b-09	1.0E-02	1.2E-03	9.5E-02	5.2E-02	1.0E-02	2.9E-02	1.0E-03
Pailas de Barro							
RVCR6-09	bdl	bdl	bdl	bdl	bdl	bdl	bdl
RVCR7-09	bdl	2.7E-03	2.4E-02	3.3E-03	bdl	2.9E-03	bdl
RVCR23-09	bdl	bdl	bdl	bdl	bdl	bdl	bdl
Hornillas	bdl	bdl	bdl	bdl	bdl	bdl	bdl

values reported in mg/l
*bdl=below detection limits

Oxide Fraction Distribution in Las Pailas Sediments

	Trace Metals						
Oxide	**Ag**	**As**	**Au**	**Ba**	**B**	**Be**	**Cd**
Standard	bdl	1.4E+00	bdl	bdl	bdl	2.6E-01	1.3E-01
Yellowstone Paint Pots	1.9E-02	1.9E-03	bdl	bdl	bdl	bdl	9.7E-04
Laguna Fumarolica	bdl	1.9E-03	bdl	bdl	bdl	bdl	bdl
Poza de Hongo	3.4E-01	bdl	bdl	1.9E-01	bdl	7.8E-03	3.7E-03
Pailas de Agua II							
RVCR4-09	1.2E-02	bdl	bdl	1.8E-02	bdl	5.9E-04	2.5E-02
RVCR8-09	1.7E-03	bdl	bdl	1.5E-01	bdl	7.2E-04	7.5E-03
RVCR13-09	bdl	bdl	bdl	1.1E-01	bdl	1.5E-03	3.9E-03
RVCR14-09	bdl	bdl	bdl	4.3E-02	bdl	5.9E-03	2.5E-02
RVCR65-09	2.3E-03	bdl	7.0E-03	2.6E-01	bdl	1.6E-03	1.6E-03
Pailas de Agua I							
RVCR1-09	2.6E-02	3.8E-03	bdl	8.2E-02	bdl	3.0E-04	3.2E-03
RVCR9-09	bdl	2.0E-03	8.5E-03	1.6E-01	bdl	5.7E-04	2.4E-03
RVCR12-09	bdl	3.8E-02	bdl	bdl	bdl	1.3E-02	2.7E-02
RVCR17g-09	3.2E-03	bdl	1.2E-02	bdl	1.8E-01	1.6E-03	2.0E-03
RVCR17r-09	bdl	bdl	bdl	bdl	bdl	4.9E-03	1.3E-02
RVCR17b-09	bdl	7.2E-03	bdl	bdl	bdl	2.7E-03	5.8E-03
Pailas de Barro							
RVCR6-09	bdl	bdl	bdl	bdl	bdl	bdl	bdl
RVCR7-09	bdl	1.3E-03	bdl	bdl	bdl	bdl	bdl
RVCR23-09	bdl	bdl	bdl	5.2E-02	bdl	6.7E-03	5.0E-03
Hornillas	5.7E-04	bdl	bdl	1.5E-01	bdl	bdl	8.2E-03

values reported in mg/l
*bdl=below detection limits

	Trace Metals							
Oxide	**Co**	**Cr**	**Cu**	**Li**	**Mo**	**Ni**	**P**	**Pb**
Standard	2.8E-01	8.7E-01	bdl	1.7E-02	bdl	1.8E-01	2.3E+01	6.5E-01
Yellowstone Paint Pots	bdl	3.5E-02	bdl	bdl	bdl	bdl	2.5E+01	bdl
Laguna Fumarolica	bdl	bdl	bdl	bdl	bdl	bdl	bdl	bdl
Poza de Hongo	2.7E-02	7.6E-02	bdl	bdl	bdl	bdl	2.7E+01	bdl
Pailas de Agua II								
RVCR4-09	bdl	1.6E-01	bdl	bdl	bdl	bdl	8.7E+00	bdl
RVCR8-09	6.7E-04	6.8E-02	bdl	bdl	bdl	bdl	bdl	bdl
RVCR13-09	1.6E-03	7.3E-02	bdl	bdl	bdl	bdl	2.4E+01	bdl
RVCR14-09	3.5E-03	1.8E-01	bdl	bdl	bdl	bdl	2.3E+01	bdl
RVCR65-09	9.4E-04	2.8E-03	2.4E-03	3.5E-03	bdl	6.3E-04	bdl	2.1E-02
Pailas de Agua I								
RVCR1-09	bdl	4.7E-02	bdl	bdl	bdl	0.0E+00	2.6E+01	bdl
RVCR9-09	3.0E-03	1.1E-02	6.3E-02	bdl	bdl	1.8E-03	bdl	2.5E-03
RVCR12-09	2.7E-03	8.7E-02	6.7E-02	bdl	bdl	5.7E-03	4.2E-01	1.1E-02
RVCR17g-09	1.7E-03	1.6E-02	1.1E-01	bdl	bdl	4.8E-03	7.7E-01	9.3E-04
RVCR17r-09	3.3E-03	6.4E-02	2.2E-01	bdl	bdl	3.8E-03	1.0E+00	1.4E-03
RVCR17b-09	2.7E-03	5.8E-03	5.8E-03	1.0E-02	bdl	1.9E-03	bdl	2.0E-03
Pailas de Barro								
RVCR6-09	bdl	bdl	bdl	bdl	bdl	bdl	bdl	bdl
RVCR7-09	bdl	bdl	bdl	bdl	bdl	bdl	bdl	bdl
RVCR23-09	3.4E-03	8.0E-02	bdl	bdl	bdl	bdl	1.6E+01	bdl
Hornillas	7.7E-04	8.2E-02	bdl	bdl	bdl	bdl	2.6E+01	bdl

values reported in mg/l
*bdl=below detection limits

	Trace Metals							
Oxide	**S**	**Sb**	**Se**	**Sr**	**Ti**	**Tl**	**V**	**Zn**
Standard	bdl	bdl	bdl	1.7E-02	bdl	bdl	bdl	5.7E-01
Yellowstone Paint Pots	bdl	bdl	bdl	bdl	bdl	bdl	bdl	bdl
Laguna Fumarolica	bdl	bdl	bdl	bdl	bdl	bdl	bdl	bdl
Poza de Hongo	6.1E+00	bdl	bdl	bdl	bdl	bdl	bdl	1.8E-01
Pailas de Agua II								
RVCR4-09	3.7E+01	bdl	bdl	bdl	bdl	bdl	bdl	bdl
RVCR8-09	7.0E+00	bdl	bdl	bdl	bdl	bdl	bdl	bdl
RVCR13-09	4.1E+00	bdl	bdl	bdl	bdl	bdl	bdl	bdl
RVCR14-09	2.0E+01	bdl	bdl	bdl	bdl	bdl	bdl	bdl
RVCR65-09	1.9E+00	1.4E-02	2.6E-02	3.6E-02	1.6E-02	6.0E-03	1.8E-02	bdl
Pailas de Agua I								
RVCR1-09	1.2E+00	bdl	bdl	bdl	bdl	bdl	bdl	bdl
RVCR9-09	3.8E+00	1.4E-02	bdl	2.1E-01	2.4E-02	1.0E-02	3.8E-02	1.6E-01
RVCR12-09	9.9E+00	1.6E-02	bdl	1.7E-01	1.9E-02	7.3E-03	1.2E+00	9.1E-02
RVCR17g-09	4.6E+00	2.3E-02	3.0E-02	1.8E-01	2.1E-02	1.0E-02	2.0E-01	bdl
RVCR17r-09	8.9E-01	1.2E-02	bdl	4.3E-01	5.3E-02	bdl	3.8E-01	bdl
RVCR17b-09	bdl	2.4E-02	3.9E-02	1.4E-01	9.2E-03	bdl	2.5E-01	1.2E-02
Pailas de Barro								
RVCR6-09	bdl	bdl	bdl	bdl	bdl	bdl	bdl	bdl
RVCR7-09	bdl	bdl	bdl	bdl	bdl	bdl	bdl	bdl
RVCR23-09	4.7E-01	bdl	bdl	bdl	bdl	bdl	bdl	bdl
Hornillas	6.6E+00	bdl	bdl	bdl	bdl	bdl	bdl	bdl

values reported in mg/l
*bdl=below detection limits

Organic Fraction Distribution in Las Pailas Sediments

	Trace Metals						
Organic	**Ag**	**As**	**Au**	**Ba**	**B**	**Be**	**Cd**
Standard	7.3E-02	1.9E-01	bdl	4.0E-02	bdl	9.4E-04	3.1E-03
Yellowstone Paint Pots	bdl	2.1E-03	bdl	bdl	bdl	bdl	bdl
Laguna Fumarolica	1.2E-03	bdl	bdl	1.5E-01	bdl	9.7E-04	1.5E-03
Poza de Hongo	bdl	bdl	bdl	bdl	bdl	bdl	1.4E-04
Pailas de Agua II							
RVCR4-09	1.6E-03	0.0E+00	bdl	bdl	bdl	2.5E-03	7.8E-04
RVCR8-09	3.3E-05	0.0E+00	bdl	4.0E-01	bdl	bdl	2.3E-04
RVCR12-09	4.1E-02	1.7E-01	bdl	bdl	bdl	3.7E-03	2.0E-02
RVCR13-09	bdl	bdl	bdl	8.2E-02	bdl	bdl	2.7E-04
RVCR14-09	1.5E-03	0.0E+00	bdl	1.9E-02	bdl	1.1E-03	7.9E-04
RVCR65-09	4.0E-02	1.9E-01	bdl	2.1E-02	bdl	bdl	2.0E-02
Pailas de Agua I							
RVCR1-09	3.5E-03	0.0E+00	bdl	4.3E-02	bdl	1.1E-04	3.1E-04
RVCR9-09	1.2E-01	0.0E+00	bdl	bdl	bdl	bdl	6.8E-02
RVCR17g-09	3.9E-02	1.8E-01	bdl	bdl	bdl	bdl	2.1E-02
RVCR17r-09	3.6E-02	1.5E-01	bdl	bdl	bdl	bdl	2.2E-02
RVCR17b-09	3.6E-02	1.9E-01	bdl	bdl	bdl	bdl	2.2E-02
Pailas de Barro							
RVCR6-09	1.2E-02	bdl	bdl	bdl	bdl	1.3E-04	2.5E-04
RVCR7-09	bdl	bdl	bdl	bdl	bdl	2.0E-03	bdl
RVCR23-09	3.2E-03	bdl	bdl	8.4E-03	bdl	1.5E-03	9.3E-04
Hornillas	5.3E-03	bdl	bdl	2.2E-01	bdl	4.3E-04	1.4E-03

values reported in mg/l
*bdl=below detection limits

	Trace Metals							
Organic	**Co**	**Cr**	**Cu**	**Li**	**Mo**	**Ni**	**P**	**Pb**
Standard	2.9E-03	5.3E-02	bdl	bdl	bdl	bdl	1.8E+00	bdl
Yellowstone Paint Pots	bdl	bdl	bdl	bdl	bdl	bdl	bdl	bdl
Laguna Fumarolica	bdl	bdl	bdl	bdl	bdl	bdl	bdl	bdl
Poza de Hongo	bdl	bdl	bdl	bdl	bdl	bdl	bdl	bdl
Pailas de Agua II								
RVCR4-09	bdl	7.2E-03	bdl	bdl	bdl	3.8E-03	bdl	bdl
RVCR8-09	bdl	5.8E-04	bdl	bdl	bdl	bdl	1.7E+00	bdl
RVCR12-09	1.5E-02	7.0E-03	6.2E-02	1.6E-02	2.6E-03	4.1E-02	4.0E-01	1.2E-01
RVCR13-09	3.7E-03	4.5E-03	bdl	bdl	bdl	bdl	bdl	bdl
RVCR14-09	bdl	2.1E-03	bdl	bdl	bdl	bdl	4.2E-02	bdl
RVCR65-09	1.5E-02	bdl	4.7E-02	1.8E-02	bdl	3.8E-02	8.5E-01	1.2E-01
Pailas de Agua I								
RVCR1-09	3.9E-04	5.9E-03	bdl	bdl	bdl	bdl	4.9E+00	bdl
RVCR9-09	9.5E-02	2.2E-01	4.5E-01	1.5E-02	bdl	9.7E-02	1.5E+00	1.4E-01
RVCR17g-09	3.0E-02	1.2E-02	6.1E-01	1.3E-02	bdl	4.7E-02	3.1E-01	1.2E-01
RVCR17r-09	3.3E-02	2.7E-02	4.9E-01	4.3E-03	5.2E-03	5.4E-02	2.1E+00	1.2E-01
RVCR17b-09	2.7E-02	1.3E-02	2.3E-01	1.2E-02	1.4E-03	4.8E-02	5.1E-01	1.3E-01
Pailas de Barro								
RVCR6-09	2.7E-04	bdl	bdl	bdl	bdl	bdl	6.8E-01	bdl
RVCR7-09	bdl	6.8E-03	6.0E-02	bdl	9.7E-03	bdl	1.2E+00	bdl
RVCR23-09	1.2E-03	5.5E-03	bdl	bdl	bdl	2.1E-03	2.0E+00	bdl
Hornillas	bdl	2.6E-03	bdl	bdl	bdl	bdl	4.2E-01	bdl

values reported in mg/l
*bdl=below detection limits

	Trace Metals							
Organic	**S**	**Sb**	**Se**	**Sr**	**Ti**	**Tl**	**V**	**Zn**
Standard	bdl	bdl	bdl	bdl	bdl	bdl	bdl	bdl
Yellowstone Paint Pots	bdl	bdl	bdl	bdl	bdl	bdl	bdl	bdl
Laguna Fumarolica	1.5E+01	bdl	bdl	bdl	bdl	bdl	bdl	bdl
Poza de Hongo	bdl	bdl	bdl	bdl	bdl	bdl	bdl	bdl
Pailas de Agua II								
RVCR4-09	6.2E+00	bdl	bdl	bdl	bdl	bdl	bdl	2.5E-02
RVCR8-09	bdl	bdl	bdl	bdl	bdl	bdl	bdl	bdl
RVCR12-09	2.8E+00	5.2E-03	2.9E-02	3.1E-01	2.3E-02	4.5E-02	3.8E-01	bdl
RVCR13-09	2.2E+01	bdl	bdl	bdl	bdl	bdl	bdl	bdl
RVCR14-09	bdl	bdl	bdl	bdl	bdl	bdl	bdl	bdl
RVCR65-09	bdl	bdl	bdl	1.2E-01	bdl	bdl	bdl	bdl
Pailas de Agua I								
RVCR1-09	bdl	bdl	bdl	bdl	bdl	bdl	bdl	bdl
RVCR9-09	3.6E+02	6.9E-03	bdl	2.3E-01	9.0E-02	4.4E-02	4.2E-02	bdl
RVCR17g-09	3.4E+01	1.1E-03	9.5E-04	2.5E-01	1.7E-02	2.5E-02	1.8E-02	bdl
RVCR17r-09	2.2E+01	1.0E-02	4.0E-02	2.5E-01	1.8E-02	6.5E-02	4.9E-02	bdl
RVCR17b-09	2.1E+01	bdl	bdl	1.7E-01	6.7E-03	3.2E-02	1.8E-02	bdl
Pailas de Barro								
RVCR6-09	bdl	bdl	bdl	bdl	bdl	bdl	bdl	bdl
RVCR7-09	3.8E+00	7.1E-03	4.5E-02	5.9E-01	1.5E-01	3.4E-02	7.0E-02	bdl
RVCR23-09	1.4E+00	bdl	bdl	bdl	bdl	bdl	bdl	1.0E-01
Hornillas	1.3E-01	bdl	bdl	bdl	bdl	bdl	bdl	5.4E-02

values reported in mg/l
*bdl=below detection limits

Residual Fraction Distribution in Las Pailas Sediments

	Residual Fraction						
Residual	**Ag**	**As**	**Au**	**Ba**	**Be**	**Cd**	**Co**
Standard	exploded						
Yellowstone Paint Pots	2.4E-07	8.1E-06	5.6E-06	bdl	1.8E-05	bdl	bdl
Laguna Fumarolica	bdl	bdl	bdl	bdl	2.4E-05	5.8E-05	6.3E-06
Poza de Hongo	bdl	bdl	bdl	bdl	1.2E-04	bdl	1.8E-06
Pailas de Agua II							
RVCR4-09	bdl	bdl	bdl	bdl	2.3E-04	bdl	7.1E-06
RVCR8-09	not yet analyzed						
RVCR13-09	1.4E-06	bdl	bdl	bdl	1.3E-03	bdl	3.6E-06
RVCR14-09	bdl	5.0E-07	bdl	bdl	2.8E-04	bdl	2.2E-06
RVCR65-09	2.8E-07	bdl	bdl	bdl	2.9E-03	bdl	3.2E-07
Pailas de Agua I							
RVCR1-09	6.2E-07	bdl	bdl	bdl	4.7E-04	bdl	5.6E-07
RVCR9-09	bdl	bdl	bdl	bdl	4.7E-04	bdl	3.9E-06
RVCR12-09	bdl	bdl	bdl	bdl	4.3E-04	bdl	1.1E-05
RVCR17g-09	4.1E-06	bdl	bdl	bdl	1.7E-02	bdl	3.0E-05
RVCR17r-09	bdl	bdl	bdl	bdl	1.2E-05	bdl	1.7E-07
RVCR17b-09	bdl	bdl	bdl	bdl	2.5E-05	bdl	2.3E-07
Pailas de Barro							
RVCR6-09	bdl	bdl	bdl	bdl	4.0E-04	bdl	5.0E-07
RVCR7-09	2.1E-07	bdl	bdl	bdl	1.7E-04	bdl	5.2E-07
RVCR23-09	bdl	1.2E-06	bdl	bdl	3.8E-04	bdl	1.3E-06
Hornillas	bdl	bdl	bdl	bdl	1.1E-04	bdl	3.7E-07

values reported in mg/l
*bdl=below detection limits

Residual Fraction

Residual	Cr	Cu	Li	Mo	Ni	P	Pb	S
Standard				exploded				
Yellowstone Paint Pots	6.6E-07	9.2E-06	4.2E-05	6.3E-07	bdl	1.7E-04	1.6E-05	1.5E-04
Laguna Fumarolica	2.2E-06	9.2E-05	6.5E-07	bdl	1.5E-06	5.8E-04	1.0E-06	6.7E-03
Poza de Hongo	1.5E-05	9.0E-05	9.7E-05	3.2E-07	4.3E-06	3.9E-04	bdl	5.3E-03
Pailas de Agua II								
RVCR4-09	1.2E-05	2.7E-05	3.0E-06	bdl	3.1E-06	7.8E-04	3.3E-06	2.3E-02
RVCR8-09				not yet analyzed				
RVCR13-09	4.2E-05	3.9E-04	4.2E-06	2.0E-06	1.5E-06	3.6E-03	6.1E-06	3.1E-01
RVCR14-09	8.9E-06	6.2E-05	4.1E-06	bdl	7.2E-07	7.3E-04	7.0E-07	1.4E-02
RVCR65-09	bdl	3.2E-06	bdl	bdl	1.4E-06	bdl	bdl	4.1E-04
Pailas de Agua I								
RVCR1-09	1.5E-05	1.4E-05	4.3E-06	1.1E-06	6.2E-07	6.4E-04	2.4E-06	2.1E-02
RVCR9-09	1.8E-05	6.5E-05	1.7E-05	6.2E-07	1.9E-06	7.1E-04	5.4E-06	7.1E-02
RVCR12-09	1.6E-05	3.5E-04	4.5E-06	bdl	5.8E-06	1.0E-03	2.3E-06	2.0E-02
RVCR17g-09	8.0E-04	3.0E-03	3.4E-04	8.0E-05	6.9E-05	2.6E-02	2.2E-05	2.0E+00
RVCR17r-09	1.2E-06	4.4E-06	3.2E-07	1.3E-07	1.7E-07	4.8E-05	1.7E-07	7.8E-04
RVCR17b-09	2.5E-06	8.5E-06	1.1E-06	1.6E-06	1.5E-07	9.9E-05	1.8E-07	1.7E-03
Pailas de Barro								
RVCR6-09	1.6E-05	2.5E-05	8.8E-06	bdl	9.8E-07	8.5E-04	bdl	1.1E-02
RVCR7-09	1.4E-05	1.9E-05	1.0E-05	7.1E-07	1.0E-06	9.0E-04	1.5E-06	8.6E-03
RVCR23-09	1.5E-05	3.2E-05	1.3E-05	4.9E-07	1.0E-06	8.2E-04	bdl	9.8E-03
Hornillas	4.1E-06	1.5E-05	1.3E-06	1.6E-07	1.2E-06	2.3E-04	bdl	1.5E-03

values reported in mg/l
*bdl=below detection limits

Residual Fraction

Residual	Sb	Se	Sr	Ti	Tl	V	Zn
Standard				exploded			
Yellowstone Paint Pots	7.9E-07	2.2E-06	bdl	9.2E-04	bdl	8.1E-06	5.9E-05
Laguna Fumarolica	bdl	bdl	1.2E-07	8.4E-04	bdl	1.0E-03	1.5E-05
Poza de Hongo	3.6E-06	0.0E+00	8.0E-07	7.4E-03	bdl	3.4E-04	7.7E-05
Pailas de Agua II							
RVCR4-09	3.9E-06	bdl	7.7E-07	6.5E-03	bdl	5.0E-04	1.1E-05
RVCR8-09				not yet analyzed			
RVCR13-09	1.5E-05	bdl	2.7E-06	2.5E-02	bdl	5.4E-04	4.3E-05
RVCR14-09	2.8E-06	bdl	2.1E-06	5.2E-03	bdl	2.8E-04	1.1E-05
RVCR65-09	2.9E-06	6.1E-06	0.0E+00	5.6E-06	bdl	6.5E-07	bdl
Pailas de Agua I							
RVCR1-09	5.6E-06	bdl	2.9E-06	9.0E-03	bdl	2.1E-04	1.7E-05
RVCR9-09	5.5E-06	bdl	2.2E-06	9.6E-03	bdl	1.8E-04	2.0E-05
RVCR12-09	4.8E-06	bdl	3.0E-06	9.3E-03	bdl	6.8E-04	1.9E-05
RVCR17g-09	1.7E-04	bdl	1.1E-04	4.6E-01	bdl	1.4E-02	8.0E-04
RVCR17r-09	4.1E-07	bdl	4.3E-08	6.6E-04	bdl	2.2E-05	1.0E-06
RVCR17b-09	6.9E-07	bdl	1.0E-07	1.4E-03	bdl	5.6E-05	1.0E-07
Pailas de Barro							
RVCR6-09	4.6E-06	bdl	2.8E-06	8.9E-03	bdl	3.0E-04	1.1E-05
RVCR7-09	4.2E-06	bdl	8.2E-07	7.9E-03	bdl	2.9E-04	bdl
RVCR23-09	4.1E-06	bdl	2.8E-06	8.8E-03	bdl	3.1E-04	1.7E-05
Hornillas	1.6E-06	bdl	4.2E-07	2.4E-03	bdl	2.2E-05	5.7E-06

values reported in mg/l
*bdl=below detection limits

Appendix B: Chloride-Fluoride Clay Experiments

Table 3A: High Temperature (80°C) Flouride Experiments

FeCl2

Day	0.1 mmol/l						0 mmol/l					
	No microspheres			Microspheres			No microspheres			Microspheres		
	Al	Fe	Si	Al	Fe	Si	Al	Fe	Si	Al	Fe	Si
0	bdl	3.1E+01	2.9E+00	3.3E-03	1.5E+01	6.5E+00	bdl	1.6E+01	8.4E+00	4.3E-03	1.7E+01	9.2E+00
1	7.5E-02	1.5E+01	6.3E+00	8.5E-02	1.6E+01	6.6E+00	bdl	1.5E+01	7.2E+00	1.9E-03	1.5E+01	7.3E+00
2	9.8E-02	1.5E+01	6.2E+00	1.0E-01	1.5E+01	6.0E+00	bdl	1.2E+01	5.4E+00	1.4E-02	1.3E+01	5.8E+00
3	1.4E-01	1.5E+01	6.3E+00	1.5E-01	1.6E+01	6.4E+00	bdl	1.6E+01	7.2E+00	bdl	1.4E+01	6.4E+00
4	1.7E-01	1.7E+01	7.3E+00	1.6E-01	1.5E+01	6.3E+00	1.1E-03	1.7E+01	7.8E+00	bdl	1.4E+01	6.1E+00
5	1.8E-01	1.6E+01	6.5E+00	1.9E-01	1.5E+01	6.4E+00	3.0E-04	1.5E+01	6.4E+00	4.1E-04	1.5E+01	6.8E+00
6	1.7E-01	1.4E+01	5.8E+00	1.6E-01	1.3E+01	5.1E+00	8.0E-04	1.5E+01	6.8E+00	bdl	1.3E+01	5.9E+00
7	2.0E-01	1.5E+01	6.1E+00	2.0E-01	1.4E+01	5.8E+00	1.9E-03	1.5E+01	6.7E+00	7.8E-04	1.4E+01	6.0E+00
11	3.0E-01	1.6E+01	6.5E+00	2.4E-01	1.3E+01	5.4E+00	1.3E-03	1.4E+01	5.9E+00	1.1E-03	1.4E+01	6.2E+00
15	3.4E-01	1.4E+01	5.6E+00	1.5E-01	1.0E+01	4.2E+00	3.7E-03	1.5E+01	6.3E+00	5.5E-02	1.1E+01	4.4E+00

*bdl= below detection limits

Table 3B: High Temperature (80°C) Oxalate experiments

FeCl2

Day	0.1 mmol/l						0 mmol/l					
	No microspheres			Microspheres			No microspheres			Microspheres		
	Al	Fe	Si	Al	Fe	Si	Al	Fe	Si	Al	Fe	Si
0	1.4E-02	1.5E+01	5.6E+00	9.8E-03	1.6E+01	6.8E+00	bdl	1.3E+01	5.0E+00	bdl	1.5E+01	7.1E+00
1	1.1E-02	1.4E+01	5.5E+00	9.8E-03	1.5E+01	6.7E+00	8.1E-04	1.5E+01	5.4E+00	bdl	1.2E+01	5.0E+00
2	6.4E-03	1.0E+01	3.9E+00	8.4E-03	9.4E+00	4.1E+00	bdl	1.4E+01	5.2E+00	bdl	1.5E+01	6.3E+00
3	9.0E-03	1.2E+01	4.9E+00	1.0E-02	1.3E+01	6.1E+00	bdl	1.1E+01	4.0E+00	bdl	1.2E+01	5.1E+00
4	1.1E-02	1.3E+01	5.3E+00	1.3E-02	1.2E+01	5.8E+00	bdl	1.2E+01	4.5E+00	bdl	1.2E+01	5.0E+00
5	1.7E-02	1.3E+01	5.3E+00	1.3E-02	1.0E+01	4.7E+00	bdl	1.3E+01	4.8E+00	4.7E-04	1.3E+01	5.3E+00
6	1.5E-02	1.3E+01	5.2E+00	1.8E-02	1.2E+01	5.7E+00	2.6E-03	1.4E+01	5.3E+00	2.1E-03	1.3E+01	5.8E+00
7	1.3E-02	1.2E+01	4.8E+00	1.8E-02	1.2E+01	5.5E+00	bdl	1.3E+01	4.9E+00	bdl	1.2E+01	5.0E+00
11	1.6E-03	7.6E+00	3.2E+00	2.1E-03	1.5E+01	6.3E+00	2.6E-02	1.4E+01	5.8E+00	2.9E-02	1.3E+01	5.8E+00
15	9.2E-03	1.5E+01	5.9E+00	3.3E-03	1.3E+01	5.4E+00	3.5E-02	1.5E+01	6.5E+00	3.9E-02	1.5E+01	6.7E+00

Table 3C: High Temperature (50°C) Flouride Experiments

FeCl2

Day	0.1 mmol/l						0 mmol/l					
	No microspheres			Microspheres			No microspheres			Microspheres		
	Al	Fe	Si	Al	Fe	Si	Al	Fe	Si	Al	Fe	Si
0	bdl	4.9E+00	2.1E+00	bdl	1.4E+01	6.2E+00	bdl	1.5E+01	6.3E+00	bdl	1.0E+01	4.5E+00
1	5.9E-02	1.7E+01	6.4E+00	4.2E-02	1.6E+01	6.2E+00	bdl	1.6E+01	6.3E+00	bdl	1.5E+01	6.1E+00
2	8.0E-02	1.6E+01	5.9E+00	6.5E-02	1.5E+01	5.6E+00	bdl	2.0E+01	7.7E+00	bdl	1.6E+01	6.1E+00
3	8.1E-02	1.4E+01	5.0E+00	6.0E-02	1.0E+01	3.8E+00	7.4E-04	1.7E+01	6.5E+00	bdl	6.7E+00	2.6E+00
4	1.4E-01	1.7E+01	6.2E+00	1.2E-01	1.8E+01	6.8E+00	bdl	1.7E+01	6.5E+00	8.9E-03	1.7E+01	6.5E+00
5	1.4E-01	1.7E+01	6.5E+00	4.3E-02	1.6E+01	6.4E+00	1.7E-03	1.7E+01	6.6E+00	7.9E-02	1.5E+01	6.1E+00
6	1.2E-01	1.6E+01	6.1E+00	1.4E-01	1.6E+01	6.6E+00	5.7E-03	1.6E+01	6.0E+00	3.3E-03	1.6E+01	6.3E+00
7	1.8E-01	1.8E+01	6.6E+00	1.7E-01	1.7E+01	6.7E+00	2.6E-03	1.7E+01	6.2E+00	8.7E-04	1.4E+01	5.2E+00
11	1.5E-01	1.4E+01	4.8E+00	1.8E-01	1.5E+01	5.3E+00	1.4E-03	1.7E+01	5.8E+00	1.7E-03	1.6E+01	5.9E+00
15	2.2E-01	1.7E+01	5.9E+00	2.3E-01	1.7E+01	5.8E+00	7.9E-04	1.7E+01	5.9E+00	2.5E-03	1.6E+01	5.9E+00

Table 3D: High Temperature (25oC) Flouride Experiments

FeCl2

Day	0.1 mmol/l						0 mmol/l					
	No microspheres			Microspheres			No microspheres			Microspheres		
	Al	Fe	Si	Al	Fe	Si	Al	Fe	Si	Al	Fe	Si
0	3.9E-03	1.6E+01	7.5E+00	5.3E-03	1.6E+01	8.7E+00	5.5E-03	1.8E+01	9.9E+00	5.4E-03	1.6E+01	8.9E+00
4	2.5E-02	1.6E+01	6.6E+00	3.2E-02	1.6E+01	6.8E+00	3.8E-03	1.7E+01	8.3E+00	2.5E-03	1.5E+01	7.4E+00
7	3.4E-02	1.4E+01	6.1E+00	3.6E-02	1.5E+01	6.5E+00	2.2E-03	1.4E+01	6.0E+00	1.2E-03	1.5E+01	6.8E+00
11	4.2E-02	1.4E+01	4.7E+00	4.2E-02	1.4E+01	5.5E+00	9.3E-04	1.4E+01	6.1E+00	1.2E-03	1.5E+01	6.8E+00
14	4.7E-02	1.4E+01	5.5E+00	4.1E-02	1.3E+01	5.0E+00	2.1E-03	1.5E+01	6.9E+00	1.2E-03	1.4E+01	5.9E+00
17	5.0E-02	1.4E+01	5.1E+00	4.6E-02	1.4E+01	5.2E+00	2.5E-03	1.5E+01	5.4E+00	3.1E-03	1.3E+01	5.7E+00
21	5.5E-02	1.3E+01	5.1E+00	6.5E-02	1.7E+01	6.3E+00	2.7E-03	1.7E+01	6.7E+00	3.1E-03	1.6E+01	6.9E+00

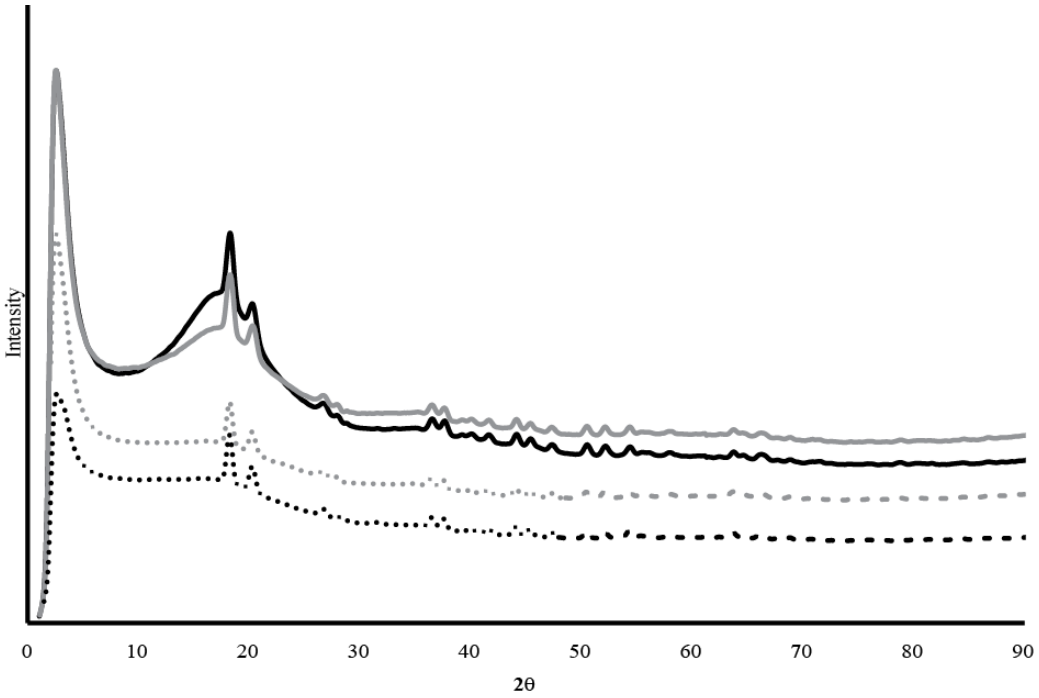

Figure 1A

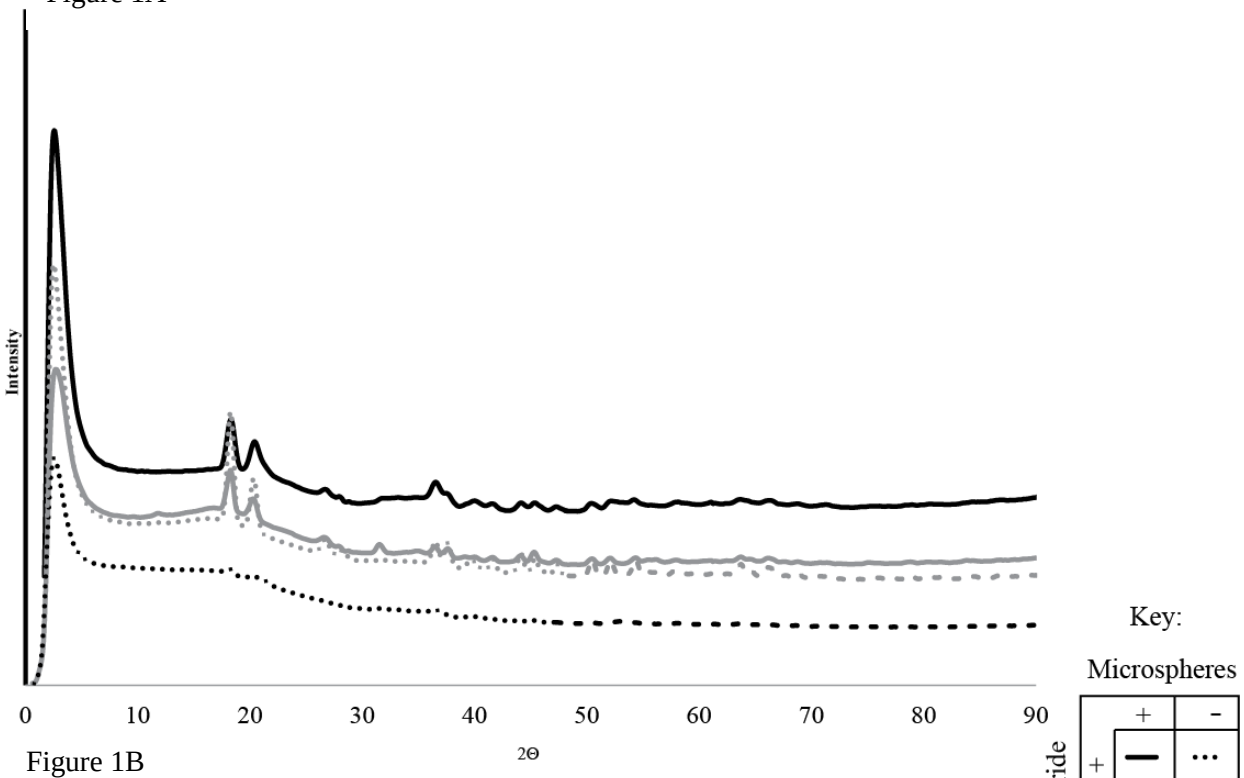

Figure 1B

Figure 1: XRD of precipitates at 80°C from (A) chloride-fluoride experiments after 7 days. Smectite peaks are more well-developed in samples containing microspheres (solid lines); however, all experimental trials form smecitites and goethite. Amorphous silica is present in samples with microspheres. (B) chloride-oxalate experiments after 7 days. Smectite peaks are more well-developed in samples containing microspheres (solid lines); however, all experimental trials form smecitites. Fe-oxides are more crystalline in the presence of microspheres.

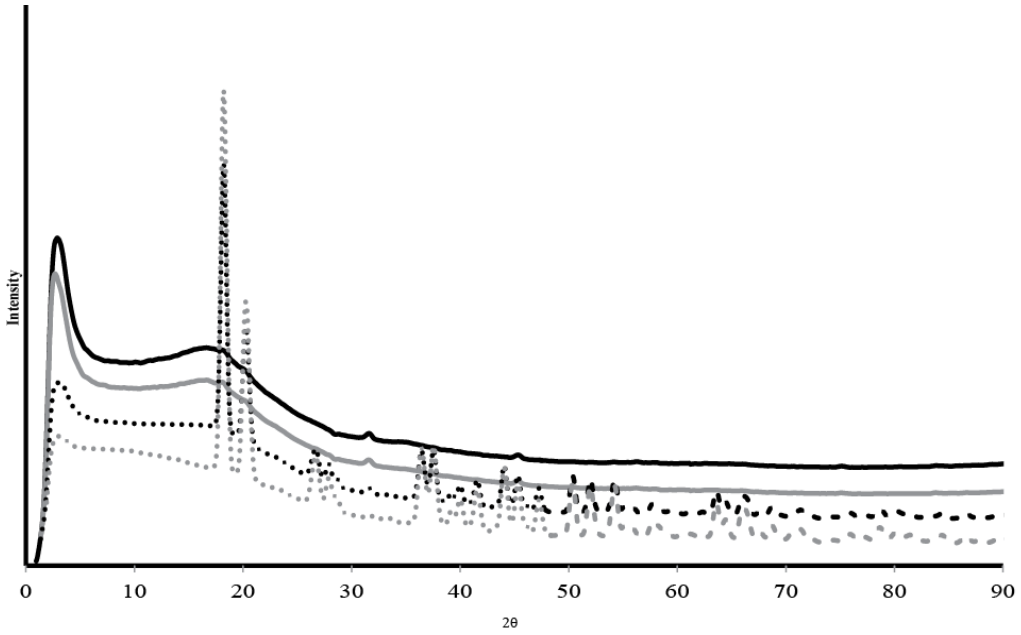

Figure 1C

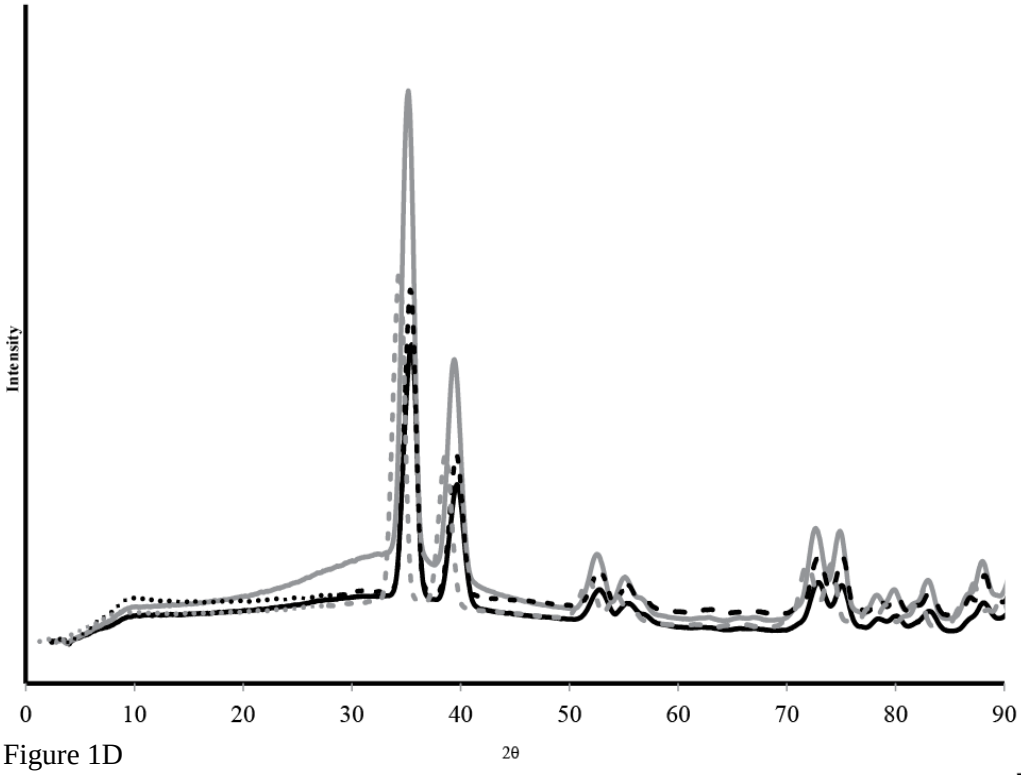

Figure 1D

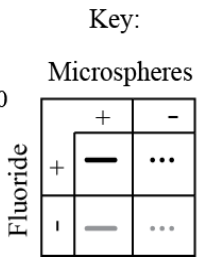

Figure 1 continued: XRD of precipitates from chloride-fluoride (C) at 50°C from experiments after 7 days. Smectite peaks are more well-developed in samples containing microspheres (solid lines); amorphous silica is also present in samples with microspheres. Fe-/Al-oxides are present in samples without microspheres (B) at 25°C from experiments after 17 days. All precipitates are similar regardless of experimental conditions. Fe-oxides form in all samples. Kaolinite may be present as well.